1 INTRODUCTION

1.1 Purpose

This Science Data Validation Plan describes the plans for validating the products generated with the team retrieval algorithms and the activities that lead to gathering these validation data.

1.2 Scope

This document includes a description of the algorithm validation approach and the measurements required for validation including the experiments and campaigns that will collect these data.

1.3 Documents

ATBDs:

Ocean Parameter Suite: F. Wentz
Rainfall: C. Kummerow, T. Wilheit and R. Ferraro
Sea Ice: D. Cavalieri and J. Comiso
Snow Water Equivalent: A. Chang
Land Surface: E. Njoku

They can be found on the web at: http://eospso.gsfc.nasa.gov/atbd/amsrtables.html

2 MEASUREMENT AND SCIENCE OBJECTIVE

In support of the Earth Science Enterprise goals, the Advanced Microwave Scanning Radiometer for EOS (AMSR-E) is flying on NASA's Earth Observing System (EOS) Aqua Satellite launched in May 4 2002. AMSR-E is a passive microwave instrument modified from the AMSR developed by the National Space Development Agency of Japan (NASDA). AMSR is flying on the Japanese Advanced Earth Observing Satellite-II (ADEOS-II) satellite launched on December 14 2002.

Atmospheric and surface parameters retrieved are: precipitation, sea surface temperatures, sea ice concentration, snow depth and water content, land surface wetness, sea surface wind speed, atmospheric cloud water and water vapor over the ocean.

2.1 The Instrument

The AMSR-E is a twelve channel, six frequency total power passive microwave radiometer system. It measures brightness temperatures at 6.925, 10.65, 18.7, 23.8, 36.5, and 89.0 GHz. Vertically and horizontally polarized measurements are taken for all frequencies.

The instrument consists of an offset parabolic reflector 1.6 meters in diameter, fed by an array of six feedhorns. The reflector and feedhorn arrays are mounted on a drum, which contains the radiometers, digital data subsystem, mechanical scanning subsystem, and power subsystem. The reflector/feed/drum assembly is rotated about the axis of the drum by a coaxially mounted bearing and power transfer assembly. All data, commands, timing and telemetry signals, and power pass through the assembly on slip ring connectors to the rotating assembly.

A cold load reflector and a warm load are mounted on the transfer assembly shaft and do not rotate with the drum assembly. They are positioned off axis such that they pass between the feedhorn array and the parabolic reflector, occulting it once each scan. The cold load reflector reflects cold sky radiation into the feedhorn array thus serving, along with the warm load, as calibration references. Calibration of the radiometers is essential for collection of useful data. Corrections for spillover and antenna pattern effects are incorporated in the Level 1 (L1) data processing algorithms.

The instrument rotates continuously about an axis parallel to the local spacecraft vertical at 40 rpm. At an altitude of 705 km, it measures the upwelling scene brightness temperatures over an angular sector of +/- 61 degrees about the sub-satellite track, resulting in a swath width of 1445 km.

During a period of 1.5 seconds the spacecraft sub-satellite point travels 10 km. Even though the instantaneous field-of-view for each channel is different, active scene measurements are recorded at equal intervals of 10 km (5 km for the 89 GHz channels) along the scan. The half cone angle at which the reflector is fixed is 47.4 degrees which results in an Earth incidence angle of 55.0 degrees. Table 2.1.1 lists the pertinent performance characteristics.

Table 2.1.1 AMSR-E PERFORMANCE CHARACTERISTICS

Center Frequencies (GHz)	6.925	10.65	18.7	23.8	36.5	89.0
Bandwidth (MHz)	350	100	200	400	1000	3000
Sensitivity (K)	0.3	0.6	0.6	0.6	0.6	1.1
IFOV (Km x Km)	75x43	48x27	27x16	31x18	14x8	6x4
Sampling Rate (Km x Km)	10x10	10x10	10x10	10x10	10x10	5x5
Integration Time (msec)	2.6	2.6	2.6	2.6	2.6	1.3
Main Beam Efficiency (%)	95.3	95.0	96.3	96.4	95.3	96.0
Beamwidth (Degrees)	2.2	1.4	0.8	0.9	0.4	0.18

2.2 Science Objectives

The geophysical standard products retrieved from AMSR-E data will primarily be used in climate change research. Over the ocean these products include rainfall, sea surface temperature (SST), surface wind speed, integrated water vapor and cloud water contents, and sea ice parameters. Over land, the standard products include soil moisture, rainfall, and snow cover water content. This wide variety of products will enable an equally wide variety of science investigations, especially those dealing with the atmospheric and surface hydrologic and energy cycles. Because some investigations will compare the relationships between the various parameters (e.g. the variability of tropical average surface winds with SST) it is important to reduce retrieval algorithm cross-talk between parameters, e.g. so that variations in wind speed are not misdiagnosed as being SST variability, and *vice versa*. Another possibility would be the misdiagnosis of temperature variability as a change in one of the retrieved parameters. Reduction of algorithm cross talk is essential to the useful exploitation of these products.

The AMSR-E's monitoring of the interannual variability in the standard product parameters will provide much insight into the climate system, helping to improve physical processes and parameterizations in climate models. These improvements, in turn, will enable more accurate predictions of global and regional climate changes associated with both natural and anthropogenic influences.

2.3 Science Data Products

The AMSR-E Science team members are developing all the retrieval algorithms. The individual development takes place on each member's science computing facility (SCF); before delivery to the Team Leader SCF (TLSCF) they are responsible for stand-alone testing of their software on the TLSCF. The generation of science data products can be divided into three groups: Level 1 - brightness temperatures (Tbs), Level 2 and higher - the EOS agreed standard data products, and special data products - research products whose retrieval algorithms are not yet proven. The generation flow of all the products is shown in Figure 2.1.1.

L 1 data will be processed at NASDA's Earth Observation Center (EOC). It is customary to have the sensor manufacturer do the L 1 processing because it involves instrument data taken during the ground calibration/qualification testing.

Level 2A (L 2A) data, are spatially consistent T_b data sets at 5 different footprint sizes corresponding to the 6.9, 10.7, 18.7, 36.5 and 89 GHz footprints.

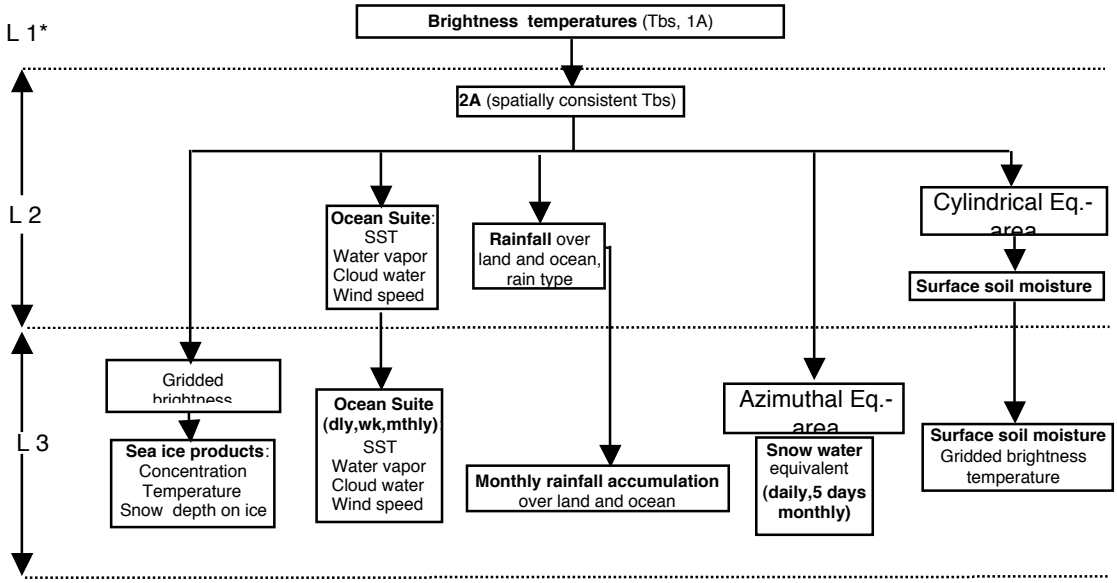

*produced by NASDA

Figure 2.1.1 AMSR-E standard products

2.4 Standard Data Products Accuracy and Resolution

a) Level 2 standard products

PRODUCT	ACCURACY	SPATIAL RESOLUTION (KM)
Brightness Temperature	0.2 – 0.7 K	5 - 56
Ocean: Sea Surface Temperature	0.5 K	56
Columnar Water Vapor	0.6 mm	25
Columnar Cloud Water	0.02 mm	25
Wind Speed	0.9 m/s	25
Rainfall: Over oceans	1 mm/hr or 20%	12
Over land	2 mm/hr or 20%	12
Type		
Land: Surface soil moisture	0.06 g/cm^3	56

b) Level 3 standard products

PRODUCT	ACCURACY	GRID RESOLUTION (KM)	TEMPORAL RESOLUTION
Ocean: Sea Surface Temperature	0.5 K	_ x _ degrees	daily asc and dsc weekly, monthly
Columnar Water Vapor	0.6 mm	_ x _ degrees	daily asc and dsc weekly, monthly
Columnar Cloud Water	0.02 mm	_ x _ degrees	daily asc and dsc weekly, monthly
Wind Speed	0.9 m/s	_ x _ degrees	daily asc and dsc weekly, monthly
Rainfall: Over oceans	20%	5 x 5 degrees	monthly
Over land	30%	5 x 5 degrees	monthly
Sea Ice: Concentration	□5%	12.5, 25	daily asc and dsc
Temperature	□4 K	25	daily asc and dsc
Snow depth on ice	□5 cm	12.5	5 days
Gridded brightness temp	0.3 – 0.6 K	6.25, 12.5, 25	daily
Land: Surface soil moisture	0.06 g/cm^3	25	daily
Gridded brightness temps	0.3 - 0.6 K	25	daily
Snow: Water equivalent	10 mm or 20%	25 (EASE grid)	Daily, 5 days, monthly

3 VALIDATION/ALGORITHM DEVELOPMENT ACTIVITIES

The AMSR-E validation program has two distinct phases: Pre-launch, where both the software stability and algorithm capability to retrieve valid products (by comparing them to ground truth data) are implemented, and Post-launch, where the latter is continued for 1 to 2 years after launch.

The **pre-launch** activities are:

1) Demonstrate the stability of the software by using TRMM TMI (and to a smaller extent SSM/I) data for the algorithms that do not require the lower frequency channels.

2) Demonstrate the validity of the retrieved products with ground truth data, where possible.

The algorithms using the lowest frequency (6.9 GHz) channel have to be calibrated post-launch.

Post-launch: the activities started before launch will continue and add, wherever possible, new campaigns and field truth data.

3.1 Ocean Parameters (submitted by F. Wentz)

There are four primary ocean parameters that require validation: sea surface temperature (SST) T_S (C°), near-surface wind speed W (m/s), columnar water vapor V (mm), and columnar cloud water L (mm). These parameters will be validated through intercomparison with other satellite and in-situ data products as described below. The intercomparisons will probably reveal some differences between the AMSR-E products and the validation data sets. When these differences indicate a problem with the AMSR-E products, physical coefficients in the AMSR-E radiative transfer model will be adjusted so as to make the AMSR-E products agree with the validation data set. Care will be taken to ensure that the validation data set is sufficiently accurate to warrant a change in the AMSR-E model. In addition we expect that small offsets will need to be applied to each of the AMSR-E channels to remove absolute biases in the radiometer calibration and/or in the radiative transfer model.

These calibration/validation methods are currently being applied to the SSM/I and the TRMM TMI. In this way, our cal/val methods are developed and tested before launch, and the AMSR-E retrieval algorithm and radiative transfer model can be improved based on current radiometer missions. These methods will also be used for the ADEOS-II AMSR whose launch is planned in late 2002.

3.1.1 Validation Criteria and Method

Computer simulations discussed at length in the AMSR-E Ocean ATBD indicate the rms accuracies given in Table 3.1.1 should be achieved by AMSR-E. These accuracies are for a 60-km spatial resolution for T_S and 25 km for the other three parameters. In view of the high accuracies, it will be necessary to carefully quality control the various validation data sets. The calibration and validation of the first 3 ocean products (T_S, W, and V) will be based on intercomparison of buoy and radiosonde observations and on SST and wind retrievals coming from other satellite sensors. Because there are no reliable ancillary data sets for calibration or validation of cloud liquid water, we will rely on a histogram analysis similar to that done by *Wentz* [1997]. The following sections more fully explain each of the calibration data sources.

Table 3.1.1. Predicted Accuracy for AMSR-E Ocean Products

Ocean Parameter	Calibration methods	Rms. Error
Sea-Surface Temperature (T_S)	Satellite, Buoy	0.5 C
Wind Speed (W)	Satellite, Buoy, GCM	0.9 m/s
Columnar Water Vapor (V)	Radiosonde	0.6 mm
Columnar Cloud Water (L)	Histogram	0.02 mm

In validating the ocean parameters, the spatial-temporal mismatch between the calibration source (i.e., in situ observation or other satellite product) and the AMSR-E product must be considered and errors in the calibration source be accounted for. For example, the true wind speed averaged over a 25 km AMSR-E footprint will, in general, not equal the wind speed measured by a buoy because the buoy wind is a point observation taken at a different time and contains measurement error. Similar problems exist for the SST and vapor intercomparison.

Thus in the intercomparison statistics, we will first compute the rms difference between the AMSR-E product and the calibration source. For this difference we will then subtract (in a root-mean-squared sense) the spatial-temporal mismatch error and the calibration source measurement error. The residual will then be the indicator of the accuracy of the AMSR-E retrieval. Our validation criterion is that this computed accuracy meets or exceeds the accuracy given in Table 3.1.1.

The spatial and temporal mismatch error depends on the size of the collocation window, which is defined as the maximum allowable space-time difference between the AMSR-E observation and the *in situ* observation. To minimize the spatial-temporal mismatch error, the collocation criteria must be carefully selected. Table 3.1.2 gives the spatial and temporal windows we plan to use for the different types of *in situ* validations. The buoy collocation window

for wind is smaller than that for SST because wind has a higher spatial-temporal variability. Ideally, we would like to have the collocation window for the vapor versus radiosonde intercomparisons as small as the collocation window used for wind. However, since the radiosonde observations come from islands, a larger spatial window is required to capture the adjacent AMSR-E ocean observations. In addition, a larger temporal window is required because radiosonde flights only occur every 12 hours, as compared to the hourly buoy observations. Thus the vapor collocation window is larger than that for wind.

Table 3.1.2. Collocation Windows for In Situ Validation

AMSR-E Product	In Situ Calibration Source	Spatial Collocation Window	Temporal Collocation Window
SST	Ocean buoys	50 km	3 hours
Wind	Ocean buoys	30 km	1 hour
Vapor	Radiosondes	60 km	6 hours

The validation of cloud water is different than that for SST, wind, and vapor. There is no reliable calibration source for the total columnar cloud water, and hence we have to rely on the histogram technique (i.e., an error model) described below. For cloud water, the validation criterion is that the histogram alignment meets or exceeds the accuracy given in Table 3.1.1.

Geophysical parameters generated as part of the Level 2B data set (i.e., sea surface temperature, wind, vapor, and cloud) will be temporally averaged by day, week, and month, and gridded as part of the Level 3 data sets. The spatial resolution of the gridded data sets will be _ degree, resulting in data volumes of approximately 2 Megabyte for each data set, or a total of 8 Megabytes per time period for the entire suite of ocean parameters.

The accuracy of each of the temporally averaged data sets will be better than that of the corresponding instantaneous Level 2B measurements, although the amount of improvement attained through temporal averaging will differ by parameter and time period. Because the AMSR-E instrument will not view the entire Earth within a single day, some Earth locations will not be measured even once in the daily averaged products, while a few locations will have the benefit of more than one observation. Thus, the primary purpose of the daily Level 3 product will be to arrange the observations on a common Earth grid rather than to average them. In contrast, weekly and monthly averages will generally enjoy a substantial temporal averaging benefit.

3.1.2 Operational Surface Networks

The two operational surface networks that will be used are the moored ocean buoys and island radiosonde stations. Moored buoys will be used to validate SST, and wind speed, and the radiosondes will be used to validate the columnar water vapor. The moored buoy data are available as hourly data and are described below. The radiosonde stations are part of the World Meteorological Organization (WMO) and daily radiosonde reports can be obtained from National Center for Atmospheric Research (NCAR).

Buoys are frequently used to validate satellite SST measurements even though satellites measure the ocean skin temperature (temperature of the first millimeter for microwaves and the first several microns for the infrared) while buoys measure the ocean bulk temperature. Moored buoys typically measure T_S at a depth of one meter. The buoy data are obtained from the US National Data Buoy Center (NDBC), the NOAA Pacific Marine Environmental Laboratory (PMEL), and the Marine Environmental Data Service (MEDS) - a branch of Canada's Federal Department of Fisheries and Oceans. NDBC and MEDS maintain networks of buoys in coastal regions around the continental United States and Canada, Alaska and Hawaii. Currently, approximately 35 NDBC buoys and 18 MEDS buoys are distanced greater than 30 km from shore and can be used for AMSR validation. (AMSR cannot retrieve ocean parameters too close to shore because of land contamination in the antenna pattern.) PMEL provides data from the 70-buoy Tropical Atmosphere-Ocean (TAO/TRITON) network in the equatorial Pacific and the 12 buoy Pilot Research Moored Array in the Tropical Atlantic (PIRATA). NDBC and MEDS hourly measurements are available by anonymous ftp in near real time whereas the hourly and 10 minute TAO and PIRATA data are only available after

buoy servicing or recovery, a process that occurs approximately once per year for each buoy. Fortunately, daily averages of the hourly TAO and PIRATA data are available in near real time.

Wind observations from these moored buoys will be used to validate the AMSR-E wind speed product. The buoys measure barometric pressure, wind direction, wind speed, wind gust, air and sea temperature, and wave energy spectra (i.e., significant wave height, dominant wave period, and average wave period). NDBC wind speed and direction is measured during an 8-minute period prior to the hour of report. Exactly when the data is collected prior to report and the height of the anemometer depends on the type of payload on the moored buoy. The locations of NBDC moored buoys in service as of June 2002 are mapped in Figure 3.1.1.

Seven MEDS buoys are located along the Canadian coast in the Atlantic and 11 in the Pacific. Surface winds, gusts, barometric pressure, air temperature and SST observations are made each second for a 10 minute period centered on 20 minutes after the hour. Both scalar and vector averages are provided in the hourly buoy data files. Wind observations are either at 5 m or 4 m depending on the type of buoy (nomad or 3m discus). Sea surface temperatures observations are made at a depth of 0.8 m. The locations of the MEDS buoys are shown in Figure 3.1.1.

The TAO array covers the tropical Pacific Ocean at intervals of approximately 10 to 15 degree longitude, and 2° to 3° degree latitude. They measure air temperature, relative humidity, surface winds, SST, and subsurface temperature to 500 meters. Wind measurements are made at a height of 4 m at 2 per second for 2 minutes centered on the hour and every 10 minutes after. The data are vector averaged. The TAO/TRITON buoys measure T_S at 1-meter depth. These T_S samples are taken once every ten minutes. To conserve battery power, hourly data is transmitted only 8 hours each day, 0600 to 1000 and 1200 to 1600 buoy local time. Three to four hours of T_S and wind data are available in near-real time from the GTS. These data are considered preliminary until the buoy is serviced and the stored hourly data is processed. Figure 3.1.1 includes the TAO/TRITON buoy network.

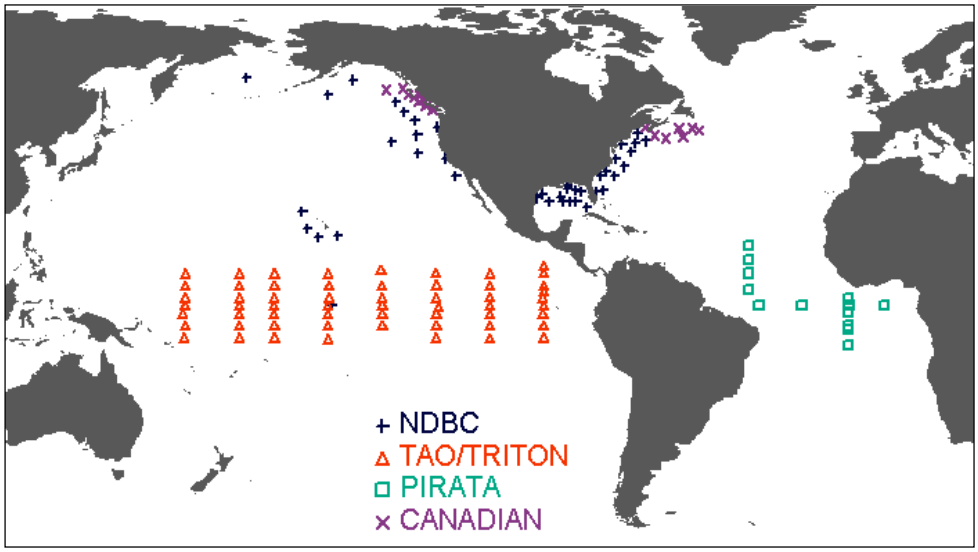

Fig. 3.1.1. Location of open-ocean moored buoys in operation from 2000 to the present that are part of the Remote Sensing Systems quality controlled buoy database used for calibration/validation work.

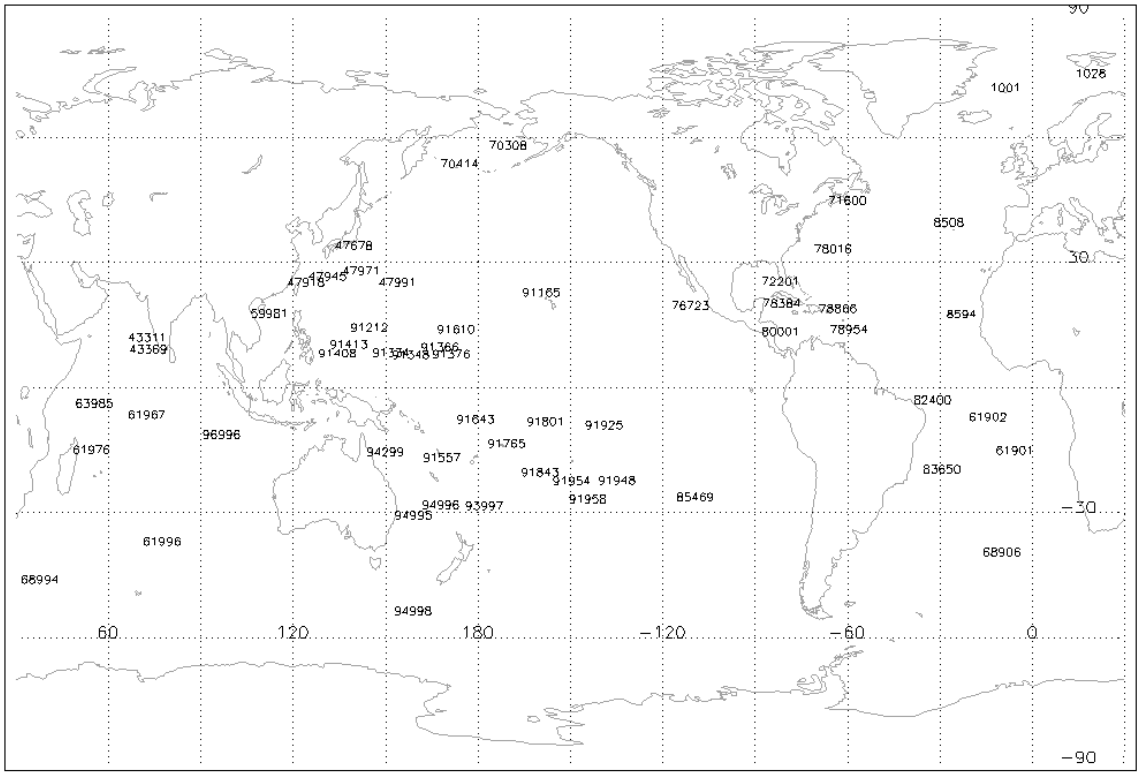

Fig. 3.1.2. Small island radiosonde stations operating as of June 2002

The PIRATA moored buoy array in the Atlantic Ocean operates in a similar manner as the Pacific TAO/TRITON buoy array but is much smaller. Currently 13 buoys are deployed and measure air temperature, relative humidity, surface winds, SST, and subsurface temperature to 500 meters. Measurements are made in the same manner as the TAO/TRITON array. Surface SST measurements are at 1 m. Figure 3.1.1 also includes the PIRATA buoys.

Anemometer height z varies for each buoy or buoy type. The NDBC moored buoys in general have z equaling 5 or 10 m, the MEDS are at 4m or 5m, and the TAO/TRITON and PIRATA anemometers are at 4 m above the sea surface. All buoy winds W_B will be normalized to an equivalent anemometer height of 10 m (1000-cm) assuming a logarithmic wind profile

$$W_{B,10M} = [\ln(1000/h_0)/\ln(h/h_0)]\, W_{B,Z} \quad (1)$$

where h_0 is the surface roughness length, which equals 1.52×10^{-2} cm assuming a drag coefficient of 1.3×10^{-3} [*Peixoto and Oort*, 1992]. Some researchers argue that buoy wind estimates must be transformed to the standard height using a boundary layer model and the auxiliary quantities measured by the buoy to estimate atmospheric stratification. However, recent work by *Mears et al.* [2001] shows that the main difference between using a complete boundary layer model and a simple logarithmic profile is a slightly higher wind speed by the boundary layer model correction. The bias and standard deviation between the two methods (boundary layer versus logarithmic profile) is 0.12 m/s and 0.17 m/s, respectively. Considering how small the difference is and the fact that not all buoys measure the auxiliary meteorological parameters needed for the accurate boundary layer parameterization, we choose to correct all buoy data within our validation data set to a 10-meter height with the simple logarithmic correction above.

The buoy data sets will undergo quality check procedures, including checks for missing data, repeated data, blank fields, and out-of-bounds data. A time interpretive collocation program will calculate the wind speed at the time of the nearest satellite overpass, as is described in *Wentz* [1997] and *Mears et al.* [2001].

Table 3.1.4. Island Radiosonde Locations as of June 2002

WMO No.	Name	Latitude	East Long.	Area (km^2)
1001	Jan Mayen	70.93	351.33	373
1028	Bjornoya	74.52	19.02	179
8508	Lajes / Janta Rita	38.75	332.93	
8594	Sal	16.73	337.05	
43311	Amini	11.12	72.73	
43369	Minicoy	8.30	73.00	
47678	Hachija Jima	33.12	139.78	70
47918	Ishigaki Jima	24.33	124.17	215
47945	Minamidaito Jima	25.83	131.23	47
47971	Chichi Jima	27.08	142.18	25
47991	Marcus Is.	24.30	153.97	3
59981	Xisha Is.	16.83	112.33	
61901	St. Helena	-15.96	354.30	122
61902	Ascension Is.	-7.97	345.96	88
61967	Diego Garcia	-7.35	72.48	152
61976	Serge-Frolow / Tromelin	-15.88	54.52	
61996	I. N. Amsterdam	-37.80	77.53	62
63985	Seychelles Intl	-4.67	55.52	23
68906	Gough Is.	-40.35	350.12	83
68994	Marion Is	-46.88	37.87	388
70308	St. Paul Is.	57.15	189.79	91
70414	Shemya Is.	52.72	174.10	21
71600	Sable Is.	43.93	299.98	8
72201	Key West	24.57	278.32	
76723	Socorro Island	18.72	249.05	
78016	Kindley Field	32.37	295.32	53
78384	Roberts Fld.	19.30	278.63	183
78866	San Maarten	18.05	296.89	85
78954	Barbados	13.07	300.50	431
80001	Isla San Andreas	12.58	278.30	21
82400	Fernando de Noronha	-3.85	327.58	4
83650	Trindade Is.	-20.50	330.68	10
85469	Easter Is.	-27.17	250.57	117
91165	Kauai	21.98	200.65	
91212	Guam	13.48	144.80	
91334	Truk	7.47	151.85	118
91348	Ponape/Caroline Is.	6.96	158.22	68
91366	Kwajalein	8.72	167.73	16
91376	Majuro	7.03	171.38	10
91408	Koror	7.33	134.48	8
91413	Yap	9.48	138.08	54
91557	Efate	-17.70	168.30	
91610	Tarawa	13.05	172.92	23
91643	Funafuti	-8.52	179.22	3
91765	Pago Pago	-14.33	189.29	135
91801	Penrhyn	-9.00	201.95	10
91843	Cook Isles	-21.20	200.19	218
91925	Atuona	-9.82	220.99	200
91948	Rikitea	-23.13	225.04	31
91954	Tubuai Island	-23.35	210.52	36
91958	Austral Is.	-27.61	215.67	47
93997	Kermadec Is	-29.25	182.09	34
94299	Willis Is.	-16.30	149.98	
94996	Norfolk Is.	-29.03	167.93	34
94995	Lord Howe Is.	-31.53	159.07	2
94998	Macquarie Is.	-54.48	158.93	109
96996	Cocos Is.	-12.18	96.82	14

Radiosondes measure temperature, pressure, and humidity as a helium balloon carries them aloft. The international radiosonde network will be the primary data source used to validate the AMSR-E water vapor product, and such data are available from several sources, including NCEP, NCDC, and NCAR. In many locations throughout the world radiosondes are launched twice each day (00Z and 12Z). To compare water vapor over ocean regions, only stations on small islands or ships are used. A preliminary list of 57 radiosonde stations currently operating on small islands is listed in Table 3.1.4 and is displayed in Figure 3.1.2.

Quality control measures will include discarding incomplete or inconsistent soundings, soundings without a surface level report, soundings with fewer than a minimal number of levels, and those with spikes in the temperature or water vapor pressure profiles. These measures will reduce the size of the available data set. In addition, corrections or normalizations among the various types of sensors and sensor configurations will be required since the radiosonde data are from different stations, countries and vendors. A collocation program will be used to find the AMSR-E measurements within a specific space and time of each radiosonde sounding. *Alishouse et al*. [1990] and *Wentz* [1997] give the details of collocating radiosondes with satellite observation and the associated quality control procedures.

3.1.3 Satellite Data

Observations from other satellite sensors play a vital role in our AMSR-E calibration/validation activity. In the pre-launch cal/val phase, the SSM/I and TMI microwave radiometers have been essential to our algorithm development work. And, after the launch of AMSR-E, two major satellite intercomparison projects will be done: 1) intercomparison of microwave and infrared SST retrievals and 2) intercomparison of microwave passive and active wind retrievals. We first discuss how satellite data have been used during the pre-launch phase of our investigation, and then describe the two post-launch satellite intercomparison studies.

Pre-launch algorithm testing and development has been primarily based on SSM/I and TMI observations collocated with existing buoy and radiosonde observations. Figure 3.1.3 shows the four basic steps in developing and testing the AMSR-E ocean algorithm. In the first phase of development, the Pre-Launch Version 0 algorithm was written. This first algorithm was primarily based on the SSM/I observations and radiative transfer theory. One shortcoming of the Version 0 algorithm was that there was some uncertainty about the wind component of the radiative transfer model (RTM) at 6.9 and 10.7 GHz. At these frequencies, we used SeaSat SMMR T_B's collocated with SeaSat scatterometer winds to specify the wind component of the RTM [*Wentz et al.*, 1986]. The SeaSat SMMR suffered from calibration problems, and we were concerned about the accuracy of the surface component of the RTM at 6.9 and 10.7 GHz.

More recently, using observations from TMI, we completed the next phase of algorithm development. TMI is providing well-calibrated 10.7 GHz ocean observations. We collocated these observations with wind vector measurements from ocean buoys and NCEP's global circulation model and with AVHRR SST retrievals. The combined T_B, wind, SST data set provided the means to update the sea-surface emissivity model at 10.7 GHz. The updated algorithm, called Pre-launch Version 1, has been delivered to the AMSR-E Science Computing Facility.

The Version 1 algorithm has been tested using the TMI observations as input. The primary focus of these tests was the SST retrieval. In spite of the impressive TMI SST results illustrated by Figure 3.1.4 [*Wentz et al.,* 2000], there is still room for improvement. The TMI analysis shows that the largest error in the SST retrieval is due to wind direction (not withstanding sensor calibration problems). At higher wind speeds, T_B can vary by several degrees with changing wind direction [Wentz, 1992]. Figure 3.1.5 shows the effect of wind direction on the SST retrieval. If not accounted for, wind direction variations can produce significant errors in the SST retrieval. For TMI, we use NCEP wind directions in an attempt to remove this error, but this approach is certainly less than desirable. (Figure 3.1.4 utilizes the NCEP wind direction correction.) It should be noted that the addition of the 6.9 GHz channels for AMSR-E (TMI does not have these channels) reduces the wind direction error relative to that shown in Figure 3.1.5. However, the SST error due to wind direction is still a problem and will be a primary concern during the post-launch calibration/validation for AMSR-E.

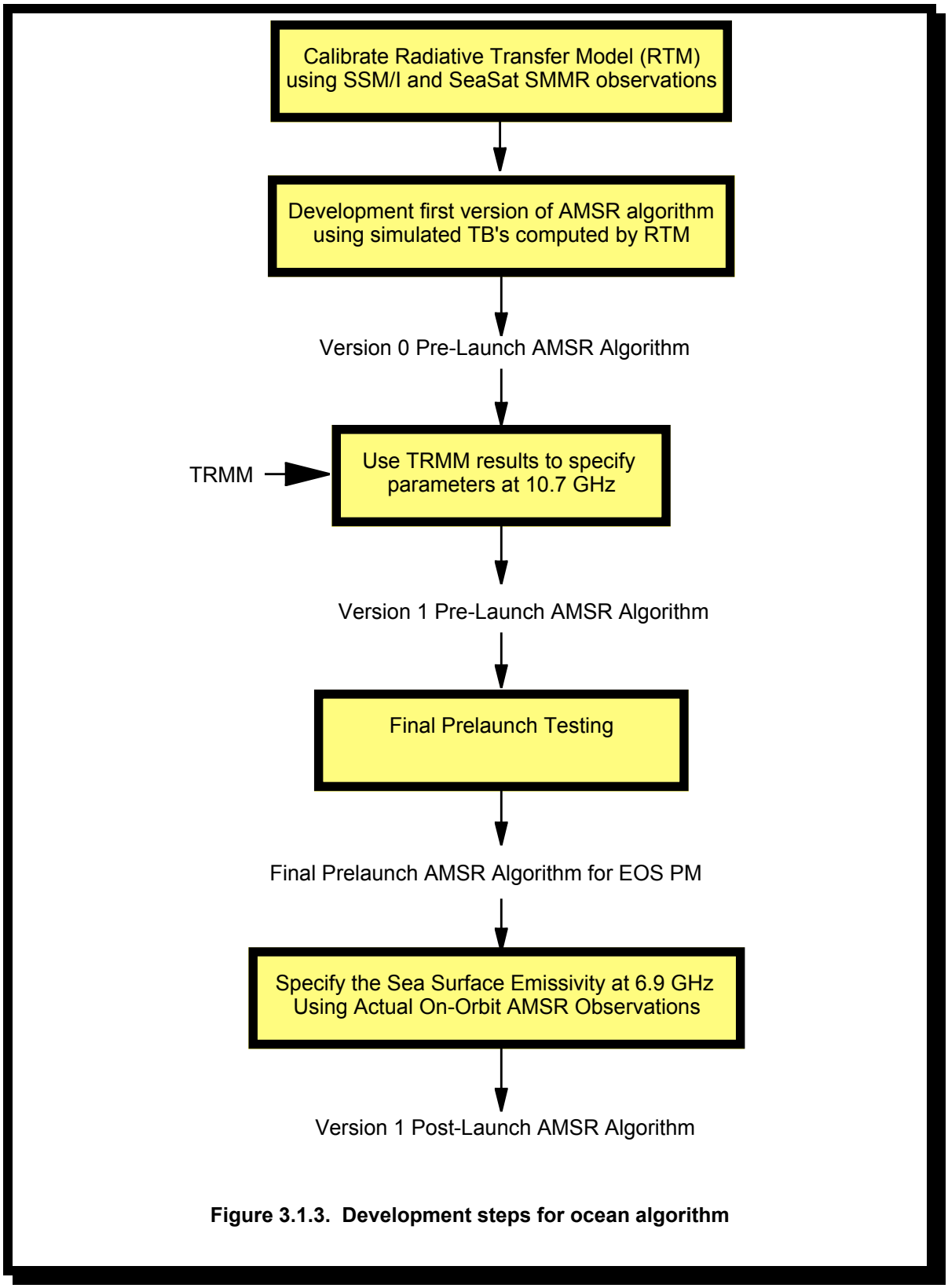

Figure 3.1.3. Development steps for ocean algorithm

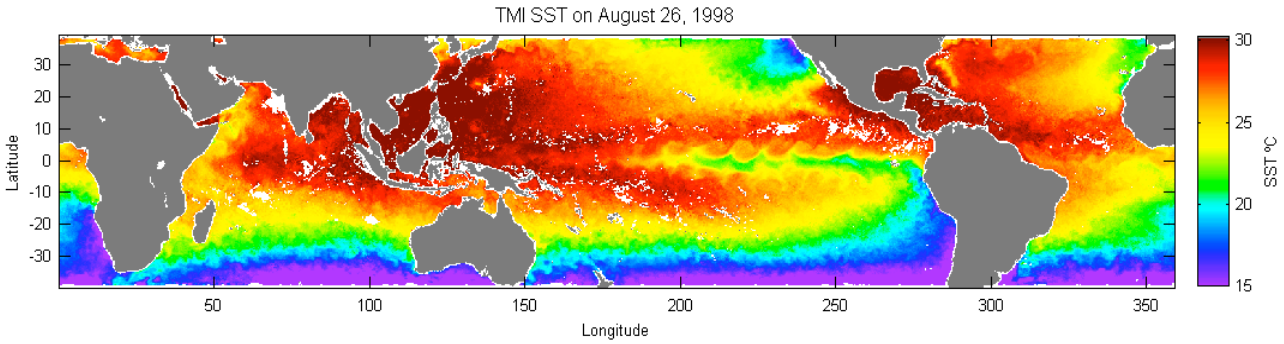

Fig. 3.1.4 TMI through-clouds microwave SST retrievals for August 25-27, 1998. Cool water directly East of Florida is cold upwelling due to the passage of Hurricane Bonnie. Tropical instability waves are propagating along both north and south of the Equator in the Pacific Ocean.

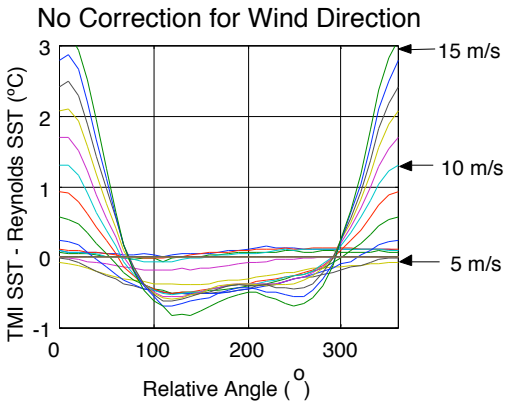

Fig. 3.1.5 The effect of wind direction on SST retrievals. Reynolds SST, which should have no wind direction dependence, is subtracted from TMI SST. No correction for wind direction has been applied to the TMI SST. This difference is binned according to wind speed and is plotted versus the relative wind direction, which is the satellite's azimuthal viewing angle minus wind direction (from NCEP). The colored curves show the results for each wind speed bin from 0 to 15 m/s, in 1 m/s steps. At low wind speeds (< 5m/s) there is no appreciable error. Above 5 m/s the peak-to-peak amplitude of the error increases to a maximum of 4ºC when winds are 15 m/s.

After AMSR-E is launched, we will begin the two satellite intercomparison studies. The first study involves comparing the microwave SST retrieval with infrared SST retrievals from a number of satellite sensors. The Advanced Very High Resolution Radiometers (AVHRR) have a two-decade heritage of retrieving T_S. They have a proven capability of measuring T_S in the absence of clouds. We will use these T_S retrievals in cloud-free areas to calibrate the AMSR-E T_S retrievals. Once calibrated in the cloud-free areas, the AMSR-E T_S retrievals should also be valid in cloudy areas because non-raining clouds are nearly transparent at 6.9 GHz. In addition to AVHRR, we will collaborate with the Aqua AIRS and MODIS Teams to do further SST intercomparison studies. The final component of the satellite SST study involves the European Along Track Scanning Radiometer (ATSR). According to some, ATSR's multiple look design currently provides the most accurate infrared SST retrievals. We are having discussions with the ATSR Team about collaborating on an AMSR-ATSR SST intercomparison.

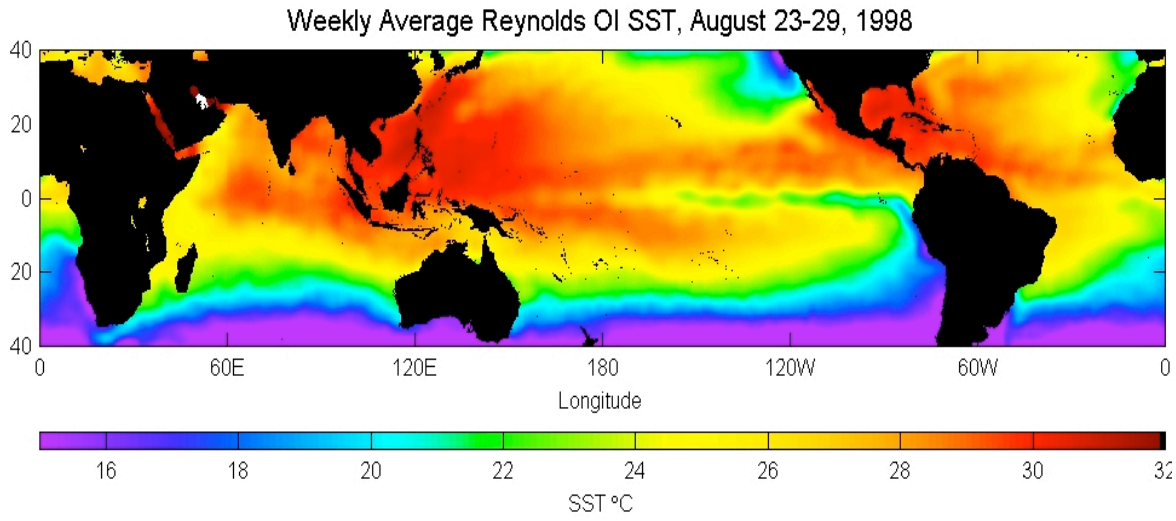

Fig. 3.1.6. An example of the Reynolds OI SST product that will be used for SST validation.

Our baseline SST for these intercomparisons will be the blended AVHRR-buoy SST data set produced by R. Reynolds using optimum interpolation (OI). This product is routinely generated on a weekly, one-degree grid, as is shown in Figure 3.1.6. The advantage of this product is that it is routinely available and has global uninterrupted coverage. This makes intercomparison with the AMSR-E observations a relatively simple task. Furthermore, a very large database of intercomparison statistics can be generated in a short time, which is ideal for a quick validation study shortly after launch. The disadvantage of the data set is its low spatial and temporal resolution and questionable accuracy in some parts of the ocean. To address these concerns, we will be doing more detailed intercomparisons with the AVHRR Pathfinder SST produced by the JPL PO-DAAC and with the AIRS, MODIS, and possibly ATSR high-resolution infrared SST products.

The second satellite intercomparison study is the AMSR-SeaWinds project, as illustrated in Figure 3.1.7. The ADEOS-II platform flies both the microwave radiometer AMSR and the microwave scatterometer SeaWinds. With this combined active/passive sensor package, we expect that the SST error due to wind direction can be virtually eliminated. Simulations show that by combining AMSR and SeaWinds the SST rms accuracy for a 3-day, 60-km product will be 0.2°C. Given this accuracy, investigators will be able to study the interaction between wind and SST in greater detail and with more confidence than ever before. The early TMI results are rich with examples of wind-SST interactions: upwellings off of the continents, cold water wakes from storms and hurricanes, and remarkably tight correlations between the tropical instability waves and the surface wind (see Figure 3.1.4). A highly accurate, combined vector wind - SST data set (through clouds) will be of enormous value to oceanography and climate research.

In addition to improving the SST accuracy, the scatterometer data will contribute greatly to our wind validation study. The microwave scatterometer provides highly accurate wind vector retrievals at a spatial resolution of 25 km. The QuikScat scatterometer (SeaWinds' precursor) is now in operation and should still be functioning when AMSR-E is launched. SeaWinds will then be launched in 2001 on ADEOS-II, and it is most probable that two scatterometers will be in operation during the AMSR-E and ADEOS-II AMSR time frame.

Inter-comparisons of the AMSR-E and scatterometer wind speed will be done on a global basis and any systematic differences will be identified. Early studies comparing SSM/I wind retrievals with scatterometer retrievals did reveal curious systematic differences in areas of upwelling. Further investigation showed an inadequate modeling of the sea surface emissivity contributed to the problem. The emissivity models were updated and all radiometer data reprocessed in 2002. The resulting SSM/I minus QuikScat wind speed difference map shown in

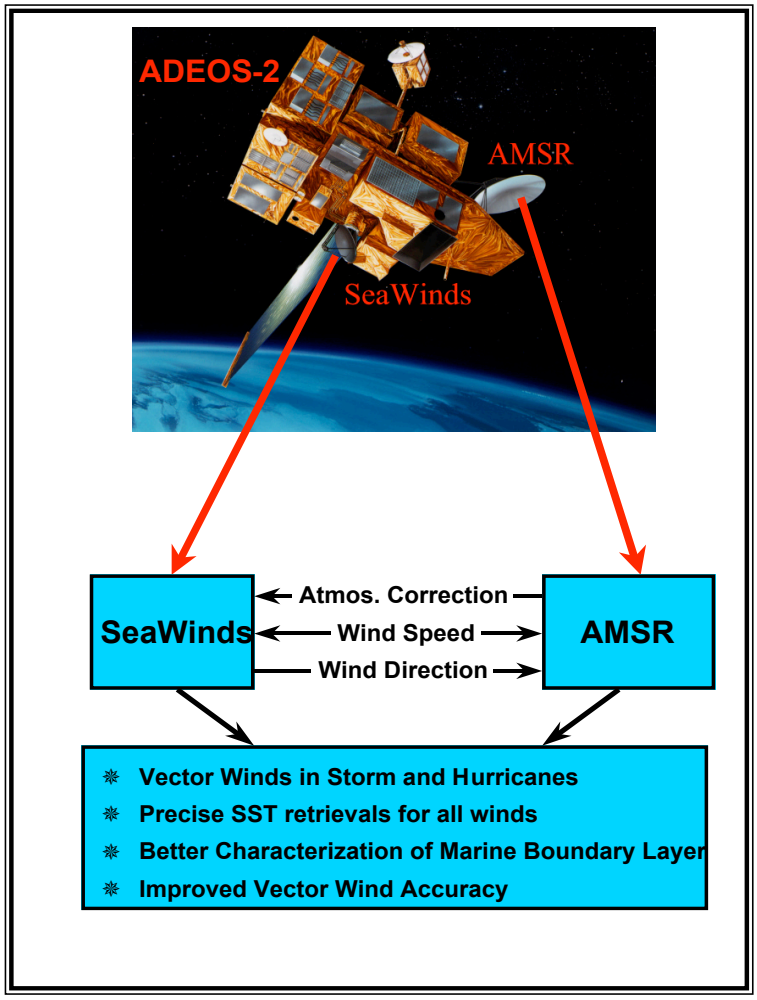

Fig. 3.1.7. Benefits derived from combining SeaWinds and AMSR

Figure 3.1.8 shows differences of less than +/- 0.5 m/s for most ocean regions. Now only a few locations, primarily in eastern boundary current regions and along ice edges, show differences greater than 0.5 m/s.

Collocated microwave T_B's and scatterometer wind vectors provide one of the best means to study wind direction effects on the T_B's and ocean products. For example, the difference between the AMSR-E and scatterometer wind speed will be plotted versus wind direction to determine if the AMSR-E wind speeds contain any systematic error related to wind direction. Likewise, the effect of wind direction on SST retrievals can be studied, as discussed above.

Finally, we point out that the QuikScat/SeaWinds Science Team will be conducting its own wind validation activity. We plan to incorporate the validation data sets and field experiments coming from the scatterometer team into our AMSR-E wind validation activity.

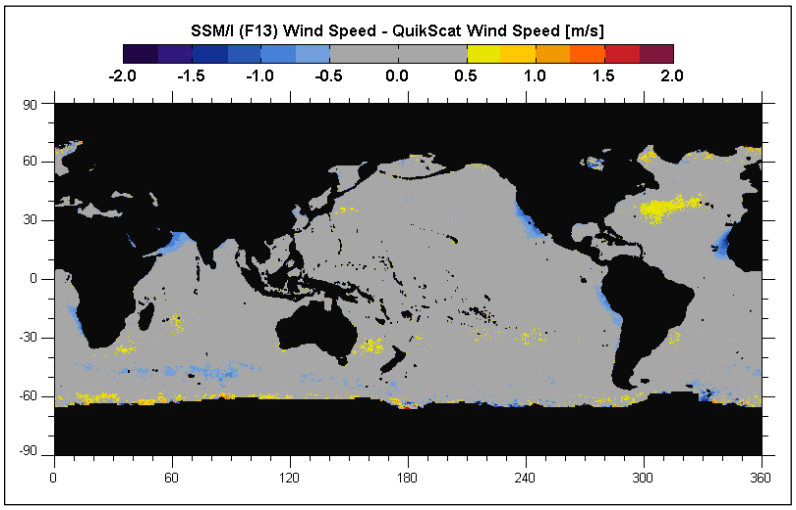

Figure 3.1.8 The difference of the version-5 F13 SSM/I wind speed minus the QuikScat Ku-2001 wind speed averaged over the year 2000. In most regions, the data agree to within +/- 0.5 m/s. Small regions with slightly larger differences are located in eastern boundary current locations (-) and along ice edges and in the Mid-Atlantic (+).

3.1.4 Validation of Wind Speed using GCM

In addition to the buoy and scatterometer intercomparisons, we will also compare the AMSR-E winds to those coming from global circulation models (GCM). Two GCM will be used: NCEP and ECMWF (if ECMEF is made available to us). The GCM comparisons have the advantage of providing global winds for every AMSR-E cell. Thus a very large database of intercomparison statistics can be quickly accumulated. The disadvantage is that the GCM winds are an analysis product rather than a direct measurement of the ocean wind field. Our approach will be to use the GCM for the initial validation period, and then as the AMSR-buoy and AMSR-scatterometer database grows with time, more emphasis will be placed on the buoy and scatterometer observations as the eventual calibration reference.

3.1.5 Histogram Validation of Cloud Water Product

Microwave radiometry is probably the most accurate technology for measuring the vertically integrated cloud liquid water L. In the 18 to 37 GHz band, clouds are semi-transparent and the absorption by the entire column of liquid water can be measured. Apart from using upward-looking radiometers to calibrate downward-looking radiometers (or vise versa), there are no other calibration sources for L. Several nations (e.g., The Netherlands) maintain upward looking radiometers or routinely make aircraft flights (e.g., Australia) to measure L in support of their meteorological operations. These data sets are increasingly made available to the scientific community over the Internet. However, comparison of the L inferred from upward looking radiometers with that inferred from downward looking satellite radiometers has limited utility. The great spatial and temporal variability of clouds makes such comparisons difficult. Also, the major problem in calibrating L is in obtaining accurate retrievals over the full range of global conditions. There are not enough upward looking radiometers to do this. Finally, when differences arise, it will be difficult to determine which radiometer system is at fault.

We prefer to use the statistical histogram method described by *Wentz* [1997]. This technique is illustrated in Figure 3.1.9. We assume the probability density function (pdf) for the true cloud water observed by AMSR-E has a maximum at L = 0 and rapidly decays similar to an exponential pdf as L increases. The pdf for the retrieved L will look similar, but retrieval error will tend to smear out the sharp peak at L = 0. Simulations in which Gaussian noise is added to a random deviate having an exponential pdf show that the left-side, half-power point of the pdf for

the noise-add L is located at L = 0. Thus we require that histograms of the L retrievals are aligned such that the half-power point of the left-side is at L = 0. Furthermore, we require this condition be met for all T_S, W, and V.

For example, the top plot in Figure 3.1.9 shows 6 histograms of L retrieved from SSM/I. The 6 histograms correspond to 6 different ranges of T_S (i.e., 0-5 C, 5-10 C, ..., 25-30 C). The middle and bottom plots show analogous results for wind and water vapor groupings. The peak of the pdf's is near L = 0.025 mm. At L = 0, all histograms are about half the peak value. The misalignment among the 6 histograms is about ±0.005 mm. We use the width of this half power point (i.e., 0.025 mm) as an indicator of the rms error in L.

This procedure effectively eliminates the bias and crosstalk error in the L retrieval, and we consider it the best available way to validate the cloud water retrievals.

3.1.6 Field Experiments

No field experiments are specifically planned for validation of the AMSR-E ocean algorithms. However, we do plan to make use of field experiments scheduled for the AIRS and MODIS SST validation and the QuikScat/SeaWinds wind validation. These field experiments will provide useful data for the AMSR-E validation that will supplement the *in situ* and satellite observations discussed above.

3.1.7 Calibration and Validation Time Line

The AMSR-E calibration and validation plan is shown above in Figure 3.1.3. We have completed the calibration and validation of the 10.7-GHz components of the model and retrieval algorithm using the TRMM TMI observations. This was the last step of the pre-launch calibration and validation phase. This pre-launch ocean algorithm for AMSR-E has benefited from two separate calibration and validation activities: SSM/I and TMI.

We originally planed to use the AMSR aboard the ADEOS-II spacecraft to further develop and test the AMSR-E ocean algorithm. Now that the ADEOS-II launch date has slipped to late 2002, this is no longer possible. Therefore, the final specification of the 6.9-GHz emissivity will need to be done after the AMSR-E launch using actual on-orbit AMSR-E observations. Given the AMSR-E 6.9-GHz observations, the dependence of the sea-surface emissivity on temperature, wind speed, and wind direction can be precisely determined. Calibration data for the SST will be obtained from buoys and cloud-free IR temperature retrievals. Buoy and scatterometer winds will be used to calibrate the wind component of the RTM at 6.9 GHz. We expect that the 6.9-GHz emissivity can be adequately specified 3 to 6 month after we begin receiving the AMSR observations.

Another post-launch activity that needs to be done as soon as possible after launch is the determination of absolute biases for each of the AMSR channels. With current technology, it is not possible to absolutely calibrate satellite microwave radiometers to better than 1 to 2 K. Also the RTM probably has an absolute bias due to uncertainty in specifying the dielectric constant of sea water and the oxygen/vapor absorption. Thus we expect that there will probably be a relative bias of 1 to 2 K between the AMSR-E observations and the RTM. Such offsets occurred for both SSM/I and TMI. These T_B offsets need to be derived after launch. This activity will run in parallel with the determination of the 6.9-GHz emissivity and will be complete 3 to 6 month after we begin receiving the AMSR observations.

We will also be looking for possible Level-1 problems during this initial cal/val period, including possible geolocation errors and sensor calibration problems. In addition, we anticipate that some unexpected problems will occur (they always do). Given the very demanding workload during this initial period coupled with the fact that this will be the first AMSR to fly, it will probably take the full 6 months to complete the initial cal/val. Once the initial cal/val is completed, the first release of AMSR-E ocean products (Version 1) will be provided to the user community.

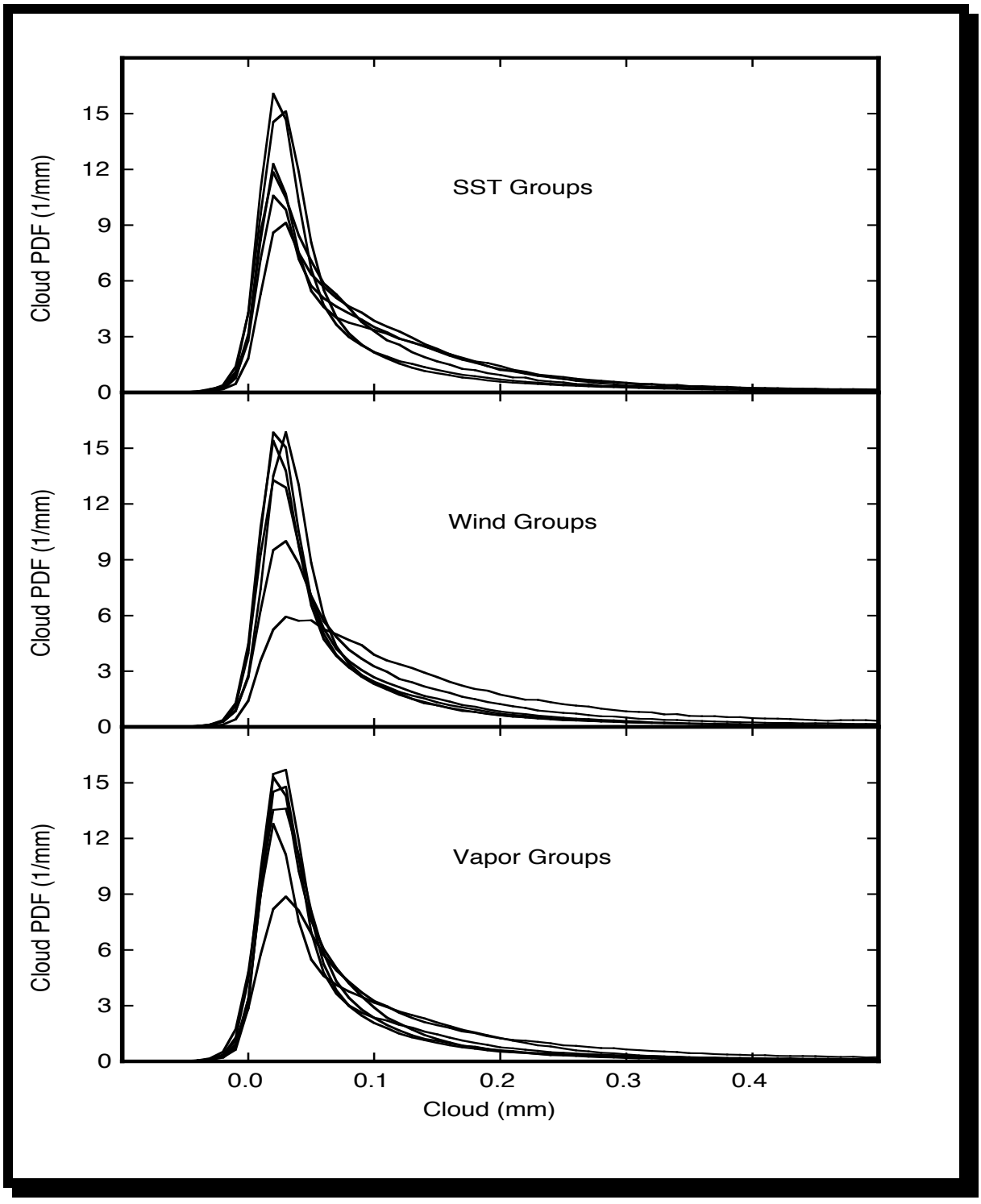

Figure 3.1.9. Probability density functions (pdf) for liquid cloud water. The cloud pdf's are stratified according to sea-surface temperature, wind speed, and water vapor. Each curve shows the pdf for a particular stratification.

The second phase of the AMSR-E validation will then begin. This will be a more thorough 1-year investigation in which a comprehensive set of *in situ* and satellite observations are used to calibrate and validate the AMSR ocean products. A precise T_B calibration will be done, and the retrieval algorithm and associated RTM will be fine-tuned. The updated algorithm coming from this activity will represent the Version 2 post-launch AMSR-E algorithm and we anticipate that it will be used to process data for several years. Once the Version-2 software is implemented, we will begin several research activities aimed towards extracting the maximum information content from the AMSR observations. Our AMSR-E investigation will conclude with an optimal algorithm for retrospective processing of the AMSR-E data.

3.2 Rainfall (submitted by C. Kummerow, T. Wilheit and R. Ferraro)

3.2.1 Approach Philosophy

There are two paradigms for validation. In the conventional paradigm, some "truth data", are collected and compared with the product to be validated. We will refer to this paradigm as ground truth (GT). The key to GT is some truth data in which you have more confidence than you have in the product being validated. In the early stages of validating a product, such as rainfall in the late 1980s and early 1990s, these techniques were useful in that they could differentiate between products that often differed by more than a factor of 2. This early success has continued to pervade the thinking of the community. Advances in space-borne technology and algorithms, however, require a shift in paradigms, at least for oceanic measurements. The TRMM radar and radiometer products now differ by less than 10% for zonal mean average rainfall, while ground-based radar data can often have uncertainties significantly larger than 10%. Validating these products calls for a better design of validation data as well as a need to begin the process of validating the assumptions that go into the algorithm and how these assumptions might hold up in areas where no conventional observations are available. We refer to this as the physical validation paradigm (PV).

A coherent validation strategy for precipitation requires that we (1) use a set of observations (possibly greater than those from the space-borne sensor itself) to define similar climate regimes (regions and time periods for which rainfall physics appear to be homogeneous), (2) determine the confidence with which we can measure area-averaged rainfall on the ground, and (3) establish that the space-borne algorithm produces similar biases/agreements in regimes defined as similar to within the uncertainty determined from the ground-based measurements. Over land, it is then possible to select regions that are representative of the different rainfall regimes and properly validate rainfall statistics that can then be merged into a global map of uncertainty. Over oceans, it is not likely that enough ground-based measurements can be made to ever produce a quantifiable uncertainty estimate and the PV approach must be used.

In the case of rainfall, there is in addition to GT and PV, the opportunity to compare results to concurrent sensors such as TRMM (in the tropics) and SSM/Is, which have been flying continuously since 1987. While these comparisons do not represent ‘truth’, these datasets have been studied extensively. In the case of TRMM, there is also a large validation effort underway. Large discrepancies with these existing datasets could therefore point at software errors and provide a straightforward opportunity to check the overall performance of the algorithm immediately following launch. These comparisons, with existing satellite products as well as existing gauge networks, constitute the basic validation of the AMSR data that will be used to release data to the public. This implementation plan deals with the more difficult task of quantifying uncertainties in the global rainfall products as well as improving the overall product quality. Before proceeding, however, it should be noted that the AMSR-E rainfall team is fully cognizant (through membership in the steering committees of both TRMM as well as GPM) of activities in those areas. The approach detailed in the next section takes both these programs into consideration.

3.2.2 Validation Approach

Over land, the high and variable emissivity of the land surface at microwave frequencies masks any useful signal from the liquid hydrometeors. One is therefore reduced to using the scattering from the ice phase to estimate the rainfall intensity. Unfortunately, the ice phase is not uniquely connected to the rain rate. A further complication related to the land algorithm is the potential for a false signal connected to cold and snow covered surfaces, which have Tb depressions that can easily be mistaken for rain signals.

There is a great deal of reasonably good rainfall data from the U.S. WSR-88 network and the Japanese AMeDAS network. These data can be used to validate the rain discrimination portion of the algorithm without too much difficulty. The operational radar networks, however, are

less reliable when it comes to generating climate quality rainfall maps. The TRMM validation effort has addressed this shortcoming by adding a layer of quality control and radar/rain gauge comparisons to the operational processing. The process is labor intensive but climate-quality radar-rainfall products can be produced. The AMSR-E team will take advantage of this framework. The WSR-88 radar at Eureka, CA, was selected by the AMSR-E team as a key validation site. The selection of Eureka was based on a number of factors: there is anecdotal evidence that microwave retrieval algorithms have had problems on the West Coast of the United States; Eureka has a relatively small beam blockage problem related to the local topography when compared to the other western United States sites; Eureka has good coverage over the oceans as well as land; and the staff at the Eureka office have been very supportive and willing to cooperate with the team for improving the local infrastructure. The infrastructure consists of additional triple-gauge clusters (needed to have complete confidence in the gauge rainfall) and disdrometers. While the AMSR-E team can supply this equipment, the team must rely on the local support for continuous maintenance. While more radar locations are certainly desirable, the AMSR-E team felt that it should concentrate its resources on a single site and insure that useful products could be derived from it.

Despite careful efforts to provide climate quality validation data, ground-based measurements have limitations. The greatest shortcoming is in the treatment of uncertainties, particularly when applied to relatively few satellite overpasses containing rainfall in any given month. The use of operational rain gauge networks is fraught with difficulties. If only the area over the gauges is considered, the TRMM team estimated that 2-3 years of data would be required in even the rainiest locations before random errors reduce to less than 10%. In the extra-tropics, seasonal variations in rainfall character would imply even longer time periods. To alleviate this problem, satellite estimates are usually made over larger domains (typically 100-500 km) surrounding the rain gauge. This, however, introduces questions about the representativeness of the gauge(s) with respect to the area-average rainfall. Even subtle topography or urban influences, for instance, can cause systematic differences in excess of 20%, which are not adequately captured by the gauge(s).

Because of the above problems, radars have been the preferred tool to validate satellite rainfall estimates. Radar, unfortunately, requires a relationship to convert the radar reflectivity to a rainfall rate (the Z-R relation). Because these relationships can be quite variable, changing from storm to storm and even within a storm, the TRMM program uses coincident rain gauge data to adjust the monthly radar accumulations. If sufficient gauges of high quality are available, this technique produces bias-free data that can be used for climate analyses. Differences between results from such analyses and the satellite products must then be ascribed to either random errors introduced by the poor temporal sampling of the satellite, or bias errors. For instantaneous rainfall estimates, the bias errors are of primary concern since random errors vanish quickly as pixels are averaged. Here, unfortunately, difficulties arise once again. The difficulties are related to the method by which biases are removed from the radar estimates (namely monthly calibrations), while the comparisons with satellite data are made on a small number of raining events. Questions about biases in the radar data for the short time period when the satellite is overhead cannot be accounted for by monthly calibration coefficients.

In contrast to the land situation, the ocean background is ideal for the passive measurement of rainfall. We are able to infer the rain rate from the emission by the hydrometeors in the centimeter wavelength range. Ocean backgrounds, however, have virtually no ground-based radar or rain gauges available. We expect that monthly rain totals over 5 degree squares will have accuracies of the order of 20% for the rainiest parts of the globe. This is a very challenging level of accuracy to validate given the poor ground-based observations. Experience with six major intercomparison projects has convinced us that the GT approach will be inadequate by itself. A combination of GT and PV methods will therefore be used over oceans.

If one considers climatological products (rainfall totals over a space-time volume) then sampling is a major source of error. AMSR-E observations are limited to two observations per day at best. We simply do not see all the rain and must infer the occurrence of rainfall between the observations. In practice, this will always be the dominant source of error. If additional observation capability is added the users will immediately demand finer space-time resolution, so that the sampling error remains at the maximum tolerable level. While the uncertainty cannot be reduced, it can be quantified.

Quantitatively, the sampling error can be thought of as the root-mean-square (rms.) difference between the actual monthly satellite estimate of rain in an area from the intermittent, near-instantaneous and sometimes partial observations and what the satellite would have measured if it could observe the entire area continuously during the month. Although this quantity cannot be directly evaluated from the satellite data, there are several ways of estimating it, each with its own advantages and limitations. One possible approach is to subsample the data taken for the GT approach to coincide with the satellite observations of the radar field of view. The rainfall totals derived from this subset will be compared with the totals from the complete dataset. Adjustments will have to be made for the areal coverage, but these are straightforward. The ground radar observations will provide sufficient information about the rain statistics in the area to allow the necessary extrapolations. The sampling error can be estimated by using resampling techniques (e.g., McConnell and North 1987, Seed and Austin 1990). As was pointed out in Bell and Kundu (2000), one needs many months of data for this method to yield useful results. This first approach estimates sampling errors that do not include random retrieval errors from the satellite system.

A second approach, that can be applied globally, is to make two separate satellite-derived estimates based on alternate days, e.g. odd and even days of the year (Chang et al., 1993). If the area covered by each estimate is doubled, the sampling will remain constant. This approach will estimate all random sources of error rather than just the sampling error. The impact of the other random sources of error can be estimated by comparing with the sampling error estimates derived from the radar data.

A third approach to the estimation of the AMSR-E sampling error is based on a method developed from studies of error estimates for TRMM and SSM/I rainfall data (Bell et al., 2001). Results obtained from radar and satellite data and models of rainfall statistics indicate that the rms. sampling error $\Box_E$ is essentially determined by the variance $\Box_A^2$ of the area-averaged rain rate in the grid box, the effective number of monthly full area visits S (i.e., the total fractional area of the box sampled by the satellite in the course of the month) and a numerical factor $\Box$ of the order unity, whose precise value depends weakly on the time correlation present in the data. Reasonable but preliminary estimates for AMSR-E can be obtained with the choice $\Box$ = 0.7, a value consistent with both radar and SSM/I data. Unfortunately, verifying the correlation time for the AMSR-E data from those data alone will prove difficult, since visits to a grid box average only once a day. However, if data from other satellites, such as, TRMM and SSM/I can be used to fill in the gaps in the AMSR-E observations, direct estimates of the correlation time needed for estimation of $\Box$ will be possible. The GT data can also yield an independent estimate of the time correlation and thus an independent estimate of $\Box$. Since, like the SSM/I, the swath of the AMSR-E instrument is wide enough to cover a grid box completely during most visits, the variance $\Box_A^2$ can be directly obtained from the full area visits. Just as in the SSM/I case, comparison between the results of this approach and the one based on differencing the data from odd and even days can provide a powerful cross-check of the validity of the error estimates. The third method has the advantage that it conveniently handles merging the AMSR-E data with data from other concurrently running satellite missions, such as, SSM/I. TRMM and perhaps others.

In addition to sampling errors, there are three major sources of uncertainty in rainfall retrievals over water. In order of importance, these are:

1. Beam-filling error (subpixel inhomogeneity in the rainfall field)
2. Uncertainty in the vertical distribution of hydrometeors
3. Errors in the freezing level retrieval

The beam-filling correction requires statistics that can be obtained either from radars or simulation and is incorporated into the Brightness Temperature—Rain Rate (TR) relationships directly (in the Level 2 algorithm) or as a multiplicative factor (in the Level 3 algorithm). To date this work has been based on limited datasets from ground- and airborne radar or hydrodynamic Cloud Resolving Models (henceforth CRMs) of which Tao's model is a well-known example [Tao and Simpson, 1999]. The relative advantages and disadvantages of each approach are fairly obvious. It is not practical to get enough airborne radar data to cover the range of possibilities adequately. Ground-based radars overcome the data volume issue, but are limited to coastal regions at best. The CRM could be run for as many situations as we choose, but we have less

confidence that the length scales are really correct. In no case do we have a sufficiently wide range of conditions to be comfortable with the corrections or even estimates of the uncertainty of the corrections. What is needed is to get reliable statistics derived from radar data for a few dozen locations in the tropics and extratropics in various seasons. TRMM is actively seeking these statistics in the tropics. A concerted effort to sample a number of different locations in the extratropics is therefore a key priority. We plan to use the Eureka, BALTEX, and aircraft data from Wakasa Bay to estimate the rainfall inhomogeneity parameters.

The vertical distribution of hydrometeors is a particularly difficult parameter to observe. CRMs are a good source of information but they still give widely disparate pictures of the liquid content in the mixed phase region just above the freezing level. This, in turn, gives widely varying effects of scattering in this region. The bright band region is of special interest. In the bright band region, the region just below the freezing level where the snow melts to form raindrops, the radiometer and radar communities model the attenuation differently. The radiometer community, on the basis of limited evidence, treats the attenuation as being the same as in the rain area below, whereas the radar community treats the bright band as having twice the attenuation of the rain below. Aircraft penetrations with simultaneous radar and radiometer observations are the best way to settle the questions. Limited observations currently in hand contain cases consistent with both the radar and radiometer communities' assumptions. The effect of the bright band is variable and we will need to quantify this variability and include it in our error models. It is important to get some airborne observations with upward-looking radiometers and a two-frequency radar (as planned in the Wakasa Bay experiment) to verify that the differential attenuation and the radiometric determinations of this excess attenuation are consistent.

If the Aqua satellite had a radar, it would be straightforward to validate the freezing level retrieval, and by implication, the thermodynamic and spectroscopic assumptions of the radiative transfer models. With TRMM data, the retrieved freezing levels are being compared with freezing levels inferred from the bright band in the radar data. This will nearly suffice for the AMSR-E freezing levels in the tropics. It will be important to extend this validation to higher latitudes (lower freezing levels). The ground-based radar at Eureka and the planned field experiments at Wakasa Bay, when scanned appropriately for this purpose, can achieve this goal by making careful measurements of the bright band height. Validating the freezing level retrieval, tests a combination of the spectroscopic and thermodynamic assumptions of the model.

3.2.3 Comparison with ground-based observations

3.2.3.1 Status of Eureka Validation Activities

The establishment of the Eureka, CA, validation site will help us learn more about the 3-D structure of stratiform, primarily winter season rainfall, that traverses over long stretches of ocean before reaching land. This type of rainfall is typical along the U.S. and Canada west coast and Western Europe and can be quite prolonged at times, resulting in monthly rainfall in excess of 200 mm in many locations. As shown in Figure 3.2.1, the Eureka site offers the best compromise of rain frequency, offshore coverage, and beam blockage due to high terrain. Rain is more frequent to the north, but those sites are located further inland and have severe beam blockages to the east and west. Sites to the south have ample offshore coverage, but it rains less frequently there. It should be noted that Eureka does suffer from beam blockages to the NE through SE quadrants of its scan.

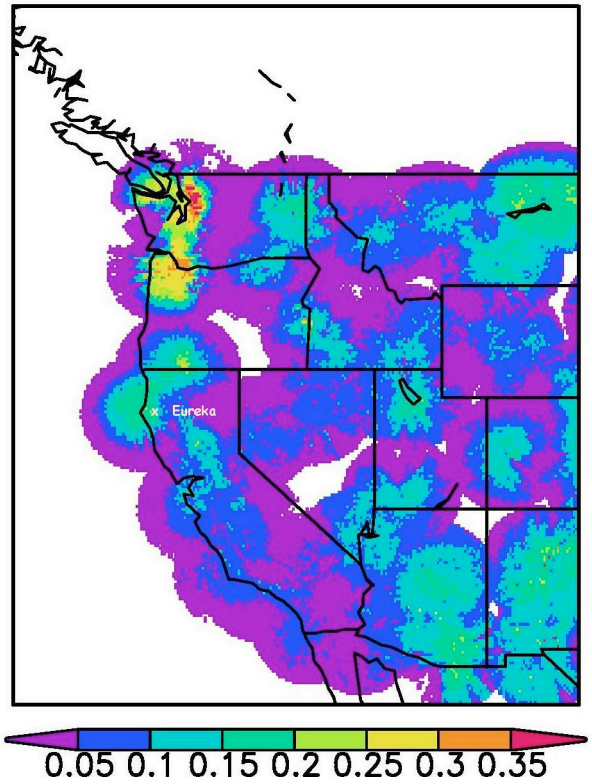

Figure 3.2.1. Annual mean rain frequency of western United States WSR-88D.

Since 2000, we have been working closely with the National Weather Service (NWS) forecast office in Eureka, CA, (Mel Nordquist, Science and Operations Officer) and the TRMM Ground Validation Team at GSFC (led by Dave Wolff) to establish a high-quality site similar to those at Houston, TX, and Melbourne, FL. At present, two three-gauge clusters with dual-data loggers have been installed within the Eureka WSR-88D range (Figure 3.2.2). One is sited at the NWS forecast office and the other is situated at Legget, which is about 50 miles to the SSE of Eureka. Preliminary results indicate that the gauge clusters are reliable and are in rather good agreement (Figure 3.2.3). NWS staff routinely downloads the data and provide the necessary maintenance to insure excellent data quality.

Finally, hardware and software to routinely acquire and transfer the WSR-88D reflectivity scans from the radar site, to the forecast office, and then directly to the TRMM GV team in Greenbelt, MD, has been installed and is undergoing final testing. Standard TRMM GV products will be generated for Eureka, as well as new ones, including freezing level height. Preliminary results and information can be found at http://trmm-fc.gsfc.nasa.gov/Eureka/index.html

Figure 3.2.2. Installation of a three tipping bucket rain gauge cluster, with dual data loggers, at Legget, CA.

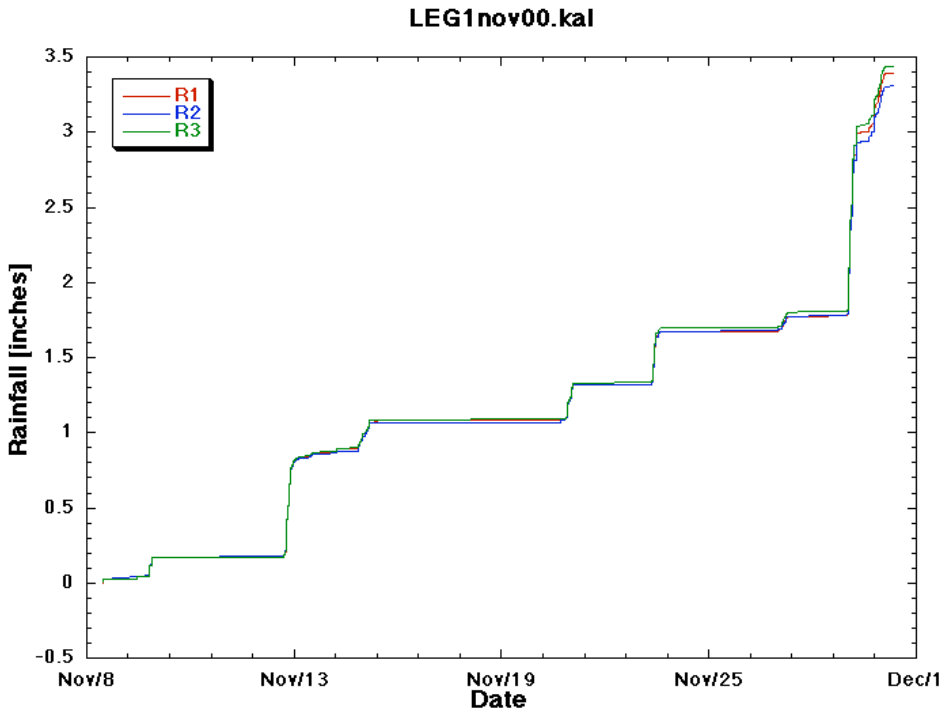

Figure 3.2.3. Rain gauge cluster data from Legget, CA, (data logger 1) for November 2000. The three colored curves represent the cumulative rainfall from the three gauges. Results from the second data logger (not shown) were essentially identical.

3.2.3.2 Further Plans at Eureka 2002-2005

Anticipating a March 2002 Aqua launch, the Eureka site will be utilized for at least three years during the AMSR mission. Summarized below are the main milestones for the next three years.

Fiscal Year 2002

The first major milestone that will be completed by December 31, 2001, will be to have all the necessary software in place and fully tested to allow the NWS forecast office to automatically download WSR-88D reflectivity scans from their radar site (about 30 miles from the office) to computers previously installed at Eureka by the TRMM GV team. This effort has been hindered somewhat during the past year due to complications arising from computer security and hardware/software compatibility.

Once the data flow is initiated, the TRMM GV team will begin routine processing of the radar data and generate preliminary standard products (defined by TRMM), as described below:

1B-51: Original radar reflectivity and radial velocity in spherical coordinates, extending to 230 km from the radar.

1C-51: Quality-controlled radar reflectivity data, extending 200 km from the radar. The QC step is designed to remove non-precipitating echo from the radar snapshots.

2A-53: Instantaneous rain rate in a 2 km x 2 km horizontal grid, extending 150 km from the radar.

2A-54: Stratiform/convective rain types in a 2 km x 2 km horizontal grid, extending 150 km from the radar. The Steiner et al. (1995) algorithm is used to determine the respective rain types.

2A-55: Three-dimensional radar reflectivity data in a 2 km x 2 km horizontal grid, extending 150 km from the radar, and 1.5 km vertical grid from 1.5 km AGL to 19.5 km AGL.

3A-53: Five-day (Pentad) rain accumulation in a 2 km x 2 km horizontal grid, extending 150 km from the radar. Note that this product will not be used by AMSR-E but is used in GPCP products.

3A-54: Monthly rain accumulation in a 2 km x 2 km horizontal grid, extending 150 km from the radar.

Rain gauge information from the two clusters, as well as additional gauges maintained by the NWS and the USGS (United States Geological Survey), will be utilized in the product generation. These products will be evaluated and collocated with existing satellite rain rate products (e.g., SSM/I and AMSU) to determine their quality and identify any problem areas. It is anticipated that the 2001-02 rainy season (November–April) will be used as a testing period.

From our preliminary analysis of Eureka WSR-88D data obtained from NCDC, it was noticed that persistent ground clutter features were evident. A mask was developed to remove such persistent features. This mask will undergo final testing by December 31, 2001. Also, low-level beam blockages are evident in the SE to NE quadrant, where high terrain exists. The TRMM GV team will alleviate this problem (only apparent in the lowest elevation scan) by developing an interpolation scheme that will use the next elevation scan to fill in the data voids below. We will also work closely with the NWS/NEXRAD group in Silver Springs to acquire and test any newly developed algorithms to alleviate such problems.

By the end of 2001, the AMSR-E rainfall team will deliver the freezing level height and reflectivity variance within the 2 km x 2 km grid.

During early 2002, an improved web site will be developed that will host many interesting features from the Eureka site. This will include daily animations of the reflectivity products and time sequences from the gauge sites.

During the summer of 2002, two major events will take place. First, improvements to the GV process will be implemented, based on our initial evaluations. Second, we will deploy two more gauge clusters at "strategic locations" that will serve to improve the GV products and benefit the NWS in the rainfall monitoring.

Finally, periodic visits (3-4 per year) will be made by members of the AMSR rainfall team and TRMM GV staff to insure our continued close working relationship with the NWS and to make site inspections of the gauges. This sort of close working relationship has been previously established and is essential to the continued success of the project.

Fiscal Year 2003

It is anticipated that during the rainy season of November 2002 – April 2003, the GV processing at Eureka will be in full operational mode. It is during this time that we expect to be fully utilizing the array of products to improve the AMSR retrieval algorithms over both land and ocean. The products will be used for both the PV and GT paradigms described earlier in this report. As previously mentioned, two more gauge clusters would have been installed during the previous summer and these will be utilized to improve the quality of the GV products. If it is deemed necessary, we will install additional gauges in data important regions.

Fiscal Year 2004

It is the desire of the AMSR rainfall team to continue to utilize the Eureka site for the following rainy season (November 2003 – April 2004). This third year of continuous operation will guarantee that the dataset will contain some extremely wet months. It is also anticipated that improved algorithms, based in part by data from this site, will be implemented by the AMSR team, so continued data would be useful to continue PV and GT exercises using "independent" data.

3.2.3.2 AMSR-E Validation Using BALTEX Radar Data Centre (BRDC) Data

Water Background

We will perform a conventional analysis using the gauge-adjusted radar data as GT. Comparing radar data observed at different altitudes with the results of the GPROF algorithm, we will be able to address the accuracy of the retrieval for different types of precipitation. The delineation of frontal and convective precipitation is of crucial importance at high latitudes. Using coincident radar and SSM/I data over the Baltic region, Bennartz and Michelson (2001) show that the response of passive microwave sensors to these different precipitation types is entirely different. We will therefore emphasize the verification of the convective/stratiform separation of the AMSR-E retrieval algorithm. Another problem at high latitudes is the usually low height of the freezing level, which is around 2-3 km for typical summer precipitation and well below 2 km in wintertime. This results in an only moderate emission signal of the liquid precipitation at low frequencies and severely hampers the retrieval accuracy at high latitudes as compared to lower latitudes. The BRDC dataset is a unique tool to address these issues associated with precipitation at high latitudes. Apart from these opportunities, the straightforward GT validation approach suffers from the limited accuracy of each validation dataset. Obviously, even the best-calibrated and gauge-adjusted radar dataset has its own associated uncertainties. Ultimately, the absolute accuracy of the passive microwave retrieval cannot be assessed from GT validation efforts alone.

We therefore plan a further, more rigid PV validation step, which allows us to associate uncertainties in the retrieval to the predominant sources of noise in the data. The main error sources are (1) the determination of the height of the freezing level, (2) beam filling for each channel, (3) the different resolution of the different channels, and (4) the variability of the vertical hydrometeor profile also including variation of ice particle density, size, and shape. As far as the

microphysical properties of the precipitation are concerned, not only the passive microwave retrieval is affected, but also in a similar manner the radar observations. Bennartz and Petty (2001) have taken some effort to develop a method that allows us to consistently describe the ice microphysical properties and their impact on radar as well as on the passive microwave observations. In conjunction with a three-dimensional Monte-Carlo radiative transfer model, this method will be used to simulate AMSR-E overpasses over the Baltic region at radar resolutions for different types of precipitation events. The resulting simulations at high spatial resolution allow us to separate the aforementioned possible error sources. First, the impact of beam filling can easily be assessed by convolving the simulated brightness temperature to the actual AMSR-E footprint size at different frequencies and by evaluating the algorithms assumptions compared to the observed inhomogeneity. Second, the impact of different hydrometeor profiles can be studied by varying the microphysical properties of the precipitation. In summary, we believe that based on this PV approach it will be possible to identify and quantify the major sources of error in the retrieval algorithm at high latitudes and to propose possible adjustments to the algorithm.

Land Background

The AMSR-E precipitation screening and quantification uses a scattering index approach. Due to the high and variable surface emissivity over land surfaces, the low frequency emission signal may not be used over land surfaces. In general, the scattering signal is only indirectly linked to surface precipitation, and therefore a pixel-by-pixel validation using radar data may reveal large scatter. However, most of this scatter appears to be associated with variations of the type of precipitation (Todd and Bailey, 1995; Kidd, 1998; Bennartz and Michelson, 2001). A second problem that arises especially at high latitudes is the distinction of snow (especially wet snow) and precipitation. We will therefore address these two issues in the following manner: We will investigate the accuracy of the snow/precipitation delineation of the AMSR-E algorithms. This will be done, by using the radar data as ground truth for the areal extent of precipitation and by using snow maps derived from surface observations to estimate wintertime snow extent. These maps are regularly produced at SMHI and will be provided for the proposed project. In addition NWP-model output will serve to at least roughly quantify the melting conditions for given overpasses via the model temperatures in 2 m altitude. Using this auxiliary information, the discrimination between dry and wet snow may be possible. In a second step, we will investigate the algorithms accuracy for those cases that successfully passed the precipitation screening. This evaluation will be done via comparison of convolved radar precipitation estimates with those obtained from AMSR-E. A GT approach will be used to evaluate the algorithm's accuracy. In addition to the overall estimates, statistics will be performed for different types of precipitation events. Comparison of AMSR-E with AMSU/HSB will reveal possible improvements in detection and quantification of precipitation by using higher frequencies.

3.2.3.3 Surface Reference Dataset: Validation Site in Iowa City, Iowa

We plan to use AMSR-E validation as the opportunity to develop a prototype rain gauge-based ground validation site for level 2 (instantaneous) satellite rainfall products. This site should have sufficient rain gauges to (1) give area-averaged rain estimates with low error, and (2) determine spatial rainfall variability so that the accuracy of the gauge estimate can be quantified. Also, the size of the site should be sufficient for comparisons with satellite estimates. Finally, the site should be in an area that is practical for deployment and operation of the gauge network.

The goal of the effort is to accurately quantify the error of level 2 satellite rainfall estimates for the first time. Many attempts using radar rainfall estimates have been made but additional work is needed to reduce the uncertainty in radar rainfall estimation. In terms of gauges, there has never been a network with sufficient density over a large enough area to be useful for level 2 satellite rainfall validation.

The validation is needed because despite the many years of development of satellite rainfall algorithms, we don't have a good estimate of their accuracy. We are learning more about regional and seasonal biases, but in terms of level 2 products, it's possible that the second order (standard deviation) errors could be 10%, 50%, 100%, or even greater than 200%; we simply haven't had the data to quantify these errors. However, level 2 rainfall estimates are being

assimilated into numerical prediction models and used in other applications such as for input into hydrologic models, so this lack of knowledge of the rainfall estimation uncertainty makes the rain estimates less useful.

Our plan is to build upon the existing rain gauge network located in Iowa City, IA, that exists as part of the research operation of Prof. Witold Krajewski at the University of Iowa, located around 40°N. Professor Krajewski has been the principal investigator for the Guam TRMM GV site and is now interested in development of the Iowa validation site. There are already 28 tipping bucket gauges organized in pairs in operation centered at the Iowa City Municipal Airport. They are spaced at different intervals from 10 m to 8 km, although most of the gauges are located within 1 km at the airport. This site is currently under the NEXRAD umbrella, and they are working on obtaining a real-time feed for the WSR-88D Davenport level II data so that they could apply their own algorithms that together with the dense rain gauge data should lead to improved validation products. The site also includes a vertically pointing X-band Doppler radar and a 2D-video disdrometer, and a wind lidar. Prof. Krajewski would like to install a C- or X-band radar near the site in the future, as well as one or two vertical profilers. The group is developing inexpensive disdrometers. The university is providing a support infrastructure for this site, and the site is maintained by IIHR-Hydroscience and Engineering (formerly Iowa Institute of Hydraulic Research) staff and students. There are plans to develop the site for validation of other hydrologic variables, including snowfall, snow cover, and vegetation characteristics. This would further enhance the utility of the site for our purposes.

The existing network is a good start for determination of the spatial rainfall statistics needed for quantification of the area-averaged gauge estimates. We would like to then increase the areal extent of the network to a 0.25-degree grid box. These developments will have support in another initiative in the state of Iowa, i.e., development of the Iowa Mesonet, modeled after the Oklahoma Mesonet. Twenty-five gauges uniformly spaced over the 0.25 degree grid box already containing the dense gauges in the center would provide us with area-averaged estimates with uncertainties that are both low and that can be quantified. This will allow us to investigate different spatial averaging scales, from the ~ 4 km x 6 km 85 GHz AMSR satellite pixel scale at the center of the site to scales containing many satellite pixels.

Krajewski et al. (2000) used the theoretical equation of Morrissey et al. (1995) to determine the uncertainty of rain gauge means over 2.5 degree boxes for validation of satellite estimates. The same equation can be applied to this site and we have done some preliminary calculations as an illustration.

Figure 3.2.4 shows the results of application of the Morrissey et al. (1995) equation to the Iowa grid box for different numbers of uniformly spaced gauges. The uncertainty of the gauge mean is expressed as a fraction of the uncertainty if one gauge was used to estimate a spatial average for an area with spatially-uncorrelated rainfall; the standard deviation of the estimate would simply be the standard deviation of the gauge accumulation about the long-term mean rainfall rate, which can be calculated from the gauge data. However, as more gauges are used for the mean and as spatial correlation is considered, this standard deviation is reduced.

For example, the point corresponding to four gauges for non-correlated rainfall is 0.5, because the variance of a random sample is reduced by n, where n is the number of random samples. In this case, the number of random samples is 4, reducing the variance by 4 and the standard deviation by 2. With correlated rainfall, the standard deviation is reduced further. The correlation length of 15-minute rain gauge accumulations has been calculated at around 5 km with data from Brazil. In Iowa, this correlation length may be up to 15 km. The results of both possibilities are shown in Figure 3.2.4.

For both possible cases, the uncertainty drops rapidly as the first several gauges are added. The standard deviation of the spatial mean can still be cut in half by going from 10 to 25 gauges, so 25 appears to be a good number for our site. The further reduction in accuracy from adding more gauges may not be worth the cost and effort at this time.

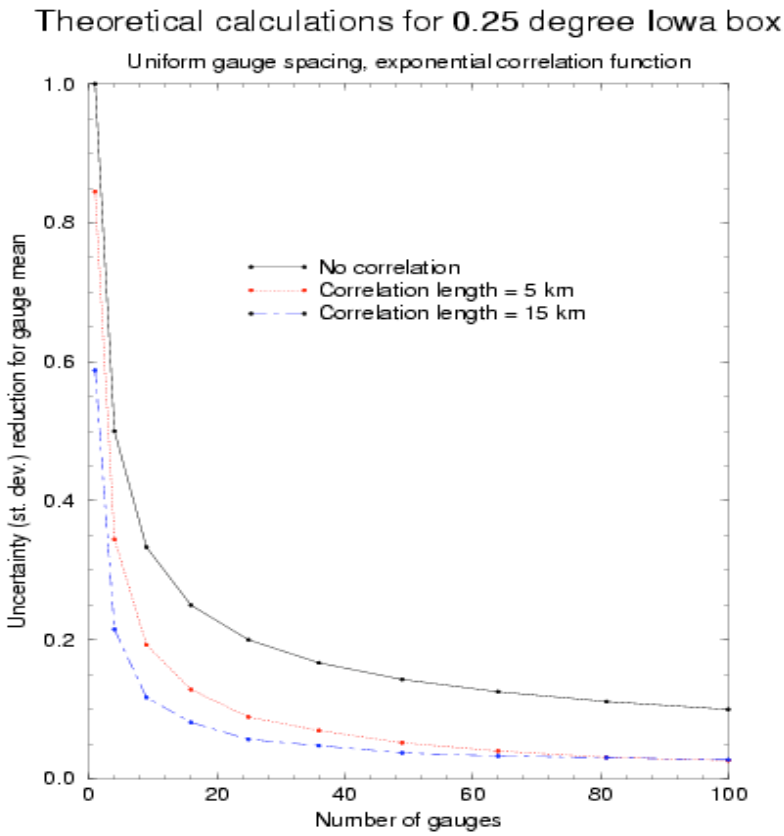

Figure 3.2.4. Results from application of the theoretical Morrissey et al. (1995) equation to the 0.25 degree Iowa site, assuming exponential correlation functions with the given correlation lengths for 15-minute rainfall. The y-axis shows the reduction in the uncertainty, expressed as standard deviation, about the gauge mean based on the sampling of the grid box from the given gauges.

Logistically speaking, the Iowa City site would provide many benefits. As mentioned, the site has already been started and the support staff is there at the University of Iowa. The land surrounding Iowa City is primarily flat farmland, and Prof. Krajewski's university team as well as Jeff McCollum of NOAA has many contacts in the surrounding areas to help facilitate deployment and maintenance of the network. For a prototype system such as this, it seems prudent to simplify the logistics as much as possible. Inevitably there will be much to learn from the experience and this knowledge can then be used for other sites with more difficult logistics until finally these sites might be deployed in different locations over the world, e.g., for GPM.

GPM will be a much more comprehensive validation campaign, and this Iowa City project would fit in well with the long-term GPM validation plan. The costs for this project are quite modest in comparison with TRMM and future GPM validation sites, but this site can provide unique information that will be useful to other validation campaigns. We would like to work closely with the GPM when it begins as a collaborative effort. However, we would like to get started as soon as possible, so that we will have ground reference data available for the entire AMSR time period, which will begin in 2002. Experience learned through this AMSR-funded activity will ultimately improve future GPM efforts. While the rainfall statistics may differ for other sites, we will be able to test methodologies for assessment of satellite estimation errors based on comparison with the ground-based gauge estimates.

For example, one methodology for bias assessment is based on determination of the spatial and temporal statistics of instantaneous area-averaged rainfall over our 25 km grid. Error models to estimate the second order error over longer time and space scales require the temporal and spatial correlation structures of the instantaneous rainfall. With these statistics, we

can use the rainfall statistical rainfall models such as Bell's to simulate long-term rainfall to determine the length of data record needed to evaluate satellite algorithm bias within a given confidence level for specified satellite overpass configurations. We will be able to assess whether there is a bias between the satellite and gauge estimates over our study to a significance level that will depend on the temporal rainfall statistics.

Time line:

Winter (Jan-Mar.) 2002	Purchase equipment and plan network configuration
Spring 2002	Install and test gauges
Spring 2002-Spring 2003	Development of error model without rain statistics
Spring/Summer 2002-completion	Data collection
Fall 2003-Winter 2004	Implementation of rainfall statistics into error model
Spring-Fall 2004	Validation and modification of error model

3.2.3.4 Physical Validation – Wakasa Bay Experiment

The U.S. AMSR-E and Japanese AMSR teams are planning a field experiment for Jan/Feb 2003 over Wakasa Bay, Japan. This experiment offers a unique opportunity to collaborate with the Japanese AMSR validation effort. The experiment is designed to (1) validate both the AMSR and AMSR-E shallow rainfall and snowfall retrieval capabilities (2) potentially begin the process of merging the two algorithms based on jointly gathered information, and (3) extend our understanding of rainfall structures through the use of new remote sensing technology. The NASA P3 aircraft will be flown as the NASA contribution to the experiment. It will carry the dual frequency precipitation radar (APR-2) operating at 14 and 35 GHz; a cloud radar operating at 94 GHz; a polarimetric microwave sensor (PSR) that simulates the AMSR observations; a high frequency passive microwave radiometer (MIR) covering from 90 to 340 GHz; and an upward looking radiometer at 21 and 37 GHz. The sensors are described in Section 3.2.3.5. The Japanese contribution to the experiment consists of a dual-polarized ground-based radar and supporting surface observations that will allow us to put the aircraft observations into the larger meteorological context. The logistics of the experiment are described in Section 3.2.3.6. This section concentrates on defining the scientific goals of the experiment.

Wakasa Bay, on the eastern end of the Sea of Japan, has fairly predictable cold air outbreaks in which cold air from the Eurasian continent blows over the relatively warm Sea of Japan. These storms generally produce rainfall near the surface, where warm boundary layer air mixes with the cold air aloft. The depth of the rain layer, however, is typically very shallow and in some cases, the snowfall reaches all the way to the surface. As such, Wakasa Bay is an ideal location to study shallow precipitation systems as well as snow events over the ocean.

a. Length Scales of Horizontal Variability

Passive microwave rain estimates suffer from incomplete knowledge of the rainfall inhomogeneity in the relatively large footprint of spaceborne radiometers. This inhomogeneity causes algorithms to have a low bias unless the mean inhomogeneity is accounted for. We have pretty good numbers in the tropics–extratropical rainfall is less certain. Wakasa Bay, in addition to Eureka and BALTEX, will be used to constrain this number.

b. Freezing Level Retrieval

Because passive microwave sensors can detect only the column integrated liquid amount, it is critical to establish the height of the liquid column before meaningful surface rainfall rates can be obtained. The freezing level (FL) retrieval has been tested against TRMM radar data in the tropics but very little data from shallow, extratropical precipitation exist. APR-2 data, which can detect the height of the freezing level (bright band) directly, will be compared to passive radiometer freezing level retrievals and AMSR-E retrievals when possible. A few profiles of temperature and water vapor taken on aircraft ascents or descents through the rain will allow direct testing of the underlying thermodynamic assumptions.

c. Bright Bands–Improved Treatment in Passive Microwave

The radar and radiometric communities treat bright bands differently. The radar community uses a model that effectively doubles the emission in the bright band region, while the radiometric community has ignored the bright band issue until now. Some evidence suggests that the bright band does indeed increase the effective emission in some cases. The shallower the rainfall column, the more important the effect of the bright band is. Experiment will determine the structure of bright band from three frequency radars and AMSR-E simulator and then fly up through the bright band with the upward looking radiometers to verify that we understand the effect.

d. Snow–How Well Can Snow be Quantified Over an Ocean Background?

Unlike rainfall retrieval that has a history of several decades, the research in snowfall retrieval is just begun, and the algorithm development is at a very early stage. Due to the low density of snowflakes, the microwave snowfall signature is relatively weak compared to the scattering signature of graupel and hail associated with deep convections. One encouraging report (Liu and Curry, 1997) based on analysis of DMSP SSM/T-2 data (92 to 183 GHz) showed that the horizontal distribution pattern of retrieved snowfall over North Atlantic compares reasonably well with the snowfall frequency distribution reported by ship observers (COADS data). Unfortunately, no quantitative validation was done due to the lack of validation data. The error in this retrieval is therefore unknown. Airborne radiometer measurements over the Japan Sea showed that the 89-GHz brightness temperature decreases by ~15 K over shallow snow convections that have snowfall rates of ~1.5 mm h^{-1} (liquid water equivalent). In this case study, a forward radiative transfer model was able to reproduce the observed brightness temperatures at 89 and 37 GHz to within ~2 K. This agreement indicates the potential of quantifying snowfall over ocean from AMSR-E observations using a physically based algorithm, although higher frequencies (such as 150 GHz or above) are preferable for snowfall retrievals. The primary signature of snowfall in microwave radiation is the reduction of upwelling brightness temperature due to the scattering by snowflakes. The scattering signature increases with the amount and size of snow particles when snowfall becomes heavier. Thermal emission from water vapor and cloud liquid water, however, has a masking effect to the snow scattering, and reduce the snow signature. As a result of this masking effect, the relative locations in the vertical among water vapor, cloud liquid water and snow particles become relevant to the satellite received brightness temperatures. Therefore, information on both the vertically integrated snow amount and its vertical distribution are needed for physical snowfall retrieval.

Two microwave radiometers (MIR and PSR; covering the frequency range from 10 to 340 GHz) and two radars (APR-2 and a cloud radar; frequencies: 14, 35 and 94 GHz) will be used in the validation campaign (Table 3.2.1). From the radar measurements, attenuation-corrected profiles of cloud and snow can be inferred. With the combination of 14 and 35 GHz radar data, snow particle size distribution can also be retrieved. Cloud liquid water path, vertical distribution of water vapor and surface wind speed may be derived from AMMR and MIR observations. A very important first step in analyzing these data is to examine how passive microwave brightness temperatures at PSR and MIR frequencies respond to the observed various snow profiles, which in turn can be used to improve the representations of snow density, snow dielectric constant and snow particle distribution in the forward radiative transfer model used for the AMSR snowfall algorithm so that it, in turn, can correctly reproduce the observed brightness temperatures. This step lays the foundation of the physically based retrieval algorithm for snowfall. The characteristics and variability of both horizontal and vertical snowfall distributions are then analyzed using the high-resolution validation dataset. The analysis provides the needed information for beam-filling correction and the construction of the database of hydrometeors' vertical profiles in snowfall environments. One question here is whether (or how much) a beam-filling correction is needed for the snowfall algorithm. Radiative transfer modeling indicates that the brightness temperature–snowfall rate relation at high frequencies is much closer to linear than brightness temperature–rain rate relation at low frequencies (e.g., 19 GHz). This implies that the beam-filling effect for snowfall retrieval may not be a significant error source. Simultaneous radar

and radiometer observations in the validation campaign will help define an answer to this question. The knowledge obtained from the aforementioned physical validation can lead to the improvement to the AMSR-E snowfall retrieval algorithm. Finally, snowfall rate retrievals from satellite AMSR-E data will be compared with coincident aircraft validation data ("ground truth"). Interpretation of the "agreement" and "disagreement" should be done, while keeping in mind the limitations of the ground truth data.

Table 3.2.1. Instruments to be used in validation campaign

Instruments	Frequencies
APR-2	14, 35 GHz
Cloud Radar	94 GHz
MIR	89, 150, 183±1, 183±3, 183±7, 220 340 GHz
PSR-A	10.7, 18.7,23.8, 36.5, 89.0 GHz

This campaign is the first opportunity ever to observe snowfall using high frequency microwaves with coincident radar data. Evaluating the ability of measuring snowfall from high frequency microwaves based on these observational data are greatly beneficial to future satellite precipitation programs, such as GPM mission.

e. The Forward Model—How Well Can We Model Microwave Brightness Temperatures?

A critical test of any physical inversion scheme is whether or not brightness temperatures can be correctly predicted when the atmospheric and rainfall structures are known. Unfortunately, the community has never seriously undertaken an experiment to measure the bulk hydrometeor contents in such a way that a test of the forward model could be performed. Work to predict TMI brightness temperatures on TRMM, based upon the precipitation radar, quickly reveal that the drop size distribution assumed by the radar was crucial in determining agreement or disagreement between the two sensors. The sensors on the P3 aircraft will allow us to improve upon previous work. In particular, the dual frequency radar package (APR-2) will allow us to determine the mean drop diameter that is critical in converting radar reflectivity to liquid water content. In addition, the combination of 35 GHz and 94 GHz cloud radar and the high frequency radiometer will allow us to determine properties of the ice water content above the freezing level. By constructing the vertical hydrometeor profile from these sensors, it is then possible to use existing cloud model simulations and radiative transfer methods to compute the brightness temperatures that are being viewed simultaneously by AMSR channels.

The AMSR retrieval of instantaneous rainfall rates relies on a Bayesian methodology. In this methodology, profiles are selected from an a priori database of cloud resolving model profiles based upon uncertainties in (1) the observed brightness temperatures–or the sensor noise, and (2) the uncertainties in the forward model. The latter have never been well defined as they include a whole range of uncertainties that we know little about. The main purpose of this forward modeling experiment is therefore to quantify our current ability to do this forward modeling. Differences between observed and modeled Tb represent errors in our ability to forward model brightness temperatures, when the hydrometeor field is known, to the highest precision possible. Differences in the modeled and observed Tb therefore represent our best guess as to the inherent uncertainties in our forward modeling ability and will form the basis—once confirmed in selected other locations—for estimating the uncertainties in the forward modeling needed by the Bayesian retrieval scheme. As such, this portion of the experiment is exploratory in nature. If successful, however, it will lead to a fundamental improvement in how uncertainties are quantified in microwave rainfall estimation schemes.

f. Snow Over Land – Can Higher Frequencies be used to Quantify Snowfall Rates Over Land?

There are two major areas that limit the AMSR-E set of frequencies in the detection of falling snow over land. The first is simply, is there enough scattering present in falling snow that can be

detected at 85 GHz? This same question is being addressed over ocean. The second is trying to separate the surface scattering due to snow cover, which is typically very strong, from the potential scattering signature that is occurring in the precipitating clouds, which is an order of magnitude less. These two issues will be addressed below.

If the precipitating clouds contain a sufficient density of ice water equivalent, from snow crystals, graupel, or both, then a depression at 85 GHz is likely (Bennartz and Petty, 2001). This situation would likely arise in well-developed storm systems that have large-scale precipitation shields and have cloud systems extending upwards of 8 km. On the other hand, if the precipitation is more of a local nature (i.e., lake effect snow) or is shallow (4 km or less), the depression at 85 GHz may not be as apparent. That is the challenge that AMSR faces in detecting falling snow.

Fortunately, the recent launch of the NOAA Advanced Microwave Sounding Unit (AMSU), first placed into operation in 1998, has for the first time, given us the opportunity to examine precipitation characteristics at sufficient spatial resolution, up to 183 GHz. It has shown tremendous promise in utilizing measurements at 150 GHz to improve the detection of light rain over land and minimize the effect of the underlying surface (Ferraro et al, 2000). Prior to that, the DMSP SSM/T2 was the only operational sensor that spanned such a high measurement frequency, but has FOV's on the order of 75 km. Despite its poor spatial resolution, it has also shown promise in improving the retrieval of rain over land (Bauer and Grody, 1995).

To better demonstrate this concept, Figure 3.2.5 shows actual measurements taken from the NOAA-16 AMSU on February 22, 2001 over a wide range of land surface conditions. The features that exhibit similar spectral characteristics are given the same symbol on the curves. Note that surfaces over vegetated land and deserts have a relatively flat response, with over the frequency range of 23–183 GHz. The TB increases noted at the highest frequency are due to higher absorption by water near the 183 GHz absorption band. The response of convective rain is clearly distinguishable from the land surfaces, and shows a continued strong decrease in TB with increasing frequency. Snow surfaces in various phases of age behave in a fairly similar manner over the frequency range. The major differences noted are simply due to the physical temperature of the snow surface and atmosphere. Contrasting this to the rain signature, there is no additional decrease in TB beyond 89 GHz due to the large size of the snow grains (i.e., geometric optical limit, so no additional scattering). Thus, the use of high frequency measurements allows for a fairly unique separation between falling rain and snow on the ground in most instances. This is an important aspect that may be useful in a combination AMSR-E/HSB scheme to separate snow aloft from that on the ground.

Also on this day, a small, fast moving snowstorm affected the Middle Atlantic States, where no prior snow existed on the surface. Although still under investigation, we believe that there were some measurements taken by AMSU where the snow was falling from clouds, but not yet reaching the ground (e.g., virga), which allows us to determine if there is a signal at these frequencies of the snow precipitation process (yet, not having to worry about a snow signature on the ground). The spectral response to this precipitation system is noted by the dashed curves, which were taken at different locations across the storm system. There is virtually no indication of scattering at 89 GHz, yet, there is a modest decrease (~10 K) noted at 150 and even at 183 ± 7 GHz in some parts of the storm system (note that the pink curve is very flat throughout, yet, light snow was falling at this time with approximately 5 cm of snow on the ground at this location). Thus, it appears that the use of high frequency measurements above 85 GHz show promise in the detection of falling snow over land.

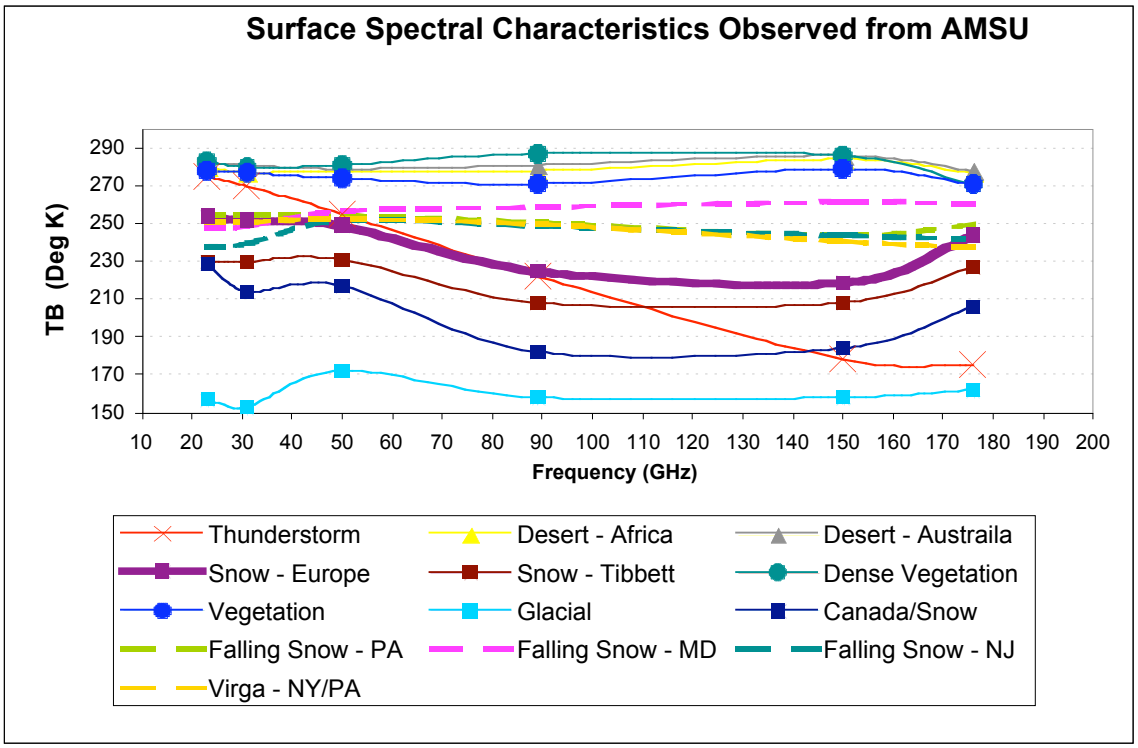

Figure 3.2.5. Surface spectral characteristics as determined from NOAA-16 AMSU measurements from February 22, 2001. Observations made at 23.8, 31.4, 50.3, 89, 150, and 183 ± 7 GHz were used and are indicated by the points in the graph.

The field experiment at Wakasa Bay will be an excellent opportunity to further explore the potential of using high frequency measurements to detect falling snow and snowfall rate. The instrument suite is listed in Table 1. We will offer guidance in planning the flight paths during the field experiment to obtain measurements of falling snow over land. If possible, we will try to get measurements over a variety of surface conditions ranging from bare ground to deep, snow cover. Additionally, the Aqua satellite will contain the HSB sensor that, in conjunction with AMSR, will offer us a full complement of spectral measurements ranging from 6 to 183 GHz. This will be the first time that such a set of measurements will be available from a space borne radiometer. Results from this unique set of satellite observations, in conjunction with those made aboard the aircraft used in Wakasa Bay should help answer the question regarding the detection of falling snow and the retrieval of snowfall rates.

g. Cloud Water Retrieval

Because the P3 aircraft will carry a cloud radar for the detection of light snowfall rates over ocean and land, as well as help with constructing the vertical hydrometeor column, the Wakasa Bay experiment also offers a unique opportunity to validate the cloud water retrievals from AMSR. Cloud liquid water retrievals utilizing 94 GHz cloud radar data (Austin and Stephens, 2001) have been developed for the CloudSat mission (Stephens et al., 2002). These retrievals are currently designed for non-precipitating clouds; there are radar-only and radar-visible optical depth versions of the retrieval. The radar-only version can be utilized for any Wakasa Bay flight. The more precise radar-visible optical depth version may be employed for flights where visible optical depth information is available from Aqua/MODIS overflights (as will be utilized for CloudSat data) or possibly from GMS, although this data will involve compromises in horizontal resolution. An algorithm for precipitation retrievals using the 94 GHz cloud radar has also been recently developed (L'Ecuyer and Stephens, 2002), and work is planned over the coming year to bridge the algorithmic gap between the drizzle-free and precipitating regimes. The Wakasa Bay flight should provide valuable opportunities to compare the cloud water retrievals for the very light

precipitation regimes where they are expected to be most accurate and to examine how the cloud water retrieval information degrades under differing degrees of precipitation. The flights will also provide data for the exploration of combined algorithms that take advantage of synergies between AMSR-E and CloudSat.

3.2.3.5 Wakasa Bay Experiment/Sensors and Aircraft

Polarimetric Scanning Radiometer (PSR)

The PSR that will be flown in the Wakasa Bay experiment is described in section 3.3.3.2

The Millimeter-Wave Imaging Radiometer (MIR)

The Millimeter-Wave Imaging Radiometer (MIR) is an airborne, total power, cross-track scanning radiometer that measures radiation at seven frequencies, 89, 150, 183.3±1, 183.3±3, 183.3±7, 220, and 340 GHz. The sensor has a 3-db beam width of 3.5 degrees at all frequencies. It can cover an angular swath up to ±50 degrees with respect to nadir. In every scan cycle of about 3 sec, it views two external calibration targets in addition to the 100-degree scene scan; one of these targets is heated to a temperature of 330 K and another remains at the ambient temperature of the aircraft cruising altitude. The temperatures of these calibration targets are closely monitored to within ±0.1 K. The temperature sensitivity, for all frequencies, is on the order of 0.5 K and the calibration accuracy is about ±1 K in the brightness temperature range of 240-300 K. The measurement accuracy at low end is less certain; based on the calibration studies in the laboratory, the accuracy near the liquid nitrogen temperature of 77 K is estimated to be ±3 K.

- Calibrated brightness temperatures at 57 beam positions covering 100 degrees swath.

- Water vapor profiles and cloud information (liquid clouds, or ice water path from storm-associated clouds) can be obtained from these brightness temperatures with appropriate algorithms.

Second Generation Airborne Precipitation Radar (APR-2)

The Second Generation Airborne Precipitation Radar (APR-2) is the airborne simulator of the next generation of the space borne rain-mapping radars, which would follow the highly successful single-frequency precipitation radar (PR) (Kozu et al., 2001) of TRMM. The APR-2 science observations will consist of vertical structures of rain reflectivity at both 13.4 and 35.6 GHz and at both co-polarization and cross-polarization, as well as the vertical Doppler measurements. Such comprehensive sets of measurements from a highly mobile sensor is intended to provide information for the detailed studies of the microphysics and dynamics of rainfall, snowfall, and dense or precipitating clouds in various climatic regimes and geolocations.

Developed and operated by NASA/JPL, the APR-2 is the successor of the Airborne Rain Mapping Radar (ARMAR) (Durden et al., 1994). The APR-2 operational geometry is shown in Figure 8; it looks downward and scans its dual-frequency antenna beams across the flight track, with each scan beginning at 25 degrees to the left of nadir and ending at 25 degrees to the right. The APR-2 scanning antenna consists of a 0.4-m offset reflector antenna with a mechanically scanned flat plate, and a 13.4- and 35.6-GHz dual-frequency antenna feed. The feed is configured such that the aperture at 35.6 GHz is under illuminated to provide matched beams at the two frequencies. The RF electronics subsystem consists of a digital chirp generator (DCG) used to synthesize a linear frequency-modulated chirp waveform, an upconverter and four receiver channels. The DCG generates the shaped, linearly frequency-modulated pulses with sidelobe levels below -60 dB. The chirp waveform is generated at an IF frequency and upconverted to both 13.4 GHz and 35.6 GHz. The signals are amplified to the desired radiated powers using the 13.4 and 35.6 GHz traveling wave tube amplifiers (TWTA) to the dual-frequency

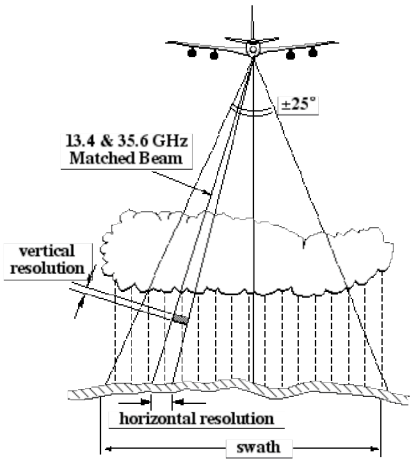

Figure 3.2.6. APR-2 operational geometry showing cross- track scan.

antenna. There are four receiver channels, two for 13.4 GHz (H- and V-pol) and two for 35.6 GHz (H- and V-pol). Table 3 shows the system characteristics for APR-2.

Table 3.2.2. APR-2 system parameters.

Parameters	Ku-band	Ka-band
Frequency	13.4 GHz	35.6 GHz
Polarization	HH, HV	HH, HV
Antenna effective diameter	0.4 m	0.14 m
Antenna gain	34 dBi	34 dBi
Antenna sidelobe	-30 dB	-30 dB
Antenna scan angle	±25˚	±25˚
Polarization isolation	-25 dB	-25 dB
Peak power	200 W	100 W
Bandwidth	4 MHz	4 MHz
Pulse width	10 - 40 ms	10 - 40 ms
Pulse Repetition Frequency	5 kHz	5 kHz
Vertical resolution	37 m	37 m
Horizontal resolution	800 m	800 m
Ground Swath	10 km	10 km
Sensitivity (at 10 km range)	10 dBZ	5 dBZ
Doppler precision	0.3 m/s	0.9 m/s

At each beam position of each scan, APR-2 acquires simultaneous vertical profiling measurements of the following set of parameters:

- Co-polarized (HH) radar reflectivity at 13.4 GHz
- Cross-polarized (HV) radar reflectivity at 13.4 GHz
- Doppler velocity at 13.4 GHz
- Co-polarized (HH) radar reflectivity at 35.6 GHz
- Cross-polarized (HV) radar reflectivity at 35.6 GHz
- Doppler velocity at 35.6 GHz

These measurements are acquired at the horiztonal resolution of 800 m and the intrinsic vertical resolution of 37 m. The APR-2 has successfully completed its maiden field campaign, the

CAMEX-4, in Aug-Sep, 2001. Figure 3.2.7 shows an example of the APR-2's quick-look data acquired during this experiment.

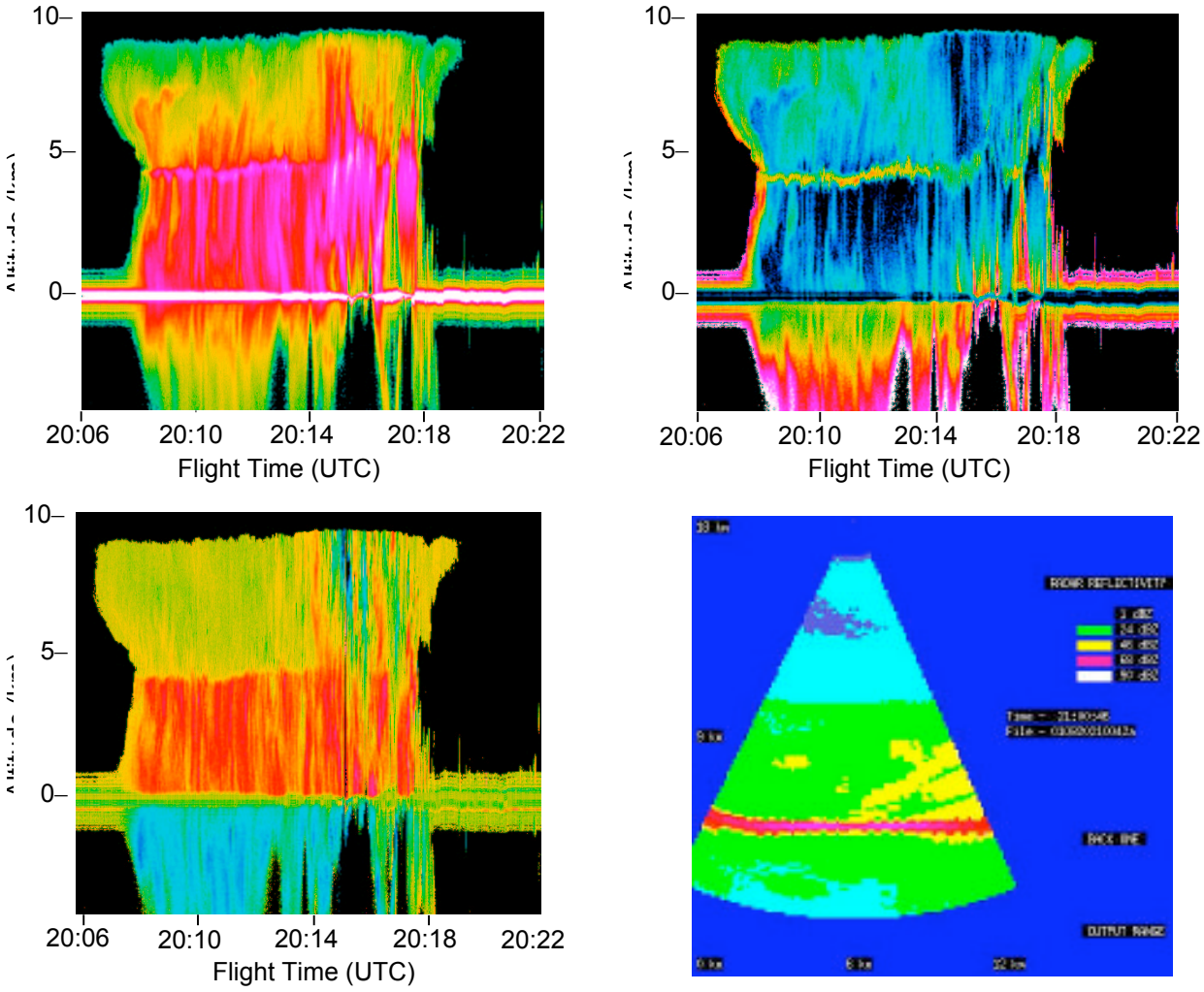

Figure 3.2.7. Vertical rainfall profiles of Tropical Storm Chantal were acquired by the PR-2 radar on the NASA DC-8 aircraft during the second flight of the Fourth Convection and Moisture Experiment (CAMEX-4) on August 20, 2001. The quick-look image at top left shows the nadir cut of the 14-GHz co-polarized radar reflectivity profiles along the flight path. Detailed structures of both the melting layer (at left) and the intense convective region (at right) of the observed rain system can be seen in this image. The ocean surface returns are shown as a white line. The portion below the white line corresponds to the mirror images (double bounces) of the radar returns from rain above the surface. The top right image is the corresponding profile of the Linear Depolarization Ratio (ratio of cross-polarized to co-polarized reflectivities). It accentuates the ice particles at the melting layer. The image on the bottom left shows the vertical Doppler velocity. At left the velocity sharply changes at the melting layer as the ice particles fall slowly and then melt, increasing in speed to 5-10 m/s at lower altitudes. At right, larger Doppler velocities are seen associated with downdrafts and updrafts in the convective area. During operations, PR-2 performs ±25° scans across the nadir track. An example of the cross-track co-polarized reflectivity is shown on the bottom right.

Airborne Cloud Radar (ACR)

The Airborne Cloud Radar (ACR) is a 94-GHz radar designed to facilitate measurements of vertical layer structure, as well as the radar backscatter and radiative properties, of all prevalent types of clouds over a wide range of geophysical locations. The ACR was developed and has been operated jointly by the University of Massachusetts and NASA/JPL.

Table 3.2.3 summarizes the system characteristics of the ACR. The system consists of an RF/IF subsystem, a digital signal processor, and data handling and control electronics. The RF/IF subsystem uses a combination of frequency mixing and multiplication to generate the transmitted signal at one of the four frequencies in a 50-MHz band centered at 94.92 GHz. The power of the transmitted signal is supplied by an Extended Interaction Amplifier (EIA). The transmit RF pulses can be routed to either the V or H port of an orthomode transducer (OMT) using a ferrite switch matrix. The OMT then feeds a 30-cm lens antenna. In the receive chain, the ferrite switches route the returned signals from the OMT to a low-noise amplifier (LNA). The signal is then downconverted to the 2.5-MHz IF. The IF signal is digitized and sent to signal processor where it is digitally demodulated and filtered to achieve the final system bandwidth. The signal processor then calculates power, pulse-pair and polarimetric correlation estimates and accumulates these estimates in real time. These processed data are then combined with auxiliary data and stored.

Table 3.2.3. ACR system parameters.

Parameters	W-band
Frequency	94.905, 94.915, 94.925, 94.935 GHz
Polarization (transmit)	H or V
Polarization (receive)	H or V
Antenna diameter	0.3 m
Antenna beamwidth	0.8˚
Antenna pointing	nadir
Peak power	1400 W
Pulsewidth	0.2, 0.5, 1 ms
Bandwidth	4, 2, 1 MHz
Duty cycle	1.2%
Noise figure	9.5 dB
Vertical resolution	38, 75, 150 m
Horizontal resolution	80 m
Sensitivity (at 5 km range, 150 m resolution)	-38 dBZ

The calibration stability of the system is maintained by using a calibration path to remove fluctuations in transmitted power and receiver gain. The calibration path consists of two cross-guide couplers and two attenuators with a combined loss of 47.5 dB. The calibration signal is injected into the receiver just before the LNA during the transmit interval.

The system can be configured to operate in three different modes in order to meet specific science objectives. They are: the frequency hopping mode, the dual-PRF Doppler mode, and the polarimetric mode.

In the frequency hopping mode, The ACR hops through a sequence of four non-overlapping frequencies (see Table 3.2.3) at the PRF of 4 KHz in order to increase the number of independent samples and maximize the cloud detection sensitivity. The measured parameter in this mode is limited to the range profile of cloud reflectivity.

In the dual-PRF Doppler mode, the ACR transmits pulses at two PRFs sequentially in order to create pulse pairs that are closely spaced in time. Second-lag pulse pair approach is used to estimate Doppler velocity. In this mode, range profiles of cloud reflectivity and vertical velocity are the two measured parameters.

In the polarimetric mode, the transmit and receive polarization states are synchronized such that the co-polarized signals (HH and VV) as well as the cross-polarized component (HV) are measured in an alternate fashion from the same cloud volume of interest. Because of the increase in the polarization states of the received signals, the number of independent samples, and therefore, the sensitivity, are reduced.

Since 1996, the ACR has been deployed several times on the NASA DC-8 aircraft to study various types of atmospheric cloud systems. Figure 3.2.8 shows an example of the ACR acquired profile of the Kansas thunderstorm in 1998.

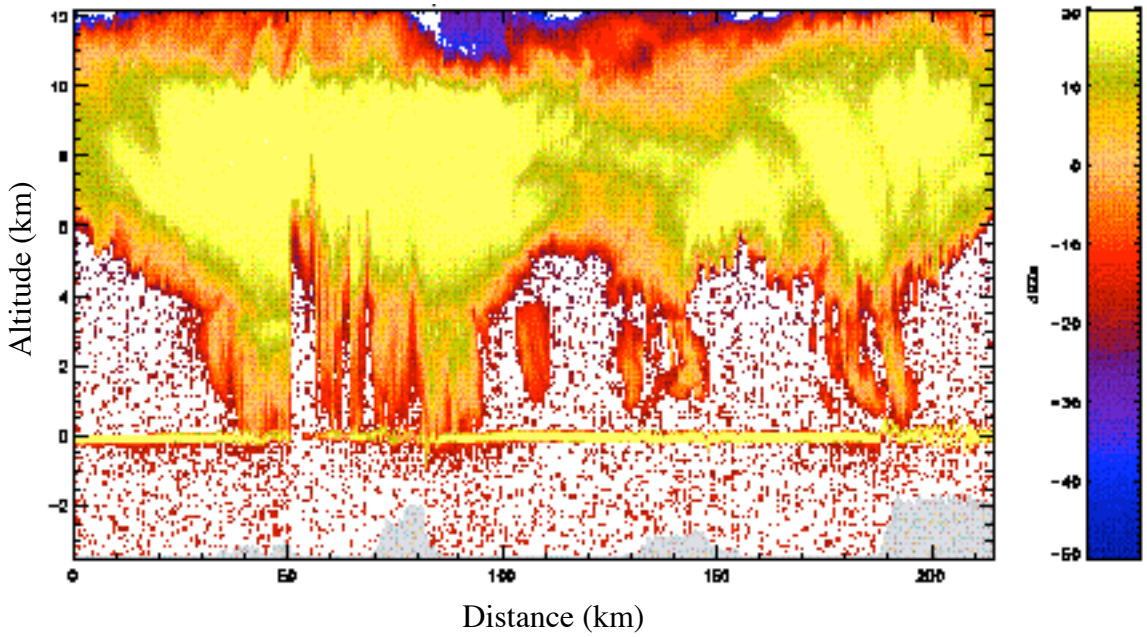

Figure 3.2.8. Vertical reflectivity profiles of the Kansas thunderstorm acquired by ACR along the flight track in 1998.

The 21/37 GHz Upward-Looking Radiometer

The upward-looking radiometer at 21 and 37 GHz is a component of AMMR (Airborne Multichannel Microwave Radiometer) that was developed in the 1970's for precipitation measurements from an aircraft. The unit has been flown in many aircraft (Convair 990, Convair 580, and DC-8) during the past three decades in various field campaigns. It has been re-furbished during year the 2000 and is ready for flights again. It is a fixed-beam Dicke radiometer with a beam width of about 6 degrees. It is currently programmed with radiometric output every second. The temperature sensitivity is < 0.5 K, and the calibration accuracy is about ±4 K. The calibration is performed on the ground by viewing targets of known brightness (e.g., sky and absorber with known brightness temperature). The unit will be installed in one of the windows of the NASA P-3 aircraft such that it will view at a 45° angle from zenith. Thus, it is necessary to spiral the aircraft gradually down to a region below the freezing level in order to make measurements effectively. Ideally, we like to have the aircraft descending at the rate of about 1 km per 5 minutes. The data can also be taken in ascent at a somewhat faster rate if the aircraft has sufficient climb capability. The system requires a bottle of N_2 gas to keep the wave guides dry during the in-flight operation. The data are given in text format tagged with date and time, which will be synchronized with those of the aircraft.

Integration and P3 Logistics

The integration and logistics will be carried out at the NASA Wallops flight facility. A preliminary layout of the instrument package on the NASA P-3 aircraft has been carried out. Figure 3.2.9 shows the details of the instrument configuration.

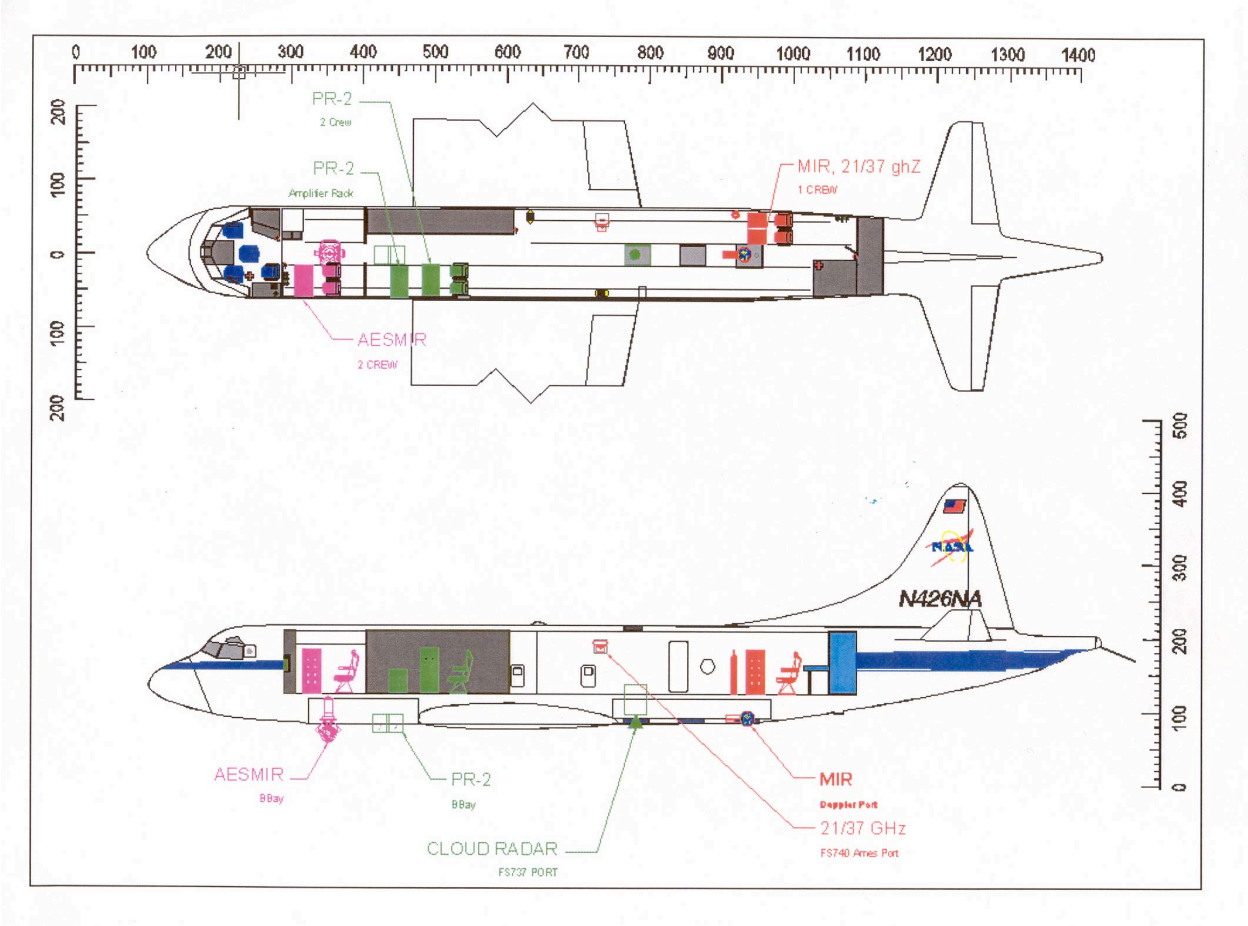

Figure 3.2.9. Accommodation of instruments on NASA P-3 for Wakasa Bay experiment.

3.2.3.5 Wakasa Bay/Japanese Contributions

The Japanese AMSR precipitation validation team will focus on solid precipitation in winter. Since solid precipitation retrievals are still in a developmental stage, it is necessary to collect comprehensive ground based observation of cloud physical variables coincident with simultaneously AMSR and aircraft measurements. The deployment of ground based sensors will follow the observational campaign of 2001.

Field Campaign of 2001

A field experiment was carried out with ground-based instruments around Wakasa Bay from 30 January to 23 February 2001. The X-band Doppler radar of NASDA (NASDA radar) was set up on Kusuyagatake (35.55N, 135.74E, 610m). Dual-frequency (23.8 and 31.4 GHz) microwave radiometers, microrain radars (10.3 GHz), and NOAH rain gauges were established on Maizuru (35.49N, 135.45E) and Hayami (35.46N, 135.26E). A snow particle observation system (SPOS) was also established on Maizuru. This system can shape and observe drop size distribution of snow particles and snowfall amount. The NASDA radar is shown in Figure 3.2.10.

Figure 3.2.10. NASDA C-band dual polarized Doppler radar.

Current research underway centers on a case study of a winter monsoon event. Heavy snowfall with meso-beta-scale snow bands passed over the target region on 14 February 2001. Radar reflectivities of the TRMM PR and the NASDA radar have been compared using scatter diagrams and the Contoured Frequency by Altitude Diagrams (CFADs) (Yuter and Houze, 1995). The qualitative patterns of the radars were similar. However, 4-5 dB biases exist between both radars in the figures. The source of this discrepancy is currently being evaluated. Good agreement was found in the time series between the NASDA radar reflectivity at 2 km height and snowfall amount measured by SPOS in 10-minute intervals. However, the scatter between these sensors dispersed. The result is partly caused by the lack of consideration of the horizontal and vertical movements of the snow particles. Super-cooled, liquid water content (LWC) and precipitable water content (PWC) was also retrieved from the ground-based microwave

radiometer data. As the results, LWC-rich regions (averaged LWC of 0.2 k gm^{-2}) were found around the snow bands. This suggests that the meso-beta-scale snow bands can be detectable over ocean by searching emission from LWC. The correspondence between LWC and surface snow intensity, however, were not very significant. Figures 3.2.11 and 3.2.12 depict the radar reflectivities and Zdr, which is a measure of the particle sphericity and thus a good discriminator of particle phase.

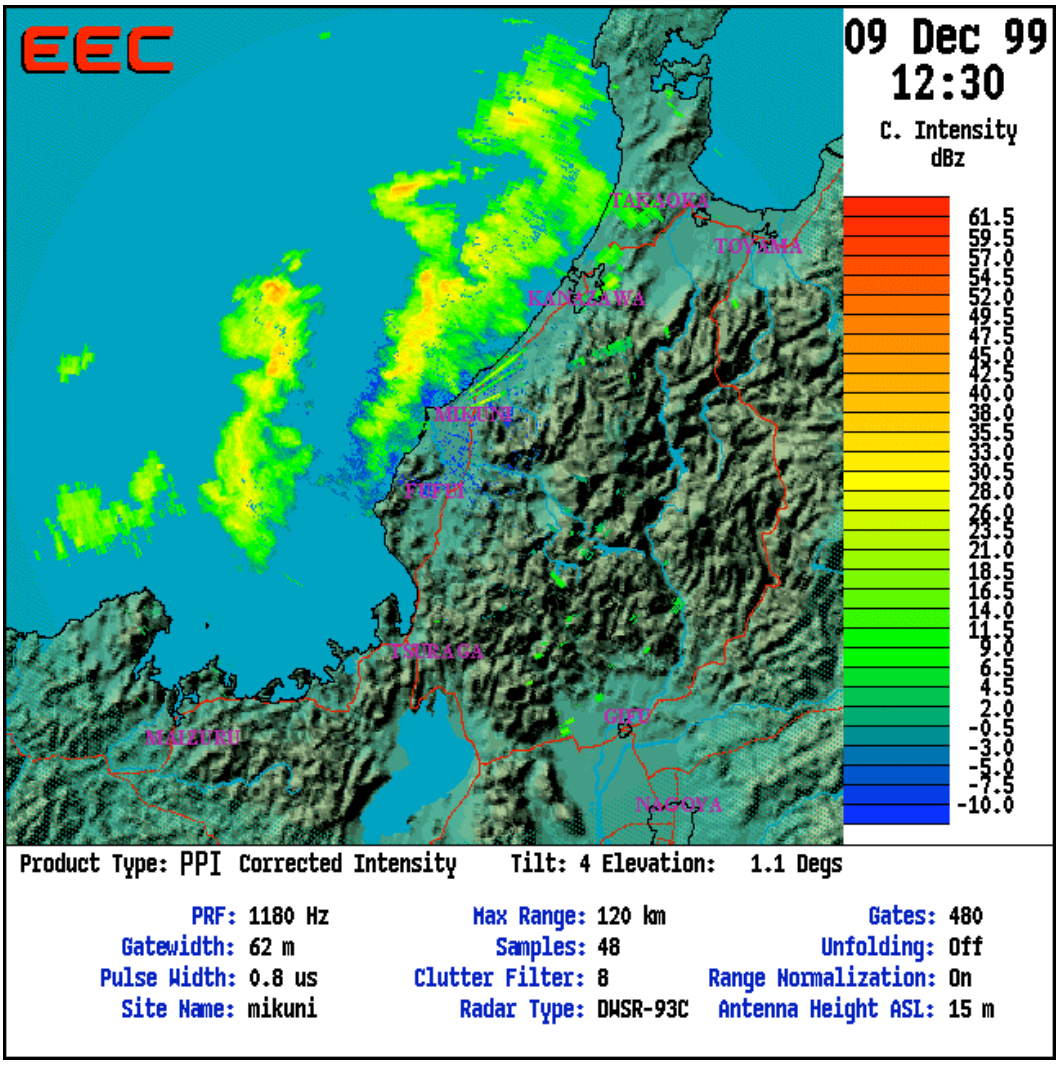

Figure 3.2.11. NASDA radar depicting reflectivities on 09 December 1999.

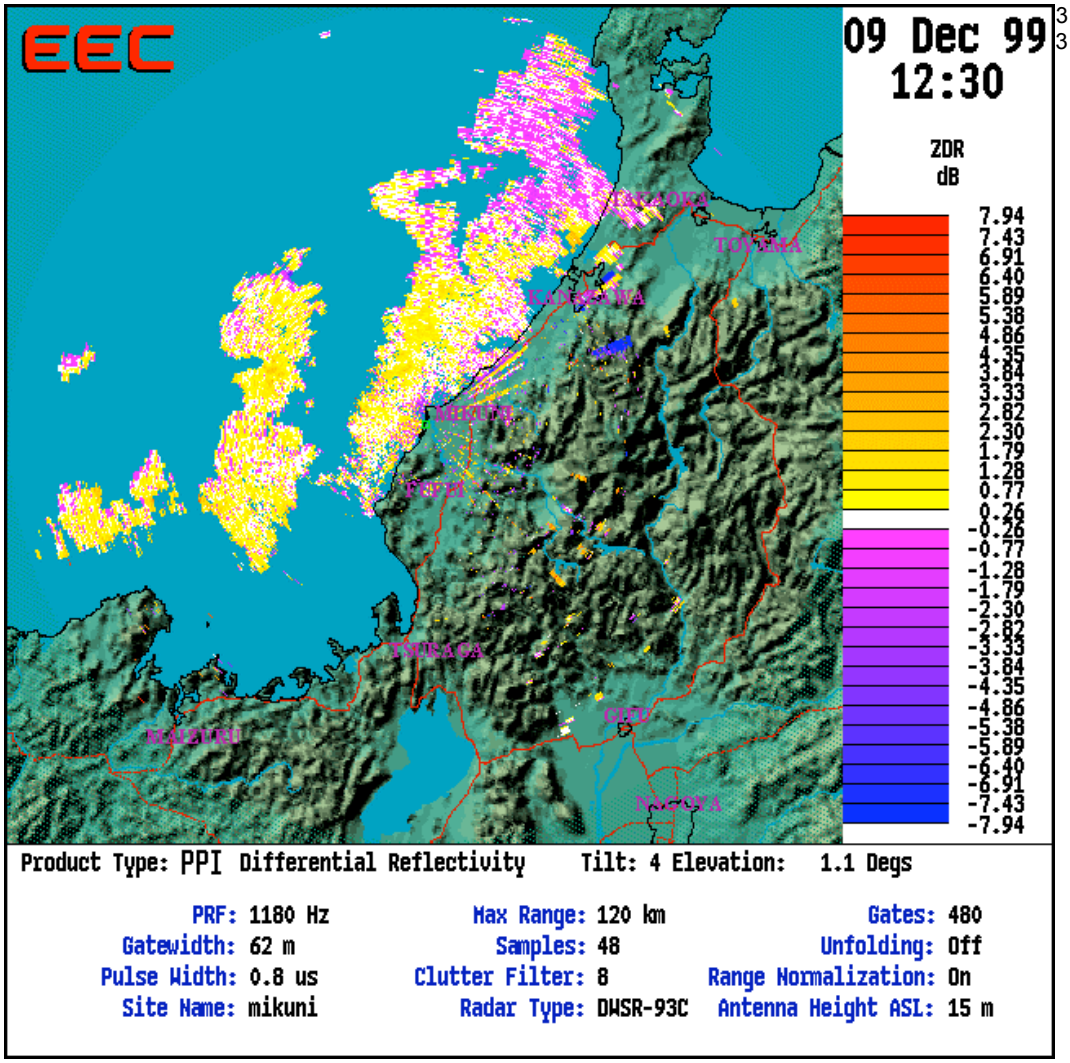

Figure 3.2.12. Cross Polarization (Zdr) observed by the NASDA radar on 09 Dec. 1999.

Current Status of the Observation Project in 2003

The Japanese AMSR precipitation validation team is preparing for the joint research observation with NASA AMSR-E team in 2003. A C-band dual polarization Doppler radar owned by a private company (Sankosha K.K.) has been agreed upon in Japan. A budget request has been submitted to NASDA to fund the contract expenses for this radar for FY of 2002. The main characteristics of the radar (Sankosha radar) are as listed in Table 3.2.4.

Table 3.2.4. C-Band radar characteristics.

Parameters	W-band
Frequency	5260-5700 MHz
Detection range	240 km (rain intensity) 120 km (Doppler velocity, dual polarization)
Antenna beamwidth	1.0˚
Peak Power	250 kW

To obtain dual Doppler coverage, it is also being planning to use the data from another C-band dual polarization Doppler radar that is routinely operated by an electric power company at (36.9 N, 137.0 E). For this end, the Sankosha radar will be installed at a site in Mikuni, Fukui prefecture (36.2 N, 136.1 E)

3.2.3.6 . Wakasa Bay Experiment, Field Phase

We have a number of goals to be addressed in the field phase as enumerated above. Many flight line possibilities will address more than one of these simultaneously. The flight lines are needed in a variety of meteorological situations, all involving fronts. The flight lines are described in Table 3.2.5.

Table 3.2.5. Flight lines. The flight lines are preliminary and will need to be refined and expanded through discussions with all the investigators and with the pilots. The letters in parentheses indicate those goals addressed by each pattern as outlined in Section 3.2.3.4.

Pattern A-WCF (a, d, e)	Extra Tropical Cyclone 1) Fly at maximum altitude. Fly from cold sector behind cold front, across cold front, across warm sector, across warm front and into overrunning in cold sector ahead of warm front until clear of precipitation. 2) Drop down to minimum altitude consistent with safety and retrace line from above to measure temperatures, to determine phase of precipitation, to document cloud liquid water. Use forecast data to determine intial flight lines, refine based on in-flight observations and ground-based radar if available. Typical flight line = 200 km.
Pattern A-O (a, d, e)	As above but across occluded front.
Pattern A-T (a, d, e)	As above but across triple point.
Pattern B-B (b, c, e)	Overfly stratiform rain at maximum altitude to find obvious bright band using JPL radar. Descend at 500 feet/min in a standard rate turn (2 min for 360 degrees) to minimum safe altitude. Drift with wind.
Pattern B-C (e, g)	As above but in stratiform cloud without precipitation.
Pattern L (f)	Overfly ground-based observations at maximum altitude.
Pattern C (radiometric calibration of AMSR)	For radiometric calibration of the satellite, overfly large (>2000 km^2) clear area coincident with a satellite overpass.

A typical flight would consist of several A and B patterns. The A patterns would be used to find good locations for the B patterns. The over-land ferry portions of the flight would be used for L patterns to the extent consistent with air traffic control constraints. If getting good land-snow data proves impossible this way, then some short flights will be dedicated to L patterns late in the deployment. Pattern C is likely to occur in transit at some point in the deployment without specifically planning for it.

The choice of a given pattern would depend on the available meteorology on a given flight day. We would keep a score sheet as we progress and seek to distribute the flight hours among the various objectives in a manner appropriate to their relative priorities.

All of these flight lines are more valuable if coincident with an Aqua overpass, but, given the physical validation nature of the experiments, a flight is still very useful without an overpass as long as the meteorology is suitable.

Flight planning would be initiated in the late afternoon based on forecast frontal positions and refined (or cancelled) the next morning. The satellite timing suggests late morning takeoffs for satellite underpasses. The initial discussion would be among the senior scientists present but no more than about a half-dozen participants. The mission scientist would then develop the flight plan with the designated member of the aircrew. Back-to-back flight days would be minimized to allow for more careful planning of the flights and review of the data between flights. However, there will be some meteorological situations that are too good to pass up.

3.3 AMSR-E Sea Ice Product Validation (D. Cavalieri and J. Comiso)

The Advanced Microwave Scanning Radiometer for EOS (AMSR-E) was successfully launched on NASA's EOS Aqua spacecraft on May 4, 2002. With the launch of this state-of-the-art radiometer, designed and built by NASDA of Japan, the sea ice research community will have available passive microwave sea ice products at a higher spatial resolution and a greater spectral range than previously possible. To make these sea ice products a useful research tool, a comprehensive AMSR-E sea ice validation program has been developed and will be implemented starting in 2003. This document outlines the program which consists of three main components: sea ice product comparisons using coincident high-resolution spaceborne data, comparisons using aircraft and surface data, and sensitivity, error, and model analyses. This validation plan outlines each component and the methods to be used to meet the validation objectives.

The two polar regions of the Earth, the Arctic and the Antarctic, have large sea ice covers that differ markedly in their physical, chemical, and electrical properties because of the very different environmental factors at work during and after sea ice formation. For these reasons and for the reason that the field campaign logistics are quite different in these two regions, this document is divided into two parts. The first part of this document covers the Arctic sea ice validation campaign, whereas the second part covers the Antarctic campaign. Both campaigns have similar validation objectives and each consists of the three main components noted above.

All the AMSR-E sea ice standard products are level 3 products and include sea ice concentration, sea ice temperature, and snow depth on sea ice. These products together with AMSR-E calibrated brightness temperatures (TBs) will be mapped to the same polar stereographic projection used for SSM/I data to provide the research community consistency and continuity with the existing 23-year Nimbus 7 SMMR and DMSP SSM/I sea ice concentration products archived on the SSM/I grid. The grid resolutions are as follows: (a) TBs for all AMSR-E channels: 25-km, (b) TBs for the 18, 23, 36, and 89 GHz channels: 12.5-km, (c) TBs for the 89 GHz channels: 6.25-km, (d) Sea ice concentration: 12.5-km, 25-km, (e) Sea ice temperature: 25-km, (f) Snow depth on sea ice: 12.5. All of the sea ice products will be validated at their respective grid resolutions.

The sea ice concentration products will be generated using three algorithms: the enhanced NASA Team (NT2) algorithm (Markus and Cavalieri, 2000; Comiso et al., 2003), the Bootstrap algorithm (BBA), and the AMSR Bootstrap Algorithm (ABA) (Comiso, and Zwally, 1997; Comiso et al., 2003). In the Arctic, the NT2 algorithm will provide the standard sea ice concentrations at both the 12.5 km and 25 km resolutions. In the Antarctic, the BBA and the ABA algorithms will provide the concentrations at the 12.5 km and 25 km resolutions, respectively. The ABA algorithm requires the 6 GHz data to reduce ice temperature effects and to generate ice temperature maps. Since the resolution of the 6 GHz is too coarse for a 12.5 km resolution retrieval, we use the BBA algorithm that makes use of the same sets of channels used in the Arctic version to generate the latter product. Differences between the algorithm ice concentration retrievals at their respective resolutions will also be provided for each hemisphere. The ice temperature will be produced from the ABA algorithm for both hemispheres and snow depth will be produced from the algorithm described by Markus and Cavalieri (1998) for both hemispheres, but excluding the Arctic perennial ice regions.

3.3.1 Arctic Sea Ice Validation

The Arctic NASA aircraft campaign integrates the requirements for obtaining the field data needed both for the validation of the standard AMSR-E sea ice products and for supporting ongoing studies of air-sea-ice interactions in Arctic coastal polynyas. This latter element falls within NASA's Cryospheric Sciences Program and has as its Earth Science Enterprise goal to understand how the Earth's climate system is changing.

The co-investigators in this campaign are listed below:

J. C. Comiso, E. Kim, and T. Markus Laboratory for Hydrospheric Processes

	NASA Goddard Space Flight Center, Greenbelt, MD 20771
A. J. Gasiewski	NOAA Environmental Technology Laboratory Boulder, CO 80305
J. Heinrichs	Dept. of Geosciences Fort Hays State University, Hays, KS 67601
W. B. Krabill	NASA Wallops Flight Facility Wallops Island, VA 23337
J. Maslanik and J. Stroeve	University of Colorado, Boulder, CO 80309
M. Sturm	Cold Regions Research and Engineering Lab USA-CRREL-Alaska P.O. Box 35170, Ft. Wainwright, AK 99703-0170
K. L. Thornhill and J. Barrick	NASA Langley Research Center, Hampton, VA 23665
B. Walter	Northwest Research Associates, Bellevue, WA 98009

3.3.1.1 AMSR-E Sea Ice products Validation

In the Arctic, sea ice conditions vary considerably from region to region. The approach taken will be to focus on those regions and conditions that are known to give rise to the largest errors and the largest differences between the two sea ice concentration algorithms. From previous comparative studies potential difficulties with both of these algorithms have been identified. These include the influence of sea ice temperature variability on the ABA algorithm retrievals and the influence of atmospheric variability on the NT2 algorithm. Other problems common to both algorithms include ice concentration biases associated with unresolved ice or surface conditions. One example is the low concentration bias associated with the presence of new and young sea ice.

Our strategy will be to utilize a combination of spatially and temporally coincident surface, aircraft, and satellite observations to provide the requisite data needed to meet the validation objectives for the sea ice concentration products. The sea ice temperature and snow depth retrievals are considerably more difficult to validate. Our strategy for snow depth will be to employ both a specially designed airborne radar as well as surface-based snow depth measurements. Temperature validation will also depend in part on surface transects coordinated with aircraft overflights. The following sections will describe in detail the objectives and approach to be taken for the validation of each of these sea ice products.

3.3.1.2 Satellite Measurements of Coastal Polynyas and Surface Heat and Moisture Flux Measurements

Polynyas located over the continental shelves of the peripheral seas of the Arctic Ocean provide a mechanism for the growth of large amounts of ice in limited geographic areas. These areas are a source of relatively large amounts of salt that maintain the cold, halocline layer of the Arctic Ocean (Figure 3.3.1 from Aagaard et al., 1981). Although polynyas cover only 3-4% of the area of the Arctic, they control up to 50% of the ocean-to-atmosphere heat transfer in winter. Recurrent polynyas in the western Arctic form on the Canadian and Alaskan coasts from Banks Island to the Bering Strait and on the Siberian coast from the Bering Strait to the New Siberian Islands and have been the subject of both modeling (Björk, 1989; Winsor and Björk, 2000) and satellite observational studies (Cavalieri and Martin, 1994; Weingartner et al., 1998). The dense shelf water formed in these coastal polynyas depends on the ice production which in turn depends on the ocean to atmosphere heat flux. The observational studies cited above crudely estimate these fluxes over the coastal polynya open water areas by using a combination

of satellite-observed open water areas and either weather station or surface weather analyses data. The sensible heat flux varies by three orders of magnitude as the polynya opens and closes. During winter and early spring large air-sea temperature differences can result in heat fluxes of 500-1000 W/m^2 (Walter, 1989).

Satellite-based measurements of polynya areas may constitute a major source of error in computing ice and dense water production (Cavalieri, 1994; Winsor and Björk, 2000). The principal sources of error result from inaccuracies in measuring the open water area (polynya size), in estimating the meteorological parameters (near-surface air temperature, humidity, wind speed), and in using bulk formulae parameterizations to calculate the heat and moisture fluxes. Another source of error results from neglecting the heat loss over thin ice areas (Figure 3.3.2).

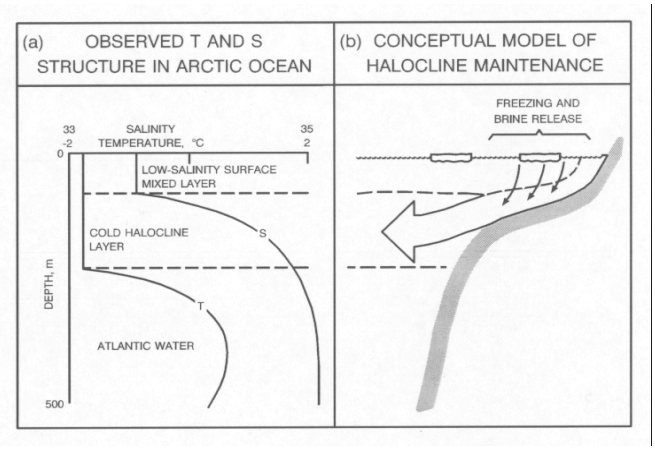

Figure 3.3.1 Schematic diagram illustrating the observed structure of the Arctic Ocean and a conceptual model of how brine release from freezing polynyas maintains the Arctic halocline. From Aagaard et al. (1981).

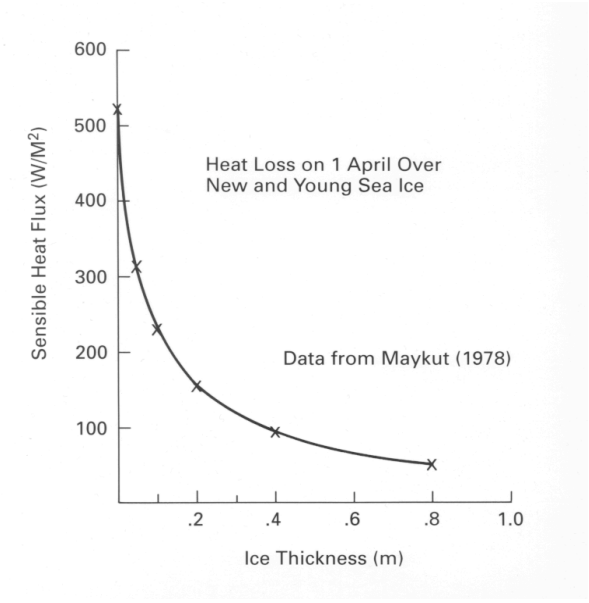

Figure 3.3.2 Heat loss on April 1 over new and young sea ice based on data from Maykut (1978).

Furthermore, modeling studies have shown that the correct parameterization of both the polynya forcing areas (open water area) and the polynya forcing fall-off region (thin ice area) is important to theFigureunderstanding of the production of dense water and its transport across the continental shelf (Gawarkiewicz and Chapman, 1995). Our approach will consist of a series of aircraft flights over selected coastal polynyas to make sea ice concentration, sea ice type, and heat and moisture flux measurements at different altitudes over the polynya and at different distances downwind coordinated with AMSR-E measurements. Specific details of the objectives and methodology are described in the following sections.

3.3.2 Objectives

3.3.2.1 Sea Ice Validation Objectives

The prime objective of the sea ice validation program is to establish statistical relationships between the sea ice parameters derived from the new AMSR-E sea ice algorithms and those same parameters derived from other data sets covering as many geographical areas as possible for different seasons. These parameters include sea ice concentration, and temperature for both hemispheres, and snow-depth on sea ice for the southern polar region and the northern polar seasonal sea ice zones only. Other objectives are to understand the limitations of each algorithm including the reasons for their particular level of performance in different regions and under different conditions, to understand the differences between the NT2 and ABA retrievals, and to suggest improvements to each of the algorithms based on the results of the validation studies.

Validation Criteria

The validation criterion to be used is that the derived AMSR-E sea ice products agree on average with the corresponding validation data set to within the estimated accuracy of the validation data set. The validation data sets will be derived from any one or a combination of field, aircraft, and high-resolution visible and infrared satellite data and are expected to provide a more accurate measure of the standard sea ice products than the AMSR-E retrieved products. The underlying philosophy of this approach is that confidence in the sea ice products derived from the AMSR-E will be achieved by showing consistency of such products with independently derived data that are spatially and temporally coincident (Comiso and Sullivan, 1986; Cavalieri, 1991; Cavalieri, 1992; Steffen and Schweiger, 1991; Grenfell et al., 1994).

Accuracy Goal

Our accuracy goal for each of the sea ice products is based on extensive experience with satellite multichannel passive microwave radiometer data. Table 3.3.1 summarizes previous validation results from SMMR and SSM/I. These goals are provided below for each standard product.

Sea ice concentration: Based on our experience with the SSM/I, the anticipated accuracy of AMSR-E sea ice concentrations will range from 4% to 10%, while that of sea ice concentrations from high resolution satellite and aircraft sensors can be significantly better. The higher the spatial resolution the less significant are errors caused by signature ambiguities within a pixel, particularly when integrated over an AMSR-E footprint. For example, the accuracy of sea ice concentrations derived from cloud free Landsat MSS imagery is estimated to be in the range of 2-4% (Steffen and Schweiger, 1991). Biases relative to the validation data can be reduced through the adjustment of the algorithm tie-points. Our accuracy goal for sea ice concentration ranges from 4% during the dry winter months to 10% during late spring and summer when surface wetness and meltponding make the emissivity of sea ice highly variable both spatially and temporally. Ultimately, we would like to achieve a 4% accuracy for all regions and seasons.

Sea ice temperature: The expected accuracy of sea ice temperatures derived from AMSR-E is estimated to be about 4K based on our experience with the Nimbus 7 SMMR. This estimate is largely dependent on the accuracy of the retrieved sea ice concentration and on the variability of the sea ice

emissivity at 6 GHz. This product represents the physical temperature of the radiating portion of the ice that provides the observed microwave signal. Generally, for first-year ice, the radiating portion is the snow-ice interface, whereas, for multiyear ice, the radiating portion is a weighted mean of the freeboard layer of the ice. The validation data set will be derived using a combination of satellite infrared data, surface field measurements including buoy data, and an ice thermodynamics model. Our accuracy goal for sea ice temperature is 4 K or better.

Snow depth on sea ice: The algorithm uses regression coefficients to derive snow depth on sea ice in seasonal sea ice regions to an estimated regional accuracy of about 4 cm based on our experience with the SSM/I (Markus and Cavalieri, 1998). A comparison of snow depth distributions from ship measurements and from SSM/I snow depth retrievals in the Southern Ocean suggests that the SSM/I retrievals underestimate the in situ measurements by 3.5 cm and that the rms difference is about 4 cm The underestimate results from microwave signal saturation at snow depths of about 50 cm so that snow depths greater than this cannot be detected with the current algorithm. On average, snow depths over first-year ice in the Arctic are typically less than this, but if necessary this limitation may be circumvented by the additional use of the 6 and 10 GHz channels. Temporal information is used to filter retrievals that have been affected by freeze-thaw processes using a threshold of 5 cm per day. Thus, our accuracy goal for snow depth on sea ice is 5 cm. Under winter conditions, the accuracy may be better.

Table 3.3.1 Quantitative Estimates of Algorithm^{+} Accuracy Based on Comparisons With Other Sources of Ice-Concentration Measurements (from Gloersen et al., 1992)

Region	Month	Sensor	Mean Diff. ±1 SD	Ref. Data Set	Ref.
Total Ice Concentration					
Bering Sea	Feb	SMMR	±5% (Thick FY)	Ship reports	(1)
Baffin Bay	Mar-May	SMMR	-3.5%	Landsat MSS	(2)
Baffin Bay	Jun	SMMR	-10%	Landsat MSS	(2)
Beaufort Sea	Oct	SMMR	-1.5%±2.6%	Landsat MSS	(3)
Weddell Sea	Oct	SMMR	0.3%±7.6%	SIR-B	(4)
Beaufort & Chukchi Seas	Sep-Nov	SSM/I	0.6%±7.4%	Landsat MSS	(5)
Beaufort Sea	Mar	SSM/I	-2.1%±3.1%	Landsat MSS	(5)
Bering Sea	Mar	SSM/I	-9.4%±6.1%$^{++}$	Landsat MSS	(5)
Greenland Sea	Sep	SSM/I	-3.7%±1.4%	Landsat MSS	(5)
Weddell Sea	Nov	SSM/I	-1.1%±3.1%	Landsat MSS	(5)
Summary		SSM/I	-3.6%±6.6%	Landsat MSS	(5)
Amundsen Sea	Dec	SSM/I	1.3%±3.6%	Landsat MSS	(5)
Beaufort & Chukchi Seas	Mar	SSM/I	-2.4%±2.4%	NADC/ERIM SAR & NOARL KRMS	(6) (6)
Multiyear Ice concentration					
Beaufort & Chukchi Seas	Mar	SSM/I	5%±4%* 12%±11%**	NADC/ERIM SAR & NOARL KRMS	(6)
Beaufort Sea	Mar	AMMR	-6.0%±14%	JPL C-band SAR	(6)

(1) Cavalieri et al. (1986)	+The algorithm has been used with SMMR, SSM/I, and AMMR data.
(2) Steffen and Maslanik (1988)	
(3) Steffen, unpubl. data (1990)	++Including new ice.
(4) Martin et al. (1987)	*Excluding data from 1 of the 4 flights which gave anomalously large and unexplained biases.
(5) Steffen and Schweiger (1991)	
(6) Cavalieri et al. (1991)	**Including data from all 4 flights.

3.3.2.2 Arctic Coastal Polynya Objectives

Satellite Measurement of Coastal Polynyas

There are two important objectives that will be addressed. The first objective is to assess the accuracy to which the AMSR-E sea ice concentration algorithms can map the size of coastal polynyas and to measure the degree of low ice concentration bias, if any, resulting from the presence of thin ice. Previous studies of Arctic coastal polynyas using SMMR and SSM/I sea ice algorithms (e.g., Cavalieri and Martin, 1994) may have overestimated polynya areas by up to 40% (Winsor and Björk, 2000). On the other hand, these observational studies measure only the open water area of the polynya and neglect the polynya thin ice areas. Neglecting areas of thin ice results in an underestimate of the sensible heat loss from ocean to atmosphere during winter. Figure 3.3.2 illustrates the magnitude of heat loss over new and young sea ice in winter. The higher spatial resolution of AMSR-E relative to SMMR and SSM/I is expected to greatly improve the mapping of coastal polynyas.

Surface Heat and Moisture Flux Measurements

The second objective is to measure directly surface heat and moisture fluxes over coastal polynyas to evaluate the parameterizations currently used in bulk formulation models and to measure the fall off of these fluxes downwind. A related issue is how the fall off of these fluxes downwind of the polynyas are related to the increase in sea ice concentration and ice thickness. The spatial dimensions of both the 'forcing' (open water area) and the 'forcing decay' (thin ice area) regions of the polynya are important parameters in theoretical models of dense water formation and its transport across the Arctic shelf (e.g., Gawarkiewicz and Chapman, 1995).

3.3.3 Validation Data Sources

The relatively large footprints of the AMSR-E sensor, the variable nature of sea ice over space and time, and the complex logistics associated with polar operations make the sea ice products particularly difficult to validate. The validation program for sea ice will therefore rely heavily on the analysis of coincident sea ice data sets from aircraft and satellite. Coordinated surface and aircraft measurements will be particularly important for providing the validation data for snow depth and sea ice temperature. The spatial resolutions of the comparison data sets range from the 25-m Landsat 7 ETM+ imagery at the high resolution end, to 100-m (at nadir) aircraft passive microwave imagery, and 1-km resolution AVHRR imagery. High (meter- to sub-meter) resolution aerial digital photographs and video from the P-3 and from uninhabited aerial vehicle flights will augment these data. The spatial resolutions of the level 3 sea ice products are 12.5 km and 25 km.

3.3.3.1 Satellite

Passive and Active Microwave

In addition to EOS Aqua AMSR-E, several other satellite multichannel microwave imaging radiometers will be in orbit within the next year. This will allow an intercomparison of sea ice retrievals

from the different radiometers and will provide a basis for assessing retrieval differences resulting from differences in calibration and in diurnal variations. Current and anticipated satellite passive microwave sensors in addition to AMSR-E include:

(a) ADEOS II AMSR launched on December 14, 2002.
(b) Special Sensor Microwave/Imager (SSM/I) on the DMSP F13, F14, and F15 spacecraft.
(c) Special Sensor Microwave Imager/Sounder (SSMI/S) to be launched in 2003 on the DMSP F16 spacecraft.

Active microwave satellite sensors are more limited in their usefulness, because of the inherent difficulties of resolving backscatter ambiguities, but are potentially valuable sources of data for validating sea ice extent and ice type (first-year and multiyear). These sensors include high-resolution RADARSAT and QuikSCAT and will be particularly useful in areas of persistent cloud cover and during periods of polar darkness where visible and IR sensors can not be used.

Visible/IR

Under favorable conditions, high-resolution visible and infrared sensors including for example Landsat-7 ETM+, DMSP OLS, ADEOS II GLI, NOAA AVHRR, and MODIS (both Terra and Aqua) imagery will be acquired. Landsat 7 ETM+ imagery is particularly useful with its 25-meter spatial resolution (including a 15-meter panchromatic band). This high resolution capability has been used to identify melt features such as melt ponds, which cause low ice concentration biases in the AMSR-E algorithms (Markus et al., 2001). Landsat imagery has also been used for the validation of Nimbus 7 SMMR and DMSP SSM/I sea ice data sets (Steffen and Schweiger, 1991; Steffen and Maslanik, 1988) as well as in sea ice algorithm comparisons (Steffen et al., 1992; Comiso et al., 1997).

3.3.3.2 Aircraft and instruments

NASA P-3B

A key component of the validation effort is the acquisition of high resolution passive microwave radiometer data at the same frequencies and polarizations as those measured by AMSR-E. The platform for acquiring these data will be the NASA Wallops Flight Facility (WFF) P-3B aircraft (Figure 3.3.3). The P-3 aircraft is a 4-engine turboprop capable of long duration flights of 8-12 hours, large payloads up to 15,000 pounds, altitudes up to 30,000 feet and true airspeeds up to 330 knots. More detailed information may be obtained from the Web site www.wff.nasa.gov. A summary of the performance of this aircraft is reproduced from the Web site and is given in Table 3.3.2.

Figure 3.3.3 NASA WFF P-3B aircraft.

Table 3.3.2. NASA P-3B Altitude, range and airspeed matrix.

	High Altitude 5-30K Feet	Medium Altitude 10-25K Feet	Low Altitude 500-10K Feet
Endurance (Hours)	12	10	8
Range (Nautical Miles)	3,800	3,000	2,400
Speed (Knots)	330	300	270

Passive Microwave Radiometry

The passive microwave radiometer to be used for the field campaign is the NOAA Environmental Technology Laboratory (ETL) Polarimetric Scanning Radiometer (PSR). The PSR system simulates all the AMSR-E bands and is compatible with the Wallops P-3 aircraft. A summary of the PSR specifications is given in Table 3.3.3.

Table 3.3.3 Polarimetric Scanning Radiometer specifications.

SCANHEAD	FREQUENCIES (GHz)	POLARIZATION	BEAMWIDTHS
PSR/A	10.6-10.8	v,h,U,V	8^o
	18.6-18.8	v,h,U,V	8^o
	21.4-21.7	v,h	8^o
	36-38	v,h,U,V	2.3^o
	86-92	v,h,U	2.3^o
PSR/CX	5.82-6.15	v,h	10^o
	6.32-6.65	v,h	10^o
	6.75-7.10	v,h,U,V	10^o
	7.15-7.50	v,h	10^o
	10.6-10.8	v,h	7^o
	10.68-10.70	v,h	7^o

Snow Radar

The snow radar (currently under development by S.P. Gogineni, T. Markus, and G. Prescott) will be an airborne stepped frequency pulse radar operating in the frequency range of 2 to 18 GHz. The anticipated vertical resolution is 2 cm. The proposed instrument provides the only means to measure adequately snow depth at spatial scales comparable to the AMSR-E. First tests of this instrument over sea ice will take place in October 2003 on the Australian research icebreaker Aurora Australis in East Antarctica. Radar development (hardware and software) is anticipated to be completed in time for the 2005 Arctic field campaign.

Infrared Radiometry and Photography

NASA Langley Research Center will operate a nadir viewing PRT-5 infrared radiometer. Aerial phototgraphy will be provided by NASA Wallops video and digital cameras for the characterization of surface conditions. In addition, a video camera and an IR radiometer (9.6-11.5 _m) will be boresited with the PSR radiometers.

Gust Probe System

The NASA Langley Research Center Turbulent Air Motion Measurement System (TAMMS) on the WFF P-3 is composed of several subsystems including: (1) distributed pressure ports coupled with

absolute and differential pressure transducers and temperature sensors, (2) aircraft inertial and satellite navigation systems, (3) a central data acquisition/processing system, and (4) water vapor instruments and potentially other trace gas or aerosol sensors.

The angle of ambient airflow relative to the aircraft is determined using the five-hole pressure port technique as described by Brown et al (1983). For this technique, five flush pressure ports (each with a diameter of ~ 0.6 cm) have been integrated into the P-3 radome in a cruciform pattern. Flow angle measurements, angle of attack and sideslip, are obtained from differential pressure measurements made between the pair of vertically aligned ports and horizontally aligned ports, respectively. The center hole is linked to existing static pressure ports on the side of the fuselage to provide required dynamic and total pressure measurements.

The differential pressure fluctuations can then be used to calculate the u, v and w velocity components relative to the aircraft. Combining these measurements with information from the Inertial Navigation System (INS) allows the calculation of the wind velocity components with respect to an earth-based coordinate system. A Global Positioning System (GPS) is used to correct for long-term drifts in the INS.

Air temperature measurements needed to determine true air speed, Ua , as well as heat flux are made within a non-deiced total air temperature Tt sensor housing using a fast-response platinum sensing element (E102E4AL).

A Lyman-Alpha hygrometer manufactured by Atmospheric Instrumentation Research, Inc (model AIR-LA-1AC) is used to provide fast response water vapor measurements. A slower response General Eastern 1011B hygrometer designed for airborne applications is mounted in close proximity and used to normalize the Lyman-Alpha signal. The Lyman-Alpha instrument will be upgraded with a new fast response water vapor sensor for the field program proposed for 2003.

The fluctuations in velocity (u', v', w'), the air temperature (T') and water vapor (q') are recorded at a frequency of 20 Hz by an onboard data system. These values are then used to calculate turbulent fluxes of momentum (u'w', v'w'), heat (T'w'), and moisture (q'w') using the covariance method.

In addition to the output of TAMMS system sensors, display of three-dimensional winds will also be provided in near real time aboard the aircraft. Work is underway to incorporate the aircraft true airspeed and vertical velocity correction algorithms into the TAMMS data acquisition software so that winds of relatively high accuracy can be calculated from the raw input signals. There are plans to provide wind information at 0.1 second intervals to facilitate direct calculation of meteorological fluxes.

NSF Aerosonde UAV

As noted earlier, a need exists to map the surface at very high resolution and below cloud cover as well as to obtain atmosphere column information coincident with AMSR-E and P-3 overpasses. Aerosonde Uninhabited Aerial Vehicles (UAVs) can provide these capabilities. The Aerosonde is a small, robotic aircraft designed to undertake a wide range of operations in a highly flexible and inexpensive mode (Holland et al. 1992; Holland et al., 2001). The aircraft, developed by an US-Australian consortium, entered limited operations in 1999. Current operations and further development are being undertaken by Aerosonde Robotic Aircraft and Aerosonde North America (See www.aerosonde.com for details.) The Aerosonde conducts a defined mission in a completely robotic mode. However, all flights are under the command of a ground controller who can change missions and respond to air traffic control requests. An NSF-funded project as part of the Office of Polar Programs' Long Term Observations program is now underway at Barrow to deploy Aerosondes for routine mapping and atmospheric sounding missions (J. Curry, PI; J. Maslanik, Co-PI). The validation effort will take advantage of these operations See http://paos.colorado.edu/~curryja/aerosonde/index-frame.html for more information. Specifications and performance of the Aerosonde are listed below, in Table 3.3.4.

Table 3.3.4 Specifications and Performance for the Operational Mark 2 Aerosonde

Aerosonde Specifications	
Weight	14 kg
Wing Span	2.9 m
Engine	24cc fuel-injected pusher-prop.
Navigation	GPS, DGPS
Aerosonde Performance	
Speed	Cruise 18-32 m s^{-1}; climb 2.5 m s^{-1}
Range	>3000 km (with 1 kg payload)
Endurance	>30 h
Altitude Range	20->7000 m (intermediate weight payload)
Communications	UHF radio, low earth orbit satellite
Payload	2 kg with full fuel load; 5 kg maximum
Instrumentation	Air temperature, pressure, humidity (Vaissala sensors), digital photography (Olympus C-3030 camera), infrared temperature (Heitronics KT-11 pyrometer), aircraft icing sensor, video camera with short-range transmission. A laser altimeter is expected to be available by spring 2003

Aerosondes operate in fully robotic mode, using onboard avionics and pre-programmed flight plans. Radio communication can be maintained with the aircraft via UHF ground link and/or via low earth orbit satellite. The latter allow flights well beyond UHF radio range of approximately 200 km. Testing is underway using LEO satellites (Iridium system) for Barrow-based operations. Up to three Aerosondes can be operated simultaneously to increase the effective payload per mission and to acquire coincident data at different altitudes.

For the AMSR-E validation effort, the types of data to be available from UAV flights will include:

- profiles of air temperature, pressure, and humidity.
- detailed photographic imaging of surface features at sub-meter resolution;
- skin temperatures along flight tracks;
- estimation of sea ice concentration, ice type, surface roughness, lead fraction, ridging fraction, and approximate ice thickness using a laser altimeter;

Flights will be conducted from the NARL airfield near Barrow. Typical flight patterns include atmospheric soundings at various locations along the flight tracks, and surface mapping missions at various altitudes. The majority of the flight hours will be dedicated to extended transects flying at relatively low altitude (200 to 400 m) for mapping of surface conditions. A typical pattern to provide statistics regarding surface conditions would involve 5 east-west flight tracks of 150 km length each, spaced evenly at 25-km apart. Such missions would require approximately 10 hours of flight time. When cloud cover is present, and for selected clear-sky cases, the flight plan will include stacked patterns (for example, below and above cloud cover) to acquire data needed to assess the effects of the atmospheric column and clouds on AMSR-E product accuracy.

A second mode will involve maintaining coverage over specific, localized areas for long durations, spanning approximately 20 hours. This continuous data collection over regions of dynamic or newly-forming ice will allow us to study how changes in pack ice and atmospheric conditions affect a time series of AMSR-E data from multiple Aqua overpasses. As discussed earlier, the two sea ice algorithms have different sensitivities to atmospheric and surface conditions, so data are needed to assess how these differences affect the products. The mission plans will focus on observing the pack ice under a range of weather and ice conditions coincident with Aqua overpasses. Details of flight operations are given in Section 3.3.5.3.

3.3.4 Surface Measurements

3.3.4.1 Barrow

The in situ data collection effort will begin with a general mapping of Barrow-area fast ice conditions prior to the P-3 flights and surface measurements using satellite SAR imagery if available, augmented by information from local ice experts and aircraft reconnaissance (Figure 3.3.4). This ice mapping will then be used to identify specific ice conditions for subsequent surface measurement. Although the precise coverage will vary depending on local conditions, the likely areas to be sampled will lie within 25 km of Barrow for in situ measurements on fast ice, with a typical maximum extent of fast ice of about 20 km from shore.

The shore-fast ice along the north coast of Alaska, particularly near Barrow, generally includes most of the major sea ice and snow classes found further north in the Arctic Basin, albeit in smaller units or floes. The fast ice parallels the coast and tends to have a banded structure, but by ranging parallel to the coast, we intend to sample a sufficient number of floes of suitable size for representative ice and snow conditions. These sampling locations will be augmented by making measurements on the saline ice which covers Elson Lagoon (an area of approximately 15 km by 50 km consisting of uniform first-year ice) and fresh-water ice on lakes in the Barrow area. The relatively fine resolution of the NASA P-3 PSR imagery will result in pure-pixel observations over the sample locations. Results of the comparisons between field conditions and brightness temperatures observed by the P-3 can then be scaled up to be appropriate to AMSR-E resolutions.

Our sampling strategy will be to make a preliminary identification of suitable floes in each ice and snow class in the fast ice zone as noted above. We will then visit these target floes during a reconnaissance traverse. Based on observed surface characteristics and sampling, we will identify the set of floes to be targeted by the aircraft (P-3 and Aerosondes). A stratified sampling technique will be used to help assure adequate sampling over the various surface types available. The measurement strategy will take advantage of experienced gained during the Surface Heat Budget of the Arctic (SHEBA) experiment, where the investigators developed an efficient system for traversing and making measurements on ice. During SHEBA, over 500 km in 20 km legs were surveyed using snow machines. No suitable aircraft are presently in place for lease in the Barrow area to assist in the sampling. A small helicopter (a Bell-47) may be available for some reconnaissance and sampling work, although the flight area is limited to fast ice only, and only one passenger and minimal gear can be carried.

A key element of the Barrow-area effort is the use of data collected at multiple scales as a means to extrapolate limited in situ data to larger areas. It is thus imperative that it be possible to match observation locations among the in situ, aircraft, and satellite data. GPS and collection of ground control points (GPS locations of particular features) will assist with this. However, we will also investigate the potential of devices such as point-source microwave transmitters, flares, targets, or other means that could be deployed on the ice to help improve the co-registration of different data sets.

A variety of tools developed over the past few years will be used to quickly, efficiently, and adequately sample those target floes for which we plan to obtain aircraft data. A GPS base station will be set-up and operated at NARL near Barrow. All snow and ice measurements can thus be associated with precise GPS positions. Measurements will be made along multiple traverse lines spanning the floes (or ridges in the case of deformed ice), and in some cases, on a grid network on individual floes. Near-continuous measurements of snow depth will be made using an automatic snow depth probe which we have developed (U.S. Patent 4600842) and a sled-mounted FM-CW X-band radar (Holmgren et al., 1998). An up-grade to the radar has just been completed which allows the radar system to collects snow depth and GPS position data simultaneously, permitting mapping of considerable areas of the snow cover on the ice in detail. In addition to providing direct comparison data for PSR and the AMSR-E algorithms, the transects of radar-derived snow information will be useful for interpreting the planned aircraft snow radar if funding is available for an in situ campaign during 2005.

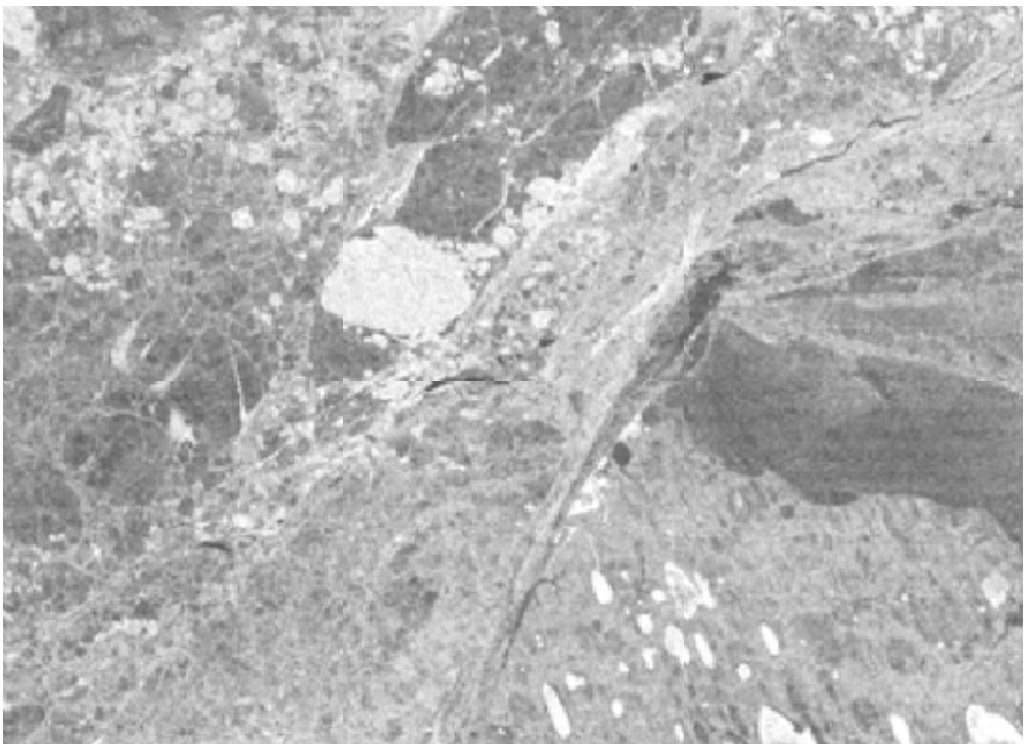

Figure 3.3.4 The Barrow in situ study area, illustrating variations in sea ice and land conditions apparent in synthetic aperture radar data (RADARSAT image courtesy RadarSAT International).

Closely-spaced (every 0.5 m) measurements of the snow-ice interface temperature will be made on traverse lines using thin probes (Patent 5815064). Continuous measurements of snow temperatures will recorded using mini-data loggers (Onset Computer Corp.) installed at the start of the intensive field campaign. At frequent intervals along traverse lines, snow texture, snow grain size, snow stratigraphy, and snow/ice interface temperatures will be determined in snow pits. At SHEBA (Sturm and others, in press) and in the Antarctic (Sturm and others, 1998) developed methods that allow rapid identification and quantification of snow characteristics. These methods will be used and improved upon for the planned work. At snow pit locations, ice thickness will be determined by drilling through the ice, and ice cores will be obtained from a sub-set of these locations for later analysis of ice type, brine pocket density, and percentage snow-ice, if any, and other properties needed for interpretation and modeling of microwave emission. Snow/ice profile temperatures will be obtained at selected locations using thermistor chain systems employed by D. Perovich.

In addition to these surface measurements, the validation effort in the Barrow area will take advantage of the ground-based remote sensing data obtained by the Dept. of Energy's Atmospheric Radiation Monitoring (ARM) site (http://www.arm.gov/docs/sites/nsa/nsaaao.html) and NOAA's Climate Monitoring and Diagnostics Laboratory site near Barrow (http://www.cmdl.noaa.gov/obop/brw/index.html), and the National Weather Service station in Barrow. These ongoing operations provide atmospheric state variables, vertical profiles, radiative fluxes, and cloud information. These data, along with atmospheric information acquired by Aerosondes and the P-3, will be used to assess the performance of atmospheric corrections and as input to modeling. We also intend to make use of the available suite of ice and atmospheric information collected during the SHEBA experiment. These data will, in particular, be useful for refining radiative transfer and ice temperature modeling.

3.3.4.2 Navy Ice Camp

Additional measurements will be made at an ice camp that will be installed by the U.S. Navy. This camp will be located in the Beaufort Sea. The camp is scheduled to be deployed on or about March 17th, leaving a window of 5 days during which the NASA P-3 will be in Alaska and the camp location will have been determined and fixed. As soon as the camp can be occupied, science personnel will proceed to the camp. At the camp, it is anticipated that extensive measurements of snow depth and ice thickness will be made on one or several lines of 1 to 3 km length. It is likely that both first-year and multiyear ice will be present near the camp, so both of these ice types will be sampled. At the current time, it is anticipated that snow depth will be measured using hand and automatic probes, and that ice thickness will be measured using the EM-31 and checked by drilling holes. Only limited snow properties (layers, density) will be recorded, and there are no plans to take ice cores. A coordination meeting hosted by the Navy is planned for February 10, 2003. At that meeting, we plan to discuss protocols for how the camp location will be transmitted to the NASA team, how line orientation will be decided, and whether laser altimetry from the aircraft is desired.

3.3.4.3 Nome

We are investigating the feasibility of carrying out Aerosonde operations based at Nome, to complement the P-3 flights over the Bering Sea during 2005. No concurrent in situ measurements are planned at this point.

3.3.4.4 Other Field Programs of Opportunity

Plans by other groups for experiments that could contribute to the AMSR-E validation effort are continuing to evolve. These include proposals for detailed study of the Barrow-area fast ice, a possible ice-research camp in the Beaufort Sea in 2003, and the Ross Island Meteorology Experiment (RIME) under consideration for 2003-2005. We intend to follow the progress of these plans, and will attempt to capitalize on such efforts where possible.

3.3.5 Approach

3.3.5.1 Sea Ice Validation Approach

The approach for meeting the validation objectives is one of compiling and analyzing spatially and temporally coincident data sets for comparison with the AMSR-E sea ice parameters. Another key element in the approach is the utilization of modeling and sensitivity studies (section 5). Coincident or nearly coincident observations will be obtained from surface measurements, coordinated NASA and NSF Aerosonde UAV underflights covering several AMSR-E footprints, and from other satellite sensors. While the focus of the planned aircraft campaigns is on winter conditions, we intend to take advantage of pond statistics derived from Aerosonde flights planned as part of the ongoing NSF effort in Barrow to assist in the validation of AMSR-E sea ice concentrations during the melt season. During June/July 2000, an AMSR-E prelaunch aircraft campaign called Meltpond2000 (Cavalieri, 2000) was undertaken to validate the NT2 algorithm under melt conditions using the airborne PSR system, but because of problems with the 89 GHz V-pol. channel validation with aircraft data could not be undertaken. Instead, Landsat 7 ETM+ imagery is currently being used.

The Arctic regions selected for the aircraft campaigns were chosen because they give rise to the largest retrieval errors during the winter season. A more detailed discussion of the attributes of each region is provided later on in this section. The approach is necessarily sea ice product specific. The following is a summary of the validation methods to be used for each standard product.

Sea Ice Concentration: The primary approach for the validation of retrieved AMSR-E sea ice concentrations is to utilized data from dedicated aircraft campaigns in conjunction with high resolution satellite data, including those from Landsat 7, Terra and Aqua MODIS and ASTER, NOAA AVHRR,

DMSP-OLS, RADARSAT, and scatterometers. The P-3 aircraft data will provide high-resolution measurements of brightness temperatures and subsequently ice concentrations for selected regions, whereas the visible and IR satellite data provide for wider spatial and temporal coverage (Figure 3.3.5). An example of the type of comparison that will be undertaken with Landsat 7 ETM+ data is illustrated in Figure 3.3.6.

Digital imagery from the Aerosonde flights will depict surface conditions at sub-meter resolution. Surface skin temperature profiles acquired by the Aerosonde yield comparison data for ice temperatures and provide information on thin-ice coverage and presence of leads. Variations in spectral albedo (for the visible channels) or changes in surface temperature (for the infrared data) can be used for proxies not only of ice concentration but also of ice thickness. The focus of the P-3 campaigns will be on those regions that exhibit large retrieval errors based on past studies. Although aircraft passive microwave data provide essentially the same type of information as the AMSR-E, the much higher spatial resolution will allow the identification of pure surface types and direct comparison with in situ measurements, and therefore the investigation on how specific surface types translate in the sea ice concentration retrievals. Furthermore, with varying aircraft altitude, the dependence of the atmospheric contribution on the retrievals can be studied. High-resolution active microwave satellite systems, such as RADARSAT, are most useful during persistent cloud cover and during polar darkness. Data from microwave scatterometers, such as those from QuikSCAT, will be utilized for identifying areas of divergence and ice drift. However, data from active systems are more difficult to interpret than those from passive and visible systems, because of unpredictable backscatter from different ice types, from open water within the ice pack, and from wind-roughened seas.

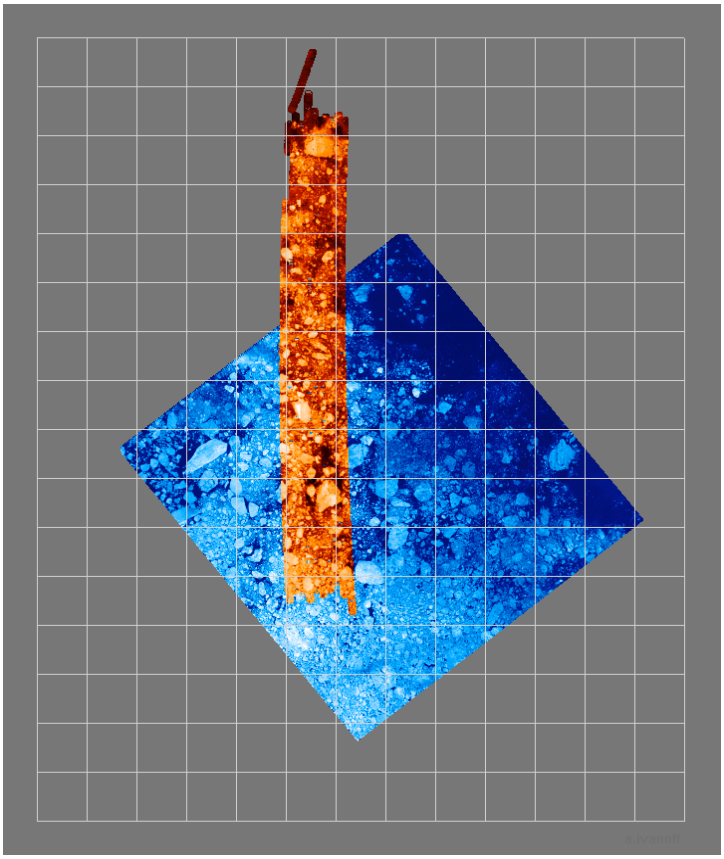

Figure 3.3.5 Landsat 7 ETM+ Image of Baffin Bay with NOAA ETL Polarimetric Scanning Radiometer brightness temperature (19 GHz, V pol.) mosaic overlain (outlined in black) for June 27, 2000. The Landsat and microwave data are gridded at a resolution of 0.5 km. The 25-km SSM/I grid is also shown for comparison.

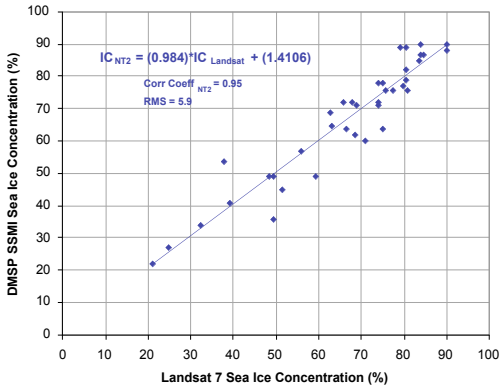

Figure 3.3.6 Comparison of DMSP SSM/I and Landsat 7 ETM+ sea ice concentrations for June 27, 2000 during Meltpond2000. The ETM+ image is shown in Figure 3.3.5.

One important aspect of the sea ice concentration validation is the effect of weather on the sea ice concentration retrievals. This is particularly important for those retrievals derived from the NT2 algorithm which makes use of the AMSR-E 89 GHz channels. To this end, we are planning a series of Aerosonde UAV flights for the purpose of mapping surface characteristics under a variety of atmospheric conditions. These will be coordinated with the NASA P-3 flights and will occur both above and below the cloud cover. The coordinated data collection effort (including the P-3, Aerosondes, surface sampling, and surface-based remote sensing) is designed to provide a suite of data extending from the surface through the atmosphere to an altitude of about 6 km. In addition to general mapping of surface features, the data collection plan is intended to support analysis of the effects of the atmospheric column and of short-period temporal variations in surface conditions on AMSR-E brightness temperatures. The UAV flights will provide profiling of the atmospheric column and transects measuring sea ice conditions out from the Alaskan coast to a distance of about 1500 km. Atmospheric observations from NOAA and DOE facilities near Barrow will provide additional data for establishing atmospheric conditions during these underflights.

Another concern is the sensitivity of the ice concentration retrievals to sea ice temperature variability. This issue will be addressed both from algorithm sensitivity analyses and from closely-spaced in situ snow-ice interface measurements made along Barrow-based transects and from temperature profiles in the ice/snow column provided by thermistor chains. These transects will be overflown by the P-3 aircraft. The P-3 will provide high-resolution measurements of brightness temperatures and surface temperatures using an IR radiometer. Details of the aircraft instrumentation are presented in section 3.3.3.2 and those of the surface measurements are presented in section 3.3.4.

Sea Ice Temperature: Sea ice temperature will be obtained using the ABA algorithm. For first-year sea ice, the ice temperature derived from the vertically polarized 6.9 GHz channel represents the temperature of the sea ice surface at the snow/ice interface, because at this frequency the snow cover is transparent to the radiation. For multiyear ice, the derived sea ice temperature represents a weighted-average of the freeboard portion of the ice. The primary technique for the validation of AMSR-E ice temperature is to make use of empirical relationships between the ice temperature and snow surface temperature in comparison with aircraft and satellite (i.e., MODIS and AVHRR) thermal infrared data. Sea ice temperature retrievals obtained with the high-resolution P-3 aircraft microwave radiometers will also be compared with the Barrow-based surface transect measurements and thermistor-chain vertical profiles to assess errors associated with the use of empirical parameters. Further refinements of the empirical parameters will be made as more field data become available and through the use of a thermodynamic model of sea ice and snow.

The retrieved ice temperatures will be further validated using surface temperature data from Arctic buoys and other platforms. While these are only point measurements, arrays of buoys exist and they provide continuous measurements that can be used to check the temporal consistency of the derived AMSR-E temperature data. The temperature algorithm was developed through the use of 6.6

GHz data that were observed by the Nimbus-7 SMMR and historical buoy and field data. The SMMR data, however, have limited value for testing the effectiveness of the AMSR-E algorithm because of very large footprint and instrumental problems associated with polarization mixing.

Snow Depth on Sea Ice: Because in situ snow depth observations over sea ice are so sparse and because surface measurements are so costly to acquire, the validation strategy is to utilize an airborne sensor to measure snow depth on sea ice. While the planned in situ snow depth measurements on Barrow fast ice will provide data to validate the algorithm using the P-3 PSR radiances, the airborne radar is the only way to provide the spatially and temporally coincident measurements needed to validate snow depth over large areas commensurate with the 12.5-km snow depth product resolution. As noted previously, an airborne radar with the capability to measure snow depth is currently under development. The development and testing of this radar is expected to occur in time for the 2005 aircraft campaign. For the 2003 campaign, our approach will be to obtain the snow depth retrievals using the P-3 airborne microwave radiometers and to compare these retrievals to the Barrow-based in situ snow depth measurements. In addition to snow depth, snow texture, grain size, and snow stratigraphy will be measured to help understand the sensitivity of the algorithm to these parameters and to make algorithm improvements. Available snow depth measurements made from ships such as those compiled by Markus and Cavalieri (1998) will be used to help validate the AMSR-E snow depth retrievals. Qualitative checks will also be made through comparisons with AMSR-E ice type maps and with MODIS, LANDSAT, and AVHRR images.

Beaufort and Northern Bering Seas (March 2003)

The rationale in selecting these regions for AMSR-E sea ice validation is that the largest errors in winter Arctic sea ice concentration retrievals occur in the seasonal sea ice zones (SSIZs). These very dynamic regions consist of various unresolved ice types and very different sea ice surface conditions. A comparison of the original NASA Team and Bootstrap algorithm retrievals using SSM/I data shows that the Bering Sea is a region showing some of the largest differences in the Arctic (Comiso et al., 1997). These differences result from the wide variety of ice types (new, young, and thin FY ice) and surface conditions (e.g., variations in snow depth) that exist in this SSIZ. In contrast, the microwave signatures of older first-year ice and perennial (multiyear) ice types found in the Beaufort Sea contrast sharply with the Bering Sea ice types. Other validation issues to be addressed in these regions include algorithm sensitivity to sea ice temperature, atmospheric, and snow cover variabilities.

The field campaign consisting of 7 coordinated aircraft flights is expected to take two to three weeks starting early March 2003. Some adjustments may be necessary just prior or during the campaign (e.g., different flight days and different location sites), resulting from unpredictable sea ice and weather conditions. Our tentative flight program is to fly 7 8-hour data flights with the NASA P-3 from Fairbanks, AK over the Beaufort and northern Bering Seas. From Fairbanks flight time to the northern Bering Sea (63^{o}N, 170^{o}W) or to the central Beaufort Sea (75^{o}N, 150^{o}W) will take about 2 hours flying 330 knots at an altitude of 25-30K feet. This leaves approximately 4 hours on site, although the transite legs will also be used for data collection coordinated with surface and Aerosonde measurements near Pt. Barrow. Flight time to Pt. Barrow is only 1 hr 30 min. Specific flight plans are discussed in the following section.

In all cases, the specific areas overflown will depend on surface and weather conditions and coordination with the Aerosonde team in Barrow. Near real-time AMSR-E or DMSP SSM/I imagery and possibly RADARSAT quick-look images will be used to guide the flight planning sessions before each flight.

When coordinating with surface and Aerosonde flights, selected flight legs will be done over the same ground track (within the limits of GPS navigation accuracy) at high altitude (ferry altitude) and at low altitude. The low-altitude leg ideally would be beneath any intervening cloud layers, but at a height sufficient to provide an PSR swath width of at least 2 km. This set of tracks is to be done over fast ice near Barrow, coincident with in situ measurements in the same area.

Flights will be timed to be as coincident as possible with EOS Aqua overpasses and with other satellite observations such as with Landsat 7 ETM+. A flight schedule that provides near-coincident coverage from multiple satellites (in particular DMSP SSM/I, RADARSAT, and possibly NOAA AVHRR) is desirable to allow intercomparison of multiple data types. We intend to fly one or more Aerosonde UAVs in concert with most of the P-3 flights.

With regard to the surface heat flux study, both regions contain persistent coastal polynyas that experience very large surface heat losses. We plan to dedicate two of the seven flights over coastal polynyas. The specific flight stategies are discussed in the following section.

Bering and Chukchi Seas (Feb/Mar 2005)

As noted earlier, an airborne radar will be flown on the NASA P-3 along with passive microwave radiometers to provide the required spatial and temporal coverage for the validation of snow depth on sea ice. From previous surface radar measurements (Jezek et al., 1998), snow depth on sea ice has been measured to within an accuracy of about 2 cm, an accuracy more than sufficient for the radar to serve as a validation tool for AMSR-E snow depth retrievals.

The Bering and Chukchi Seas provide a full range of snow depths and snow conditions. Persistent polynyas in the northern Bering Sea and off the Alaskan coast region of the Chukchi Sea provide gradients of snow depth ranging from 0 cm on new ice to 15-20 cm on first-year ice downwind of the polynya. Ridged sea ice areas generally contain much deeper snow. By late February to early March the Chukchi Sea will have an older snow cover with larger grains resulting in greater scattering. This will provide a good area to test the effects of grain size variability on the snow depth retrievals.

We plan to fly 5 flights from Fairbanks, AK over the Bering and Chukchi Seas. If possible, flights will be coordinated with Aerosonde flights out of Nome. High and low altitude patterns will be flown to provide a comparison of snow depth retrievals from AMSR-E and airborne passive microwave radiometers with the snow radar. The plan is to fly mosaic patterns over selected areas while covering as many AMSR-E footprints as possible. These flights will also provide an opportunity to collect additional sea ice validation data not collected during the 2003 field campaign.

3.3.5.2 Polynya Surface Flux Measurement Approach

The approach to be used consists of using a gust probe system on the NASA P3 aircraft with the goal of:

- mapping surface heat and moistures fluxes over the St. Lawrence Island polynya in the northern Bering Sea and/or coastal polynyas off the Alaskan coast of the Beaufort Sea,
- measuring how these fluxes change with distance downwind from the polynya and also how they vary with sea ice concentration and ice type,
- using these in situ aircraft data sets to aid in the development of methodologies for estimating fluxes from polynyas using satellite remote sensing data,
- determining the accuracy of flux estimates obtained from Aerosonde flights and bulk formulae.

Flights will be made when synoptic conditions are favorable for large, sustained polynya events. For the St. Lawrence Island polynya, our preferred site, the conditions consist of a large area of high pressure located over Siberia and a low pressure system over the Aleutians. These systems provide northerly surface winds over the Bering Sea forcing the opening of a polynya along the southern coast of the island. A crosswind multi-level stack pattern will be flown over the polynya in order to map the vertical structure of the fluxes over the polynya. Several other crosswind stack patterns will be flown downwind of the polynya to determine the relationship between changes in surface fluxes and sea ice concentration and ice types. 1-second samples of pressure, temperature, dew-point temperature and wind will be made at the following altitudes: 150, 300, and 600 ft, if approval is received as anticipated for transects below 500 ft. A PRT-5 type of downward-looking radiometer will provide surface temperature.

3.3.5.3 Arctic Flight Operations

The performance characteristics of the NASA P-3B aircraft is summarized in Table 3.3.2, while the aircraft instrumentation is discussed in section 3.3.2. The P-3 instrumentation for the Arctic2003 campaign is summarized in Table 3.3.5. The P-3 will make a total of 7 validation and science flights from

Fairbanks International Airport (FAI), Alaska. The regions that will be overflown include the Bering, Beaufort, and Chukchi seas as well as special study sites near Barrow Alaska.

The objectives for each of the 7 flights are summarized in Table 3.3.6. These objectives include both those for sea ice validation and polynya surface heat and moisture flux studies. The flight lines described here are only approximate. The final lines will depend on the regional weather and ice conditions during March 2003. The tentative lines for the Barrow flights are shown in Figure 3.3.7 and the flight lines for the other flights in Figure 3.3.8. Each of the 7 flights will be 8-hours in duration. The transit time from FAI to Barrow is approximately 1.5 hours leaving about 5 hours for data collection. For some of the other sites, for example St. Lawrence Is. in the Bering Sea, the transit time is about 2 hours leaving only 4 hours for data collection.

Table 3.3.5 NASA P-3B instrumentation for the Arctic 2003 campaign.

Sensor	Characteristics	Purpose	Sensor Scientist
Polarimetric Scanning Radiometer (PSR-A) (see Table 3.2)	Operating Frequencies (H&V-pol):10, 18, 22,37, 89 GHz	Simulate AMSR-E Measurements.	Dr. Gasiewski/NOAA/ETL
Polarimetric Scanning Radiometer (PSR-CX)	Operating Frequencies (H&V-pol): 6 ,10 GHz	Simulate AMSR-E Measurements.	Dr. Gasiewski/NOAA/ETL
Turbulent Air Motion Measurement System (TAMMS)	Pressure ports coupled with pressure transducers, temperature sensors, and water vapor instruments.	Measure turbulent heat and moisture fluxes over coastal polynyas	Dr. K. Lee Thornhill/ NASA Langley Dr. John Barrick/NASA Langley
IR radiometer	9.6-11 □m radiometer	Surface temperature	
Airborne Topographic Mapper (ATM-II)	Scanning Lidar altimeter combined with a differential GPS system	Maps ice surface topography at high resolution	William Krabill/NASA Wallops
Video and digital cameras	Tv video camera; 3 megapixel digital camera (KODAK)	Visible record of ice surface	William Krabill/NASA Wallops

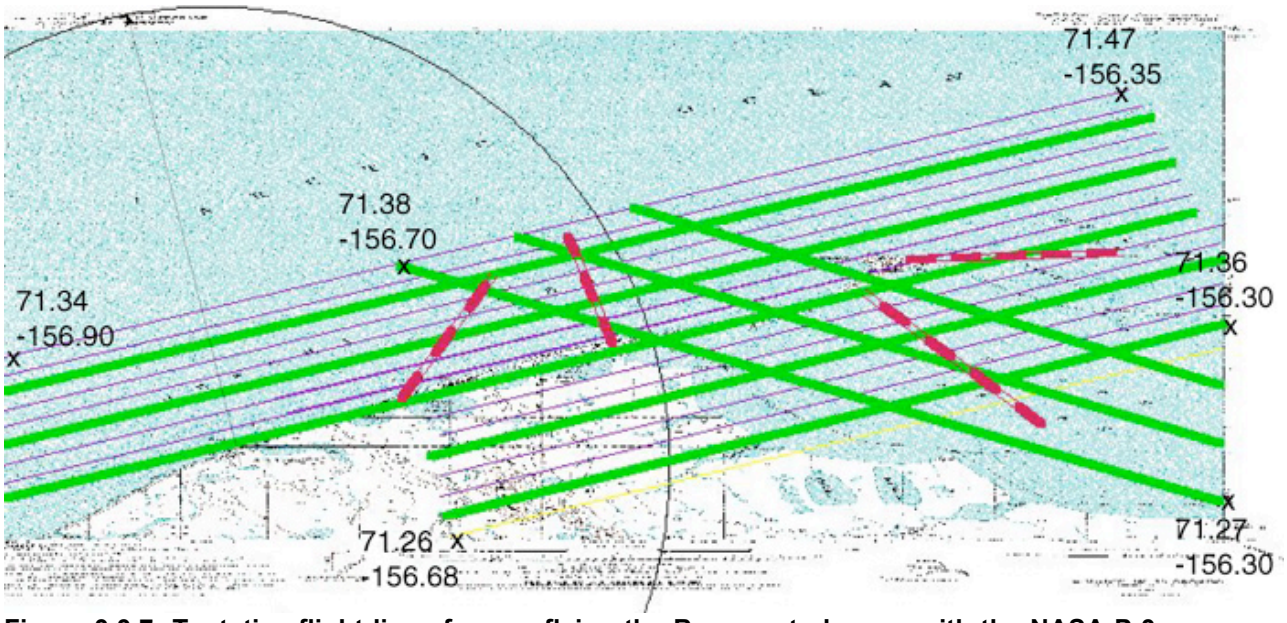

Figure 3.3.7 Tentative flight lines for overflying the Barrow study area with the NASA P-3 aircraft.

Table 3.3.6 P-3 Flight Objectives

FLIGHT NO.	OBJECTIVE	REGION	FLIGHT PATTERN / ALTITUDE	OPTIMAL WX AND SFC CONDITIONS
1	Compare P-3/AMSR-E ice concentrations in areas of new, young & first-year ice	St. Lawrence Is., Bering Sea	Hi-altitude mosaic (4,500 ft)	Clear wx; open polynya
1A	Measure sfc flux fall-off with ice conc. & type; compare computed sfc fluxes from AMSR-E & P-3	St. Lawrence Is., Bering Sea	Lo-altitude stack (500, 750, 1500 ft)	Clear wx; open polynya
2	Compare P3/AMSR-E sea ice concentrations in areas in the marginal ice zone & across the ice edge.	St. Lawrence Is., and the Bering Sea edge	Hi-altitude mosaic (21,000 ft)	Clear wx; open polynya
3	Compare P3/AMSR-E ice concentrations in areas of new, young & first-year sea ice	St. Lawrence Is., Bering Sea	Hi-altitude mosaic (4,500 ft)	Clear wx; open polynya
3A	Measure sfc flux fall-off with ice conc. & type; compare calculated sfc fluxes from AMSR-E & P-3	St. Lawrence Is., Bering Sea	Lo-altitude stack (500, 750, 1500 ft)	Clear wx; open polynya
4	Compare P3/AMSR-E ice concentrations in first-year & multiyear ice areas	Beaufort Sea	Hi-altitude mosaic (21,000 ft)	Clear wx; first-year/ multiyear ice type mix
4A	Compare P3/AMSR-E ice concentrations in first-year & multiyear ice areas	Beaufort Sea	Lo-altitude mosaic (4,500 ft)	Clear wx; first-year/ multiyear ice type mix
5	Compare P-3 snow depth & ice temperatures with sfc measurements	Barrow, AK	Lo-altitude transects (500 ft)	Clear wx
6	Compare P-3 snow depth & ice temperatures with sfc measurements	Barrow, AK	Lo-altitude transects (500 ft)	Clear wx
7	Compare P-3/AMSR-E ice concs. above/below clouds	Chukchi Sea	Hi-altitude mosaic (21,000 ft)	Clear/cloudy wx; range of ice conc.
7A	Compare P-3/AMSR-E ice concs. above/below clouds	Chukchi Sea	Lo-altitude mosaic (4,500 ft)	Clear/cloudy wx; range of ice conc.

Figure 3.3.8 Overview of the NASA P-3 flight lines for the Bering, Beaufort, and Chukchi seas.

Satellite/aircraft coordination is essential in meeting the objectives of this campaign. The swath of the EOS Aqua AMSR-E instrument (1445 km) is sufficiently wide to permit complete coverage daily over all areas to be flown with the P-3. The time of AMSR-E observations over these areas will be in early afternoon which coincides with the estimated 10 am to 2 pm time period of data collection for the P-3. The primary satellite sensors of interest are summarized in Table 3.3.7.

Table 3.3.7 Summary of satellite sensors for the AMSR-E sea ice validation campaign.

Satellite	Sensor	Range of Operating Frequencies	Maximum Resolution
EOS Aqua	AMSR-E	7-89 GHz	5 km
EOS Aqua	MODIS	0.4-14.5 _m	250 m
ADEOS II	AMSR	7-89 GHz	4 km
Landsat 7	ETM+	.5-12.5 _m	15 m
DMSP F11-F15	SSMI	19-85 GHz	12 km
RADARSAT	SAR	5.3 GHz	8 m
ICESat	GLAS	1064 nm laser	70 m

Almost all of the flights are planned for clear weather conditions (Table 3.3.6). This will allow comparisons with those sensors that require cloud-free conditions to observe the surface such as MODIS, ETM+, and GLAS. Arrangements have been made for the acquisition of data by these sensors during each of the flights. The high resolution of these sensors permits them to be used for validating the retrieved AMSR-E and PSR sea ice concentrations. While SAR does provide a high resolution capability, there are ambiguities in the interpretation of sea ice concentration arising from surface roughening of open water areas within the ice pack and at the ice edge by wind.

3.3.6 Modeling and sensitivity analyses

Radiative transfer modeling combines sea ice and atmospheric components to simulate top-of-the-atmosphere (TOA) brightness temperatures at AMSR-E frequencies. Our approach applies modeling in two ways. First, with the aid of the in situ data described above, we will calculate a synthetic AMSR-E data set that encompasses a wide range of surface and atmospheric conditions. Using these synthetic data as input to the AMSR-E algorithms, we will quantify the error statistics of the NT2, ABA, BBA, snow cover, and ice temperature retrievals as a function of local conditions. The second approach to be used is to validate the AMSR-E retrievals using forward modeling. In this approach, an ice and atmosphere "state" is defined. This state is then used to simulate TOA brightness temperatures. The simulated brightness temperatures are compared to the measured AMSR-E and/or P-3 PSR brightness temperatures. Discrepancies between the simulated and observed temperatures reflect errors in (a) the pre-defined state (the AMSR-E-derived ice concentrations, for example); (b) modeling errors; and (c) measurement errors (i.e., accuracy of the microwave radiometers). In addition, differences in sensor calibration will also be taken into account. For AMSR-E validation, we will be able to characterize the atmosphere reasonably well using UAV data and other Barrow observations, so we expect to be able to isolate the error associated with the algorithm-derived surface conditions. This method provides a direct way of quantifying product accuracies, and will allow us to identify algorithm shortcomings and thus suggest possible improvements.

The sea ice/atmospheric model to be used is that developed by Fuhrhop et al. (1997) called MWMOD, which we have applied previously for sensitivity studies (Stroeve et al., 1998). MWMOD computes brightness temperatures in the microwave frequency range for polar regions, including sea ice, open ocean and atmosphere, and has been applied by us previously for sensitivity studies (Stroeve et al., 1998). The Microwave Emission Model of Layered Snowpacks (MEMLS; Wiesmann and Metzler, 1999) will also be used to provide improved simulation of snowpack and multiyear ice. For applications of the models as a validation tool (via forward modeling of the AMSR-E-defined ice state), brightness temperatures for open water and ice can be prescribed, with the results compared to those achieved using the surface model. This will help alleviate the effects of inaccuracies in the surface modeling.

3.3.7 Program management and coordination

The overall management and coordination of the AMSR-E Team Validation Program will be the responsibility of Dr. Elena Lobl. This includes data set management and coordination among team members. The specific managerial responsibilities for the Arctic sea ice component of the validation effort is provided in Table 3.3.8. The responsibilities include the planning, coordination, execution of the task, data collection, and analysis. The data sets will be shared among investigators for intercomparison and analysis. The exchange of validation data sets between this program and Dr. Comiso's Antarctic program is essential. Exchanges of data will be undertaken as soon as final calibration and quality control are completed. This exchange of data sets will insure that all AMSR-E standard sea ice products will be validated for both Arctic and Antarctic.

An essential element of any field campaign is close coordination among field personnel. Coincident operations of the P-3 and Aerosondes (as well as any other aircraft in the area) will require development of flight plans and communications to assure safety. The study area is near the commercial airport at Barrow, so coordination with airport operations will be necessary. If possible, direct radio contact between the Aerosonde operators and the NASA P-3 during flight will be arranged for safety and also in case of delays, changes in flight plans, or other problems. It will also be necessary to have a communications plan to allow Barrow researchers and the P-3 operations to exchange information and coordinate flight times and plans prior to and subsequent to flights. This will be achieved via phone, fax, or internet.

Given the limited nature of the in situ data collection, every effort must be made to maximize the value of the data sets and assure that surface measurements are obtained at locations and times that best complement the aircraft and satellite observations. To help achieve this, we propose that the Barrow campaign begin with low altitude P-3, Aerosonde and field data collection. As soon as possible, these data should be processed in the field so that limited cross-checking of results, checking on navigation and coincident sampling can be assured. The effort will then continue with the remaining sampling plan for coverage of wider areas, but data should continue to be collected by all platforms over the selected

areas. For example, the P-3 should plan on overflying the local Barrow area at some point during each Beaufort Sea flight. This should be feasible given the small area of the field site. As the campaign continues, initial near-Barrow data will be examined for areas with high gradients or otherwise noteworthy signals that can be used to plan more field sampling of any unusual areas or undersampled conditions. The Barrow-area campaign should end with the same low altitude acquisitions as at the beginning, to ensure sampling over the longest time period possible to capture the greatest temporal changes in the area of most field data. The combined surface, aircraft, satellite data collection effort will also require maximum use of tools to aid georeferencing among the different data sets. This is essential to maximize the value of the small study area, and is further discussed in Section 3.3.4.1.

Table 3.3.8 Managerial responsibilities for the Arctic Sea Ice Validation Program

TASK	RESPONSIBLE INVESTIGATORS
NASA WWF P-3B Campaign	D. Cavalieri, A. Gasiewski, T. Markus, B. Walter
NSF Aerosonde UAV Campaign	J. Maslanik
Surface-Based Measurements	M. Sturm, J. Maslanik
Modeling and Sensitivity Studies	T. Markus, J. Stroeve, J. Heinrichs

3.3.8 Data management and availability

Overall data management for the AMSR-E Validation Program will be the responsibility of Dr. Elena Lobl. Data management and availability for each subtask listed in Table 3.3.8 will be the responsibility of the corresponding investigators. Data sets will be made available and archived as soon as the data have been calibrated and quality controlled. It is anticipated that the data will be archived no later than one year after the field campaign is completed.

ARCTIC CAMPAIGN SCHEDULE

YEAR	02				03				04				05				06			
Task/Quarter	1	2	3	4	1	2	3	4	1	2	3	4	1	2	3	4	1	2	3	4
EOS Aqua Launch		X																		
1. Satellite intercomparisons																				→
2. Beaufort/Bering a/c flights					X															
3. P-3 aircraft data analysis												→								
4. Bering/Chukchi a/c flights													X							
5. P-3 aircraft data analysis																				→
6.Prelaunch BarrowUAV flights/in situ data analysis		X			X	→														

3.3.9 Antarctic AMSR Validation Program

The Antarctic sea ice cover is one of the most seasonal parameters on the Earth's surface (Zwally et al., 1983). It is different from the Arctic ice cover in that there are no outer land boundaries that limits the growth and advance of sea ice in the region. In winter, the ice cover expands from the outer boundary of Antarctica until atmospheric and oceanic forces limit its northward advance, while in the spring and summer, the ice retreats rapidly because of its vulnerability to atmospheric and oceanic heat and wave action. Unlike the Arctic, there is no thick perennial ice cover that includes the pole but the sea ice cover is more expansive in winter and the changes with season are more dramatic. It is thus not surprising that the signature of sea ice in the Antarctic is quite different from that of the Arctic (Gloersen et al., 1992; Comiso et al., 1992). But although the signature of the sea ice cover is mainly the same as that of seasonal ice, the microwave emissivity of the surface has been observed to be spatially very variable (Comiso et al., 1989; Comiso et al., 1992; Grenfell et al., 1994). Such variations in emissivity in different seasons and under different weather conditions must be studied in detail because they affect the performance of the sea ice algorithms (Comiso and Steffen, 2001).

Since the advent of microwave remote sensing, there have been numerous remote sensing aircraft programs over sea ice in the Arctic (e.g., MIZEX experiments). However, we don't know of any similar passive microwave sea ice flight program that has been implemented over the Antarctic. This flight experiment is aimed at providing the much needed aircraft remote sensing data set in the region. The aircraft data is needed for validation because they provide intermediate resolution and spatial coverage that enables accurate interpretation of the AMSR-E data. The strategy is to obtain such passive microwave data in conjunction with simultaneous visible, infrared, and ship data to assess the real physical characteristics of the ice cover. The data set is in turn used to quantify the effectiveness of the mixing algorithms that are used to estimate ice concentrations and other data products. The aircraft is also equipped with other instruments that enable better interpretation of the data products.

Because of the vastness in its areal coverage, the only proven technique for quantifying seasonal and interannual changes in the ice cover is through satellite passive microwave remote sensing. The data also provide the longest record available and is currently the only one that can be effectively used for trend analysis studies. Significant improvements have been made in the characterization of the sea ice cover as instruments evolved from the single channel ESMR system, through the SMMR system, and currently, the SSM/I system, over a period of almost three decades. The advent of EOS-Aqua/AMSR, called AMSR-E is expected to provide a big advance in capability not only in resolution but also in accuracy due to the availability of more frequency channels.

In addition to the validation of the three algorithm parameters, the validation program will address the utility of these parameters in process and climate change studies. For example, in the study of polynyas, marginal ice zones, and divergence regions, it is important to recognize that these regions are covered primarily by new ice in winter. Heat and salinity fluxes in these areas are also vastly different from areas covered by thick consolidated ice (Maykut, 1978). The retrieval of ice concentration is frequency dependent, with the high frequency channels being much more sensitive to new ice than lower frequency channels. On the other hand, the lower frequency channels provide the best contrast in emissivity between sea ice and open water and best results for detecting new ice in leads, polynyas, and marginal ice zones. It is thus possible that different applications would require different combinations of AMSR-E channels and therefore slightly different products. The validation program will thus seek to establish which retrieved products will be most useful for the different applications.

The co-investigators of the Antarctic AMSR Validation program are listed below.

Donald Cavalieri	NASA Goddard Space Flight Center, Code 971 Greenbelt, MD 20771
Edward Kim	NASA Goddard Space Flight Center, Code 975 Greenbelt, MD 20771
Albin Gasiewsky	NOAA Environmental Research Laboratory

	325 Broadway, R/E/ETI, Boulder, Colorado, 80303
Keith Raney	Applied Physics Laboratory, John Hopkins University, John Hopkins Road, Laurel, MD 20723
Robert Cahalan	NASA Goddard Space Laboratory, Code 913 Greenbelt, MD 20771
William Krabill	Wallops Flight Facility, GSFC, Code 972 Wallops Island, VA 23337
Koni Steffens	CIRES, University of Colorado, Campus Box 216, Boulder, CO 80309
Robert Massom	Antarctic CRC, University of Tasmania, GPO Box 2520, Hobart, Tasmania, 7001, Australia
Stan Jacobs	Lamont-Doherty Earth Observatory of Columbia U. P. O. Box 1000, Palisades, NY 10964

3.3.9.1 Scientific Justification

The short term scientific justification for the validation program is to confirm the physical basis and the range of applicability of the assumptions made in the AMSR-E sea ice algorithm and to establish the accuracy of the derived geophysical parameters. Such a program provides credibility in the use of satellite geophysical data and make them useful for scientific research. The long term justification of the program is to enable the compilation of a consistent and accurate data set that is useful for process and climate change studies.

3.3.10 Objectives

3.3.10.1 Algorithm Validation Objectives

Although passive microwave satellite data have been around for a while, AMSR-E is a new high performing instrument and it is important that sea ice algorithms designed to take advantage of its added capabilities are validated and that the accuracy of the derived sea ice parameters are consistent with estimated values. AMSR-E data are expected to provide the baseline for new polar climate data sets and the means to evaluate the quality and consistency of historical satellite data. High quality and consistently derived sea ice parameters are needed to ensure that trend and mass balance studies, that makes use of these data sets, are done as accurately as possible.

3.3.10.2 Process and Climate Change Studies Objectives

Accurate and consistent data on sea ice cover are needed to fulfill some of the goals of NASAs Earth Science Enterprise, and in particular the Cryospheric Sciences Program. Among the objectives of the latter are to study processes in the polar region, to improve and verify global circulation models (GCM), and to gain insights into the changing global climate as reflected in the polar regions. For process studies, it is important to detect and quantify the small but physically significant changes in the physical characteristics of the ice cover, especially in polynya and divergence areas and in the marginal ice zones. Accurate quantification of these polynyas and divergence areas are important in that they are the primary source of global bottom water (Gordon and Comiso, 1988; Martin et al., 1992). The rate of formation of such bottom water may be changing and could impact the thermohaline circulation of the World's oceans, and therefore

climate (Comiso and Gordon, 1992). A good match of validated sea ice cover data from satellites with those derived from GCMs will also ensure that the physical and mathematical formulation of these models as well as the assumptions made are based on solid foundations. Furthermore, the historical satellite data provide the only means to evaluate inter-annual and inter-decadal variability of the sea ice cover on a global scale (Bjorgo et al., 1997; Cavalieri et al., 1999; Comiso and Steffen, 2001). Rapid changes in the ice cover have been detected in recent years (Jacobs and Comiso, 1997; Comiso, 2002). A fully validated algorithm for generating such a data set will go a long way towards providing confidence about the validity of the observed changes.

3.3.11 Coordination with other Programs

The cornerstone of the Antarctic validation program is the acquisition of a comprehensive data set on the sea ice cover after the launch of EOS-Aqua on 4 May 2002. The validation period is from 2002 to 2006. The primary data set will be the concurrent aircraft, in situ, and satellite data to be collected during the 2003 winter and 2004 spring periods as discussed in the following sections. In situ data during the aircraft experiment in 2003 will be collected with the NSF/RV Gould as the basic platform. But during the validation period, other sources of in situ data will be collected in other places and time, including those collected during the international GLOBEC program sponsored by NSF and conducted in the Bellingshausen Sea region in 2002 using the RV Nathaniel Palmer and RV Gould as platforms. The key contacts for this project are Drs. Doug Martinson and Don Perovich. Another source of in situ data is the Antarctic satellite validation project sponsored by CRC of the University of Tasmania, Australia to be conducted in the Indian Sea/Western Pacific Ocean in September/October 2003. Dr. Robert Massom, who is an EOS-Aqua validation PI, is in charge of this experiment dedicated for satellite validation studies and will be collecting in situ, helicopter, and possibly some small aircraft (Twin Otter) sea ice data with the ship Aurora Borialis as the platform. Another US program that has been collecting in situ data is the NSF/Ross Shelf Project involving the Nathaniel Palmer which started in December 2002 and will continue in 2003. Drs. S. Jacobs and A. Gordon are in charge of this program and have agreed to collect in situ ice data for the validation project. Other collaborators are Dr. Miles McPhee of the University of Washington who has been working in the Weddell Sea, Prof. Ray Smith of the University of California at Santa Barbara whose work is primarily in the Bellingshausen Sea and Dr. Peter Wadhams of the University of Cambridge and Dr. Martin Jeffries of the University of Alaska who have been doing experiments in the Ross Sea. The validation program will be coordinated with all these and other related projects, especially those with specific sea ice observation activities indicated above.

3.3.12 Algorithm Validation Issues

The basic radiative transfer equation that applies to the observed satellite brightness temperatures at a given wavelength is

$$T_B = \varepsilon T_S e^{-\tau} + \int_0^{\tau} T(z)\,\kappa(z)\,e^{-\tau+\tau(z)}\,d\tau(z) + (1-\varepsilon)\,e^{-\tau}\int_0^{\tau} T(z)\,\kappa(z)\,e^{-\tau(z)}\,d\tau(z) \quad (1)$$

where T_B is the observed brightness temperature, ε is the emissivity of the surface, T_S is the physical temperature of the surface, $\tau(z)$ and τ are the atmospheric opacities from the surface to a height z and from the surface to the satellite height, respectively, ω is an estimate of the diffusiveness of the surface reflection, and $\kappa(z)$ is the emittance at z. In equation (1), the first term represents radiation directly from the earth's surface which is the dominant contribution. The second term represents satellite observed radiation directly from the atmosphere, while the third term represents radiation from the atmosphere but reflected from the surface of the earth. A fourth term that takes into account the reflected contribution from free space, which is a small additive contribution, is not included in equation (1).

Within the ice pack, the radiation observed by the passive microwave satellite sensor comes from ice covered surface, open water, or a combination of both. The observed brightness temperature, T_B, is expressed in terms of the relative contribution from each surface by the linear mixing formulation given by

$$T_B = T_O C_O + T_I C_I \quad (2)$$

where T_O and T_I are the brightness temperatures of ice-free ocean and sea ice, respectively. C_O and C_I are the corresponding fractions of each of the two ocean surface components within the field-of-view of the instrument and add to unity (e.g., $C_O = 1-C_I$). Equation (2) forms the basis for sea ice concentration algorithms. The challenge is how to take into account temporal and spatial changes in T_O and T_I which are both functions of emissivity, temperature, and atmospheric conditions, as indicated in equation (1). Such changes can be taken into account or at least minimized through the utilization of several AMSR-E channels. The sea ice algorithms that will be used for processing AMSR-E data are indicated in the preface and discussed in Comiso et al. (2003, in press). The ABA or AMSR-E Bootstrap Algorithm (Comiso, 1995; Comiso and Steffen, 2001) will be used for the standard sea ice data in the Antarctic gridded at a resolution of 25 km. The BBA, or Basic Bootstrap Algorithm (Comiso and Zwally, 1997; Comiso et al., in press, 2003) is currently used for processing SSM/I data and will be used to derive 12.5 km products. The latter will also be used by NASDA's Earth Observation Center for generating standard geophysical sea ice products from both AMSR-E and AMSR, (the radiometer aboard ADEOS-II) for both hemispheres.

The validation criterion is that the derived AMSR-E sea ice products agree on average with the corresponding validation data to within the estimated accuracy of the validation data. The validation data sets will be derived from any or a combination of field, aircraft, submarine and high-resolution visible and infrared satellite data and are expected to provide a more accurate measure of the standard sea ice products than the AMSR-E retrieved products. The underlying philosophy of this approach is that confidence in the sea ice products derived from the AMSR-E will be achieved by showing consistency of such products with independently derived data that are spatially and almost temporally coincident (Comiso and Sullivan, 1986; Cavalieri, 1991; Cavalieri et al., 1991; Steffen and Schweiger, 1991; Grenfell et al., 1994; Comiso and Steffen, 2001). Operating within this paradigm, the following is a summary of validation methods and issues for each of the AMSR-E standard products.

Sea Ice Concentration: Sea ice concentration is defined as the areal percentage of sea ice observed within the field of view of the satellite sensor. The primary approach for the validation of retrieved AMSR-E ice concentrations is to utilized data from the dedicated aircraft campaigns in conjunction with high resolution satellite data, including those from Landsat 7, Terra and Aqua MODIS, NOAA-AVHRR, DMSP-OLS, and ENVISAT. Aircraft data will provide the means to assess the absolute accuracy in the retrieval of ice concentration at some places and some seasons while the high resolution satellite data provide better spatial and temporal coverage for all seasons. In situ ship data will be used to validate aircraft data. High-resolution active microwave satellite data such as the Envisat ASAR, are most useful during persistent cloud cover conditions and during darkness. Data from microwave scatterometers, such as those from QuickSCAT, will be utilized for identifying areas of divergence and possibly convergence. However, data from active systems are more difficult to interpret than those from passive and visible systems, because of unpredictable backscatter from different ice types, from open water within the ice pack, and from wind-roughened seas. However, after validation, such data can be extremely useful at providing some unique large scale physical properties of the ice cover in practically any time period when it is available.

The aircraft campaign will provide multi-channel passive microwave data similar to AMSR-E but at a much better resolution. The high resolution will provide the means to test the effectiveness of the mixing formulation in different ice regimes and conditions. The aircraft will also be equipped with digital and film camera system for the characterization of small features of the ice cover, a laser ranging system for surface topography studies and ice thickness estimates, and a multi-frequency radar for snow cover studies. The strategy is to apply the algorithm on co-registered and coincident aircraft and spacecraft data and evaluate how the results matches each other quantitatively and how they compare with similar analysis from high resolution visible and infrared data. Discrepancies will be analyzed and explained through the use of ancillary data and further examination of the high resolution data. Data at the ice edge, open ocean, and land/ocean boundaries will also be analyzed to validate the effectiveness and consistency of the masking algorithms.

The validation program will take into consideration the large changes in physical and radiative characteristics of sea ice during a complete ice season. During early ice growth period,

the ice cover consists mainly of new ice, pancakes, young ice, and relatively undeformed first year ice. On the other hand, during late winter, the ice cover consists of predominantly thick and vast ice floes with relatively thick snow cover. During the melt season, the vast ice floes get broken up to smaller units and the surface gets covered by slush or liquid. Such phenomenon is discussed in detail in Comiso and Steffen (2001) and is illustrated in Figure 3.3.9. For at least two periods (dry and wet periods) the changes in the radiative signature will be quantified as accurately as possible and relationships with the accuracy of the retrieved sea ice parameters will be evaluated.

Another issue is the effect of atmospheric opacity to the performance of the algorithms. The effect of clouds and adverse weather conditions can be significant (Oelke, 1997), especially at high frequency channels, as quantified using AMPR, MAS, and SAR data as illustrated in Figure 3.3.10. In this figure, the ice data over cloud free conditions are significantly different from those in cloud covered conditions even if the ice cover is basically uniform throughout the tract as inferred from the SAR data. The validation program will aim to quantify this effect more accurately and determine how well radiative transfer modeling can be used to minimize such effects in algorithms where the high frequency channels are used. Adverse weather conditions also causes bad retrievals in the open water. Open water masking has been developed but needs to be validated. Related to this is the need to check masking techniques at the land/ocean boundaries such as that developed by Cho et al (1996) and modified for the Bootstrap Algorithm.

As a complementary approach, time series of images will be analyzed to check AMSR-E retrievals for temporal consistency. The growth and decay of sea ice are limited by physical laws and environmental conditions and such time series data can provide the means to establish how well the expected time development of the ice cover is reproduced by the satellite data. This effort will help identify weaknesses in the technique that are not obvious from examination of individual images.

Sea Ice Temperature: The ice temperature derived from the vertically polarized 6.9 GHz channel represents the temperature of the sea ice layer that emits much of the signal observed by the radiometer. For first year ice, it is the temperature of the snow/ice interface because at this frequency the snow cover is transparent to the radiation and the surface is opaque due to relatively high salinity. For multiyear ice, the derived sea ice temperature represents a weighted-average of the freeboard portion of the ice. During previous Antarctic cruises, the physical characterization of the ice cover made on a regular basis included quantitative measurements of temperature profiles through the snow and ice. Such data were taken during the Weddell Sea winter and spring cruises of 1982, 1983, 1986, and 1989. These data were used to obtain empirical relationship between the snow skin-depth temperature and the snow/ice surface temperature. The snow skin-depth temperature is routinely measured by infrared (IR) satellite instruments (e.g., AVHRR, ATSR, and MODIS). The primary technique for the validation of AMSR-E ice temperature is to make use of this empirical relationship that converts IR satellite data to ice temperature data and use the latter for comparative analysis with AMSR-E data. The aircraft IR data will be converted to surface ice temperatures that in turn will be compared with ship measurements to assess errors associated with the use of empirical parameters. Further refinements of the empirical parameters will be made through the use of more field data and a thermodynamic model of sea ice and snow.

The issue is how well AVHRR reproduce the AMSR-E temperature data. Since only one set of empirical parameter is used for the entire ice cover, the formulation may not be valid for all types of ice. For example, the equation may be useful for first year ice floes which are the primary ice cover in the Antarctic and where most of the in situ measurements came from. Such equation, when applied to multiyear ice floes may not be valid because the latter are much thicker and therefore has significantly different temperatures at the snow/ice interface. This phenomenon is illustrated in Figure 3.3.11 which is a temperature map derived from AMSR-E data. The temperature map shows what is expected in the region but some areas are relatively colder (in green). These are areas which are believed to be covered by thick ice that survived the summer and were advected from the Western Weddell Sea.

The retrieved ice temperatures will be further validated using surface temperature data from buoys, ships, ice camps, and other platforms. While these are only point measurements, the horizontal variability of the snow/ice interface temperature is not expected to be large over several kilometers. Also, there exist some arrays of buoys that provide continuous

measurements and could be used to check the temporal consistency of the derived AMSR-E temperature data.

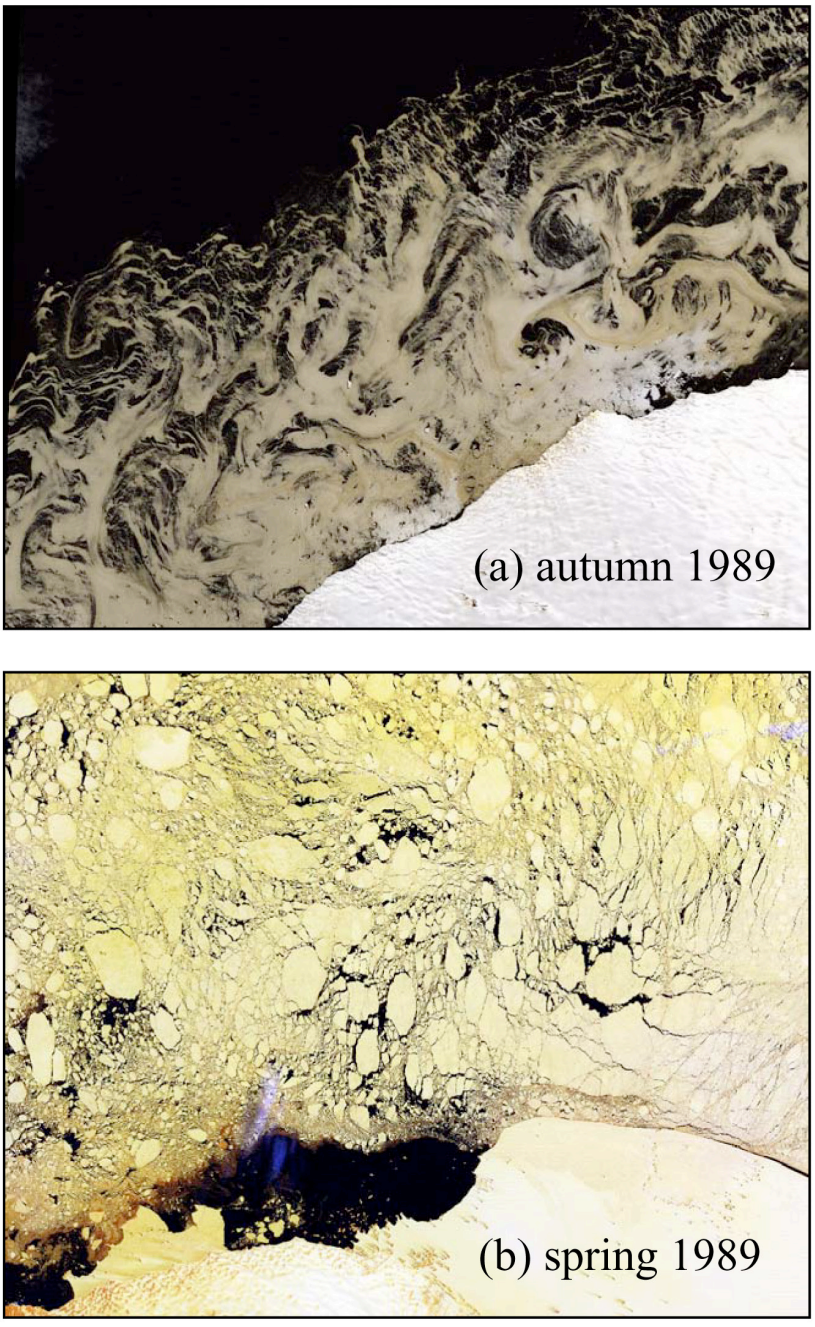

Figure 3.3.9. Landsat images showing the changes in the physical characteristics of the sea ice cover in the Indian Ocean from (a) autumn to (b) spring.

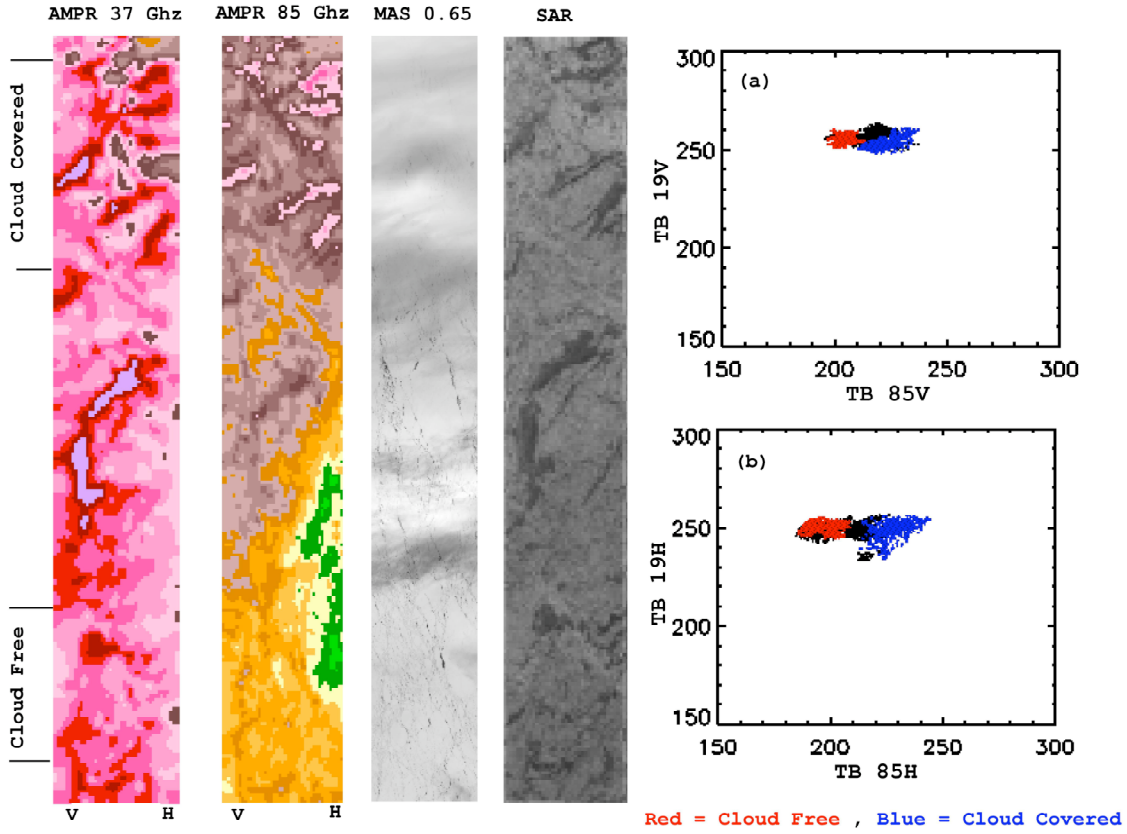

Figure 3.3.10. Tracks of AMPR, MAS, and SAR data over sea ice covered regions with and without cloud cover as detected by MAS. The scatter plots of 19 versus 85 GHz at both vertical and horizontal polarization shows significant shifts in the signature of ice from cloud free (red) to cloud covered (blue) conditions at 85 GHz channels.

Snow Depth on Sea Ice: Because snow depth observations over sea ice are so sparse and because surface measurements over areas comparable to the size of passive microwave footprints are so difficult and costly to acquire, the validation strategy is to use an airborne range-gated, step-frequency radar. A prototype of this sensor has been built and tested on the surface. The range resolution of the sensor is estimated to be 1.15 cm, which is more than adequate to provide the necessary accuracy for the snow algorithm validation. The airborne version of this radar is being built under the direction of Prof. Gogineni at Kansas University and may be available for the 2004 mission. For the 2003 winter experiment, 2 potentially good techniques will be used: one using the halo of an off-beam Lidar measurement, while the other using a combination of a Lidar and a radar altimeter to measure the snow top and the ice top elevation, respectively. The results from these measurements will be validated using ship measurements. The snow algorithm for AMSR-E is not part of ABA and is basically a regression technique developed by Markus and Cavalieri (1998). Their work will be closely coordinated with the validation activities outlined here. Qualitative checks will also be made through comparisons with ice type maps that can be inferred from multichannel AMSR-E data (Massom et al., 1998) and AVHRR or MODIS images.

.

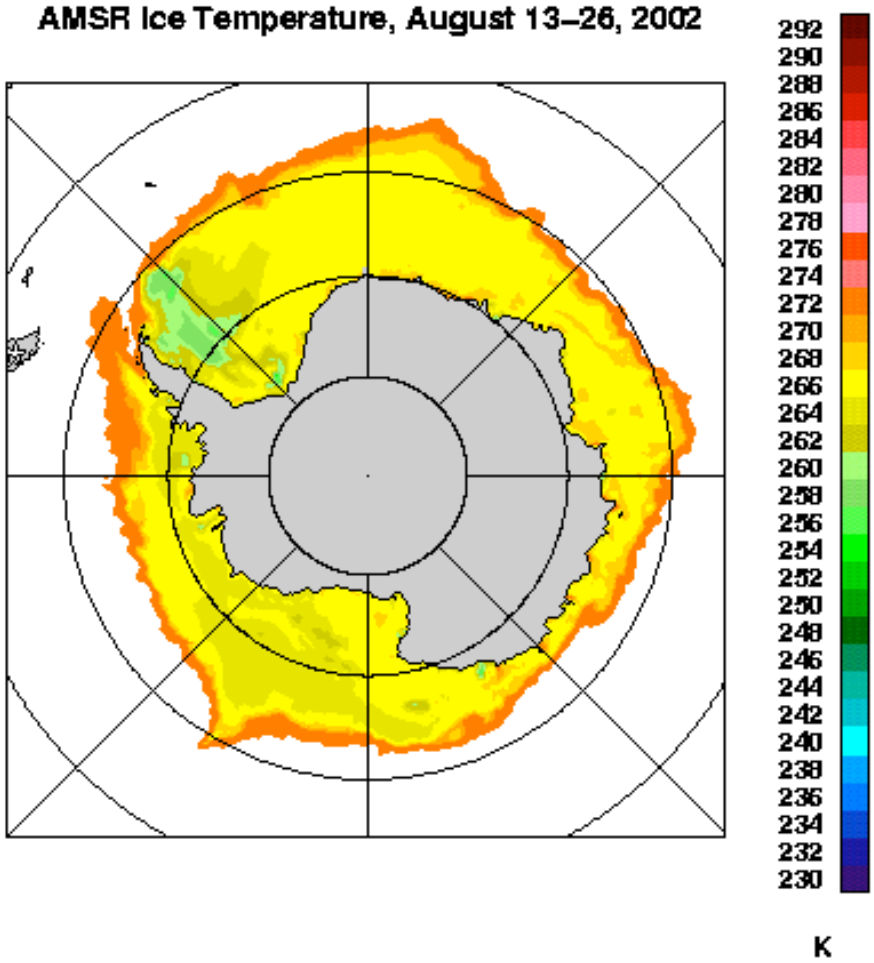

Figure 3.3.11 Color-coded surface ice temperature map from AMSR-E data.

3.3.13 Process and Climate Change Study Issues

3.3.13.1 Thin Ice/Polynya Studies

Ice concentration provides the fraction of ice within the footprint of the satellite sensor. As mentioned earlier, the sea ice cover is an entity with progressively changing physical characteristics and therefore radiative signatures. Thin ice and polynyas are therefore very difficult to quantify with ice concentration data. The strategy is for the aircraft and ship to go to coastal polynya areas, refrozen leads, and marginal ice zones where the main ice cover is new ice. To illustrate the problem, Figure 3.3.12 shows images of ice concentration in the Western Weddell Sea in early spring. In the passive microwave image (Fig. 3.3.12a), relatively low concentration ice is inferred that matches the areas where MODIS data (Fig. 3.3.12b) shows some open water and thin. The iceberg inside the small rectangle which has emissivity different from sea ice is represented as low concentration ice as well. The strategy is to be able to accurately characterize the spatial extent and physical characteristics of ice in the polynya areas as well as adjacent areas and be able to quantify the distribution of the different types of new ice.

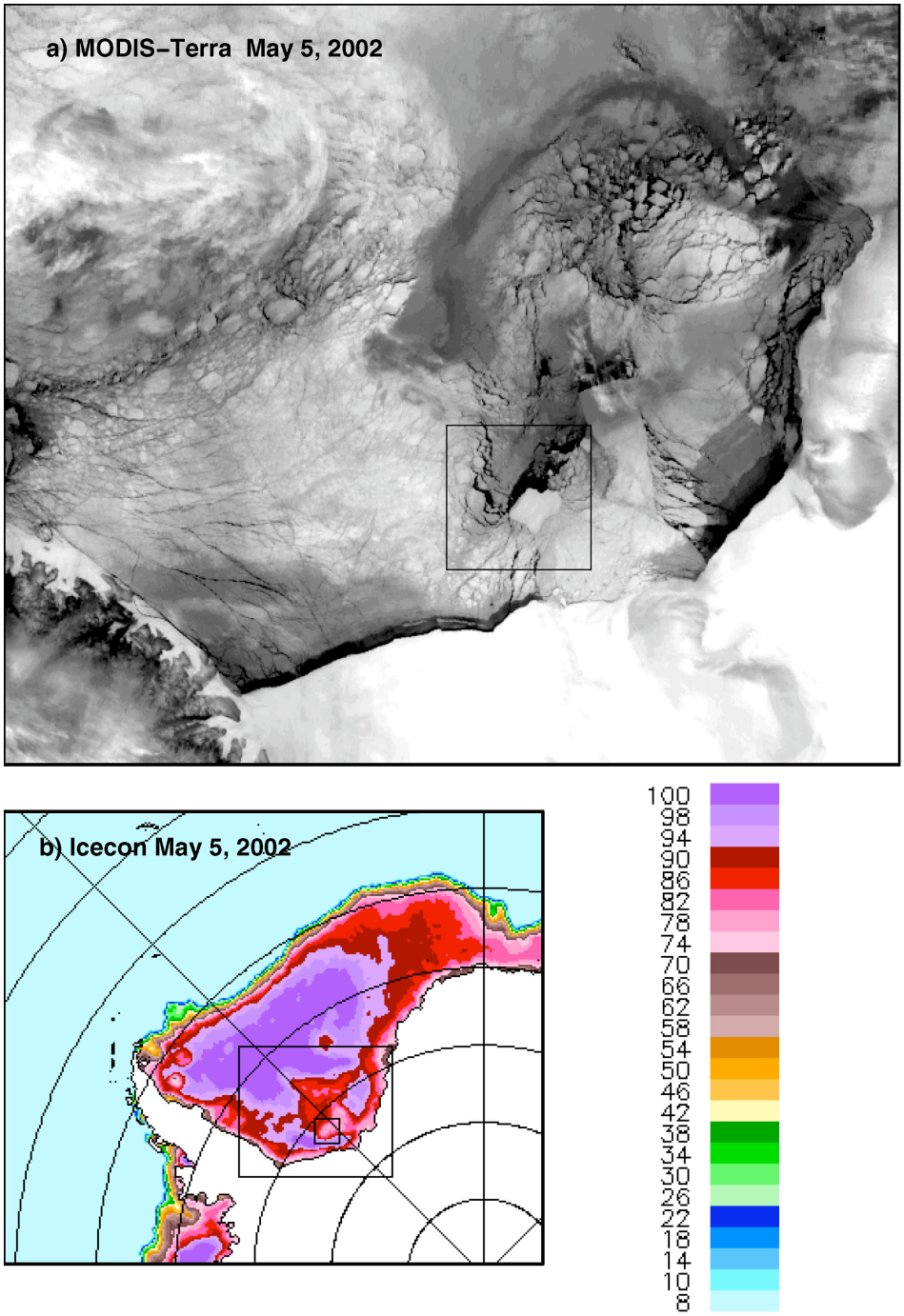

Figure 3.3.12. (a) Ice concentration map in the Weddell Sea Region; (b) MODIS image inside the large rectangle in the ice concentration map. The small rectangle indicates an area of open water, new ice, and iceberg.

3.3.13.2 Surface Heat and Humidity Fluxes

The ice cover serves as a blanket that insulates the ocean from the atmosphere in winter. But different types of ice cover provide different insulation capabilities. Previous studies have noted that fluxes from thin ice are an order of magnitude higher than those of the thicker ice types (Maykut, 1978). Fluxes from different types and different thicknesses of the ice cover are thus very import to quantify. In situ/surface measurements will include the use of 3-D eddy-correlation

instrument that measures wind speed in three dimension and physical temperature and providing the means to estimate heat and energy fluxes. Also, a Lyma instrument will be utilized to observe latent heat/vapor fluxes over leads and polynyas. These measurements will be complemented by the TAMMS instrument on board the P3 that will measure similar variables.

3.3.13.3 Thickness, Topography, and Drag Coefficients

To assess how the ice cover is changing, it is important to know as well how the thickness is changing since it is really volume and not just area that matters in mass balance studies. In situ measurements of ice thickness has been made (Wadhams et al., 1989) but the coverage is limited and the sampling may be biased compared to the true thickness distribution of the Antarctic sea ice cover because ships tend to go to the thinner regions of the ice cover to avoid being stucked in the ice. The ship data will be used to validate two lidar and one radar altimeter data of the ice freeboard that will in turn be used to extrapolate the ice thickness over much longer transects. Such technique has been demonstrated to be effective in the Arctic (Comiso et al., 1990). The scanning lidar will also provide topography and surface roughness measurements. Such data are also useful in estimating the drag coefficients in various regions as well as ridge and lead statistics that are needed in ice dynamics modeling studies.

3.3.13.4 Ice Edge/Ice Extent Studies

The satellite sensor is very good at providing a quantification of the extent and area of the ice cover. It is through the assessment of the extent and area that we get to find out if the ice cover over a long term period has been changing. With a relatively long record now accumulated from passive microwave data, the accuracy and consistency of this estimate is very important when used in decadal variability and climate change studies. The extent is defined as the area that is covered by ice with at least 15% concentration. The issue is how accurately and consistently the satellite sensor is able to find the location of the 15% ice edge. Previous studies have indicated some apparent inconsistencies of satellite data with ship observations (Worby and Comiso, 2001) as illustrated in Figure 3.3.13. The SAR image was taken from the rectangular area as shown in the passive microwave image and is shown with the 15% (black) and 30% (red) contours from the latter. While the 15% satellite passive microwave data show consistency with ship measurement in this case, it is clear that the location of the ice edge as defined by passive microwave is not consistent with that of the SAR data. The problem will be studied by using ship observations in conjunction with satellite data and aircraft transects over the marginal ice zones (MIZ) during the same period.

3.3.14 Methods and Techniques

3.3.14.1 Coordinated Aircraft Program

Two coordinated Aircraft experiments are proposed for the Antarctic region after the launch of EOS-Aqua in 2002. The first will be an austral winter program (on August-September 2003) over selected sites in the Weddell Sea, Bellingshausen, and Amundsen Seas. The second will be a spring/summer program (on October-November 2004) over either the Ross Sea if logistics allows it or the Weddell, Bellingshausen, and Amundsen Seas. The rationale, specific objectives, strategy, and coordination will be discussed in the following sections. The instrumentation for the 2003 mission is as discussed below. It is expected that the intrumentation for the 2004 mission will be basically the same.

Aircraft Instruments

The aircraft will be equipped with a set of sensors and instrumentation that are designed to meet the objectives of the validation program for the AMSR-E sea ice parameters, as indicated earlier. The following are the instruments that will be installed in the P-3 for the Antarctic mission and the rationale for using them:

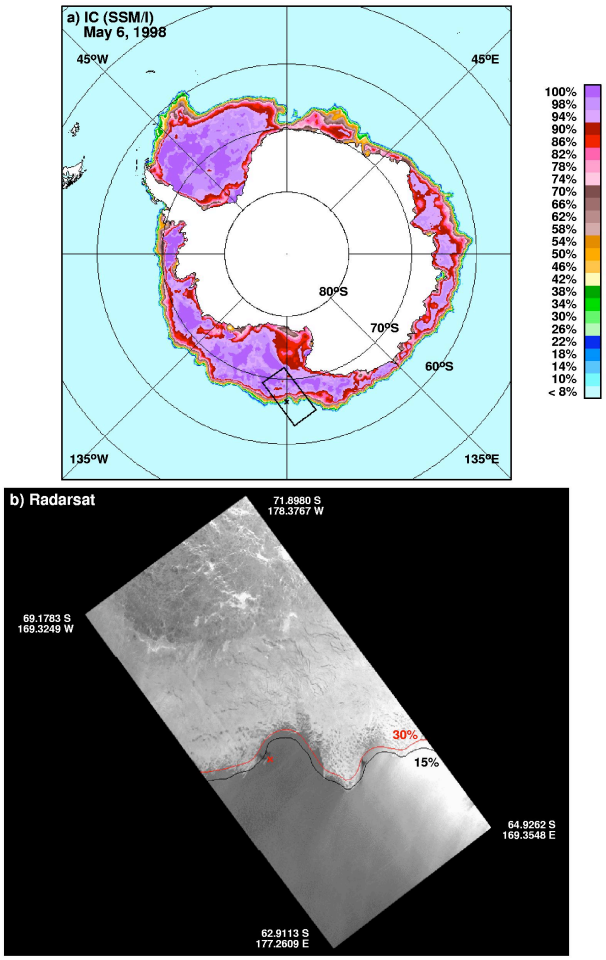

Figure 3.3.13. Ice concentration image and SAR image indicating location of the 15 and 30% ice edge in the Pacific Ocean. Ship location is indicated by x.

1. Scanning Microwave Radiometer

The primary instrument on board the P-3 that will be used for AMSR-E validation is a scanning microwave radiometer that has the same channels as the satellite instrument. One of two options will be used: the Polarimetric Scanning Radiometer (PSR-A) which has been tested for several field programs, and a newly built Airborne Earth Science Microwave Imaging Radiometer (AESMIR). The two are very similar systems and are expected to provide almost identical results. However, the PSR-A does not have the 6 GHz channel. The PSR-A has to fly together with PSR-C to match the capability of the AESMIR, but space for the PSR-C will not be available in the current aircraft configuration. At normal flying altitude of about 6,000 m, the resolution for AESMIR will be about 600 m which will enable detection of most leads and coastal polynyas. The flight program will include segments where the aircraft will be flying at low elevations to enable acquisition of radiometer data at an even better resolution. For example, at a flying altitude of about 1000 m, the resolution will be about 115 m, which is sufficient to image leads and some pancakes. The high resolution data will provide the means to test how accurately the true ice cover is depicted by the mixing algorithm. The system will also have an infrared radiometer (6.5-14 □m) to obtain high resolution surface temperature data for comparison with ice temperature retrievals and to be able to estimate surface emissivities.

2. Scanning Ranging Lidar

A scanning ranging laser instrument called the Airborne Topographic Mapper (ATM) has been developed for the Greenland ice sheet project. The predecessor of this Lidar has been used in the Arctic on board the NASA P-3 while overflying a nuclear submarine equipped with an upward looking sonar that measures the thickness of the ice. The results from the study were very encouraging and show that the thickness distribution of sea ice inferred from the submarine sonar data can be reproduced from the freeboard thickness distribution of the ice as observed by the Lidar (Comiso et al., 1991). Among the key issues in validation studies is how the emissivity of Antarctic ice changes with ice type and thickness. In addition to thickness determination, the Lidar can also be used for obtaining ice type, rafting and ridging statistics. The Lidar will thus serve as a good validation tool and with its imaging capability, the data can be co-registered with PSR/AESMIR data for detailed comparison to evaluate the effects of thickness, ice type, surface roughness, and ridging on the ice emissivity and hence the ice parameter retrieval.

3. Cloud Thickness from Off-beam Lidar Returns (THOR)

The THOR was designed primarily for cloud cover studies but has been demonstrated to be effective for snow and ice studies as well. The system which operates at 540 nm, 1 kHz, can be used to infer snow thickness and ice thickness separately from the size of the horizontally reflected diffuse "halo" at the surface. This promising capability has been tested in the field and in modeling studies, but will be used for the first time in the Antarctic. In theory, the thickness of snow is proportional to the size of the halo. Direct validation will be done using ship data while comparative analysis will be done using the other aircraft data.

4. Delay/Doppler Phase-monopulse angle measurement (D2P)

The D2P radar altimeter provides similar measurements as the Lidar but the strongest return signal comes from the snow/ice interface instead of the surface of the snow. The system in conjunction with the ATM thus provides a means to measure snow thickness and assess snow thickness distribution in a large part of the Antarctic ice cover. In conjunction with PSR/AESMIR data, the system would be useful in assessing how the snow thickness retrieved by AMSR-E data is affected by snow layering, grain size and wetness. The D2P is also a simulator to the system that will be on board the ESA/Cryosat satellite that will be launched in 2004.

Snow thickness is the most difficult to quantify on a large scale. The most dependable thickness measurements are from ships on the ground but data sampling is a problem because the snow cover in the ship's vicinity do not necessarily represent average snow thickness within the footprint of the satellite. The D2P/ATM system is currently the best bet at providing statistically robust snow thickness distributions. The ship data will be used to validate the retrievals from the D2P/ATM system. Coordination will be made during overflights such that the ship is in consolidated ice and not in newly frozen lead areas, which are the most likely path for multi-disciplinary cruises that requires the shortest possible time to get to the next destination.

A step-frequency range gated radar designed to measure snow thickness is under development at the University of Kansas by Dr. Prasad Gogenini but will not be finished on time for this mission. Such an aircraft sensor that measures snow depth would be a highly valuable complement to existing systems.

5. ESTAR

The ESTAR provides passive microwave data at L-band (1.413 GHz) and at horizontal polarization. The wavelength (~21 cm) is not one of the channels of AMSR-E but it is much more penetrating that any of the channels from the latter and will provide useful information about the thickness distribution of the ice, especially in divergence regions and in polynyas. Because of its long wavelength, the system provides discrimination between thin ice and thick ice on account of the dependence of emissivity on thickness (Menashi et al., 1993). It is a system that makes use of interferometric technique in which pairs of small antennas and signal processing are used to obtain the resolution of a single large antenna. It has been used successfully for soil moisture

studies (1997 and 1999) and for sea surface salinity studies (2001). Ability to do ice type classification using this system will be studied in conjunction with ship data.

6. Turbulent Air Motion Measurement System (TAMMS)

We intend to use the system during the flights over coastal polynya regions and also over the marginal ice zones. The TAMMS provide critical information needed for polynya and heat flux studies. Among the parameters that will be measured are wind velocity in 3-D, temperature, and humidity. These measurements in conjunction with those from PSR/AESMIR will provide unique information about polynyas that will enable accurate quantification of fluxes from the latter. The results will be compared with those derived from ship and satellites.

7. Optical and Digital Camera

Optical and digital cameras provide the best resolution data that can be acquired from the aircraft mission. These data will be invaluable in determining actual open water areas within the footprint of the radiometers and can be used to identify the different types of new ice and evaluate effects of significant ridging, rafting, and flooding. Such data will be coincident in time and space with the other measurements and will be useful for improving interpretation of other validation tools such as Landsat, SAR, and MODIS.

3.3.15 Antarctic Winter Aircraft Experiment (23 August - 15 September 2003)

3.3.15.1 Rationale and Issues

The winter sea ice cover in the Antarctic is vast and occupies an area of about 19 million square kilometers which is more extensive than that of the Arctic. An Antarctic validation program is needed to ensure that the accuracy of the retrieved sea ice products from such a large fraction of the global sea ice cover is consistent with estimates. The main issue is the absolute accuracy of retrieved sea ice parameters from ABA, especially since results from the latter differ from those of other algorithms by as much as 35% in large areas of the Antarctic in winter (Comiso et al., 1997). Such discrepancies need to be resolved and evaluated to ensure that the derived data are suitable for scientific and operational studies. The other issue is how accurately and consistently the location of ice edges and sizes of polynyas are quantified. These parameters are needed to assess interannual changes in the extent of and fluxes within the sea ice cover. Detailed studies of an apparently changing climate in at least some parts of the Antarctic, like the Bellingshausen/Amundsen Seas and the Antarctic Peninsula, as indicated earlier, require accurate validation of the changes in the ice cover as observed by passive microwave sensors.

3.3.15.2 Objectives

There are three major objectives of the validation program during this period. The first is to provide the means to assess quantitatively the performance of the AMSR-E sea ice algorithms in the Antarctic region during dry surface conditions. In particular, the accuracy of the standard sea ice products (sea ice concentration, ice temperature, and depth of the snow cover) derived from AMSR-E, will be estimated through comparative analysis with those derived from the validation data set. The second objective is to test the effectiveness of the tie-points that are currently used by the algorithm as reference brightness temperatures for 100% ice cover and open water. Such tie-points will be adjusted if necessary to optimize the performance of the AMSR-E sea ice algorithms. Finally, the spatial variability of the emissivity and temperature of sea ice will be evaluated during this period when ice is most expansive to fully assess how accurately the ice parameters are derived. With aircraft radiometer data, spatial changes in the emissivity of sea ice from one ice type to another can be better quantified because of much better resolution than that of the satellite data. Also, with the aircraft data, the unique informational content of each of the AMSR-E channels can be better evaluated for optimal utility, especially in

the use of the 6 GHz channel for deriving sea ice temperature and in improving the retrieval of sea ice concentration data.

In essence, the general objective is to obtain as accurate characterization of the sea ice cover as possible during the validation period to fully assess the accuracy and value of parameters derived by ABA. High accuracy is needed to be able to quantify the small percentage of open water and new ice in polynyas and divergence regions within the pack. Such accuracy is also required to consistently monitor the extent of actual area of the global sea ice cover and gain insight into the changing climate of the polar regions.

3.3.15.3 Flight Program and Logistics

During the austral winter program, a fully instrumented P-3 aircraft will be based at Punta Arenas, Chile. The primary study areas are the ice cover in the Weddell Sea and the Bellinghausen/Amundsen Seas. Typical transects from the base into the ice pack and back are shown in Figure 3.3.14. The locations of special interest are the areas where the Bootstrap and the Team algorithms have large discrepancies (see purple areas). Mosaic patterns are planned in these locations, as shown, to allow direct comparison of aircraft and spacecraft data. The flight program will enable a high-resolution characterization of the sea ice cover, provide accurate estimates of sea ice parameters, and help establish causes of discrepancies of the two algorithms in these regions. Flights along the coastal areas are also planned to assess the accuracy of the satellite data in quantifying open water and thin ice in these regions. The uncertainties in the retrieved ice concentration are in part due to contamination of the sea ice data by continental ice sheet data and also by unusually cold surface ice temperatures compared to adjacent regions. It is very important that retrievals in these regions are validated since these areas are regarded as ice factories and key sources of global bottom water. During each flights, the exact location of ice edges will also be quantified to assess how accurately and consistently the AMSR-E algorithm identify the 15% ice edge which has been used as the standard for ice extent analysis. The exact location of the ice edge is key to the calculation of the ice extent, which is an important climate parameter.

An example of the transect that will be used for ice edge studies is shown in Figure 3.3.15. The Bellingshausen Sea transect will coincide with the time period when RV Gould will be in the vicinity of the ice edge.

It is anticipated that the campaign will take about three weeks and will start on 23 August and end on 15 September 2003. The schedule is to fly every other day but some adjustments may be necessary, because of unpredictable weather conditions. Flight schedules will also be coordinated such that the time of aircraft coverage approximately coincides with that of AMSR-E. The size of the mosaic patterns will be optimized, as range of aircraft will allow to cover as many AMSR-E footprints as possible. The range of the P-3 is estimated at 5,940 km, assuming flight time of 10 hours and an average speed of 330 knots. This capability in range will suffice to fulfill the validation goals in the Weddell and Bellingshausen/Amundsen Seas.

The following describes anticipated flight scenarios. Some adjustments in flight days and location sites may be necessary during the campaign because of unpredictable weather conditions. The aircraft will originate at Wallops , VA (37^{o}N, 118^{o}W), and refuel at San Jose, Costa Rica (9.98^{o}N, 84.07^{o}W) before it gets to Punta Arenas, Chile (53.15^{o}N, 70.92^{o}W) which is the primary staging site. The research sites of especially interest are:

Bel/Amundsen Seas, Site #1: Mosaic pattern centered at 70°S, 80^{o}W
Bel/Amundsen Seas, Site #2: Mosaic pattern centered at 70^{o}S, 90^{o}W
Bel/Amundsen Seas, Site #3: Coastal regions in western Antarctic Peninsula
Bel/Amundsen Seas, Site #4: MIZ at around 90W
Weddell Sea Site #5: Mosaic pattern centered at 65°S, 35°W
Weddell Sea Site #6: Mosaic pattern centered at 68°S, 50°W
Weddell Sea Site #7: Coastal regions in eastern Antarctic Peninsula
Weddell Sea Site #8: MIZ at around 50°W

The order of the flights as indicated may not be strictly followed and will depend on many factors including weather and the ice condition during the period.

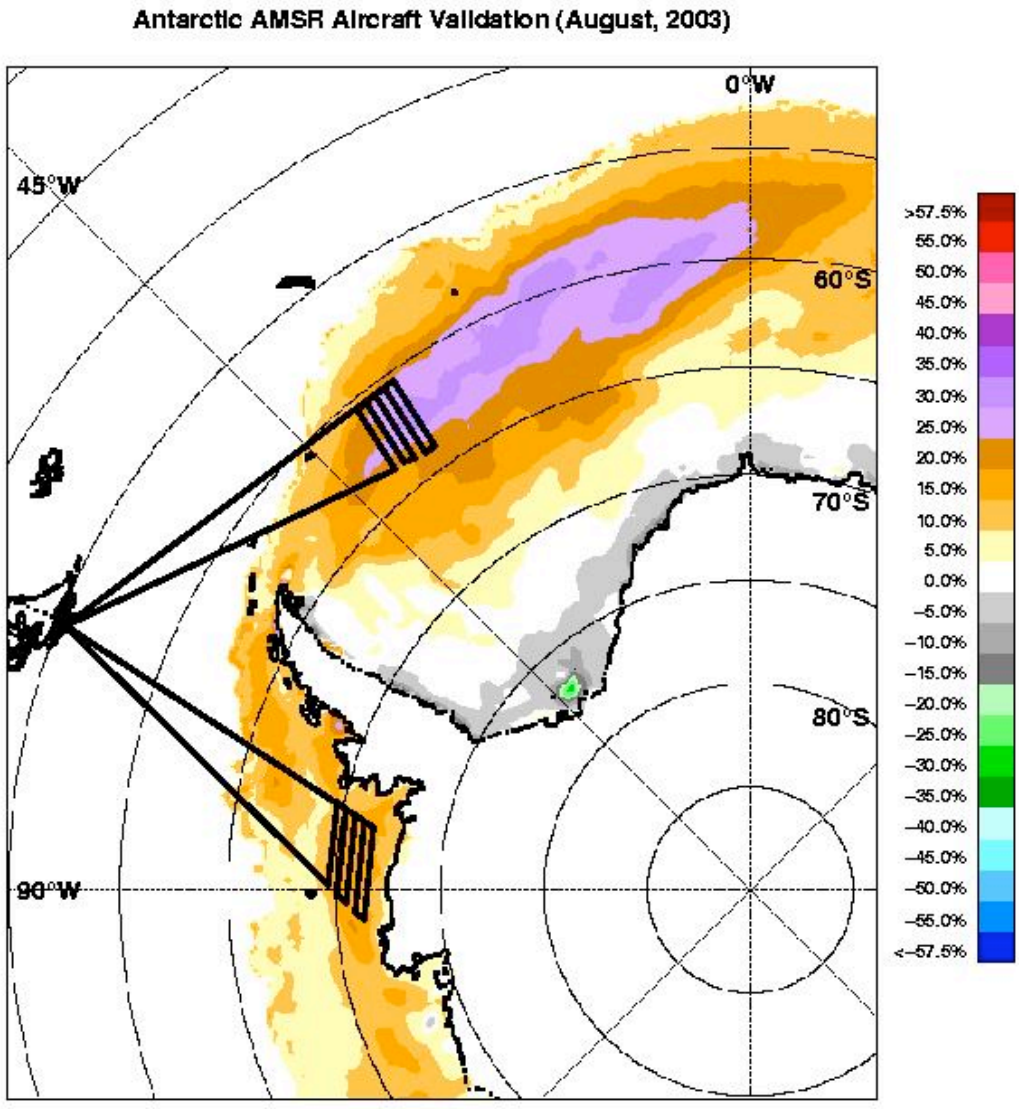

Figure 3.3.14. Sample transect for the P3 Aircraft over the middle of the ice pack in the Weddell and Bellingshausen/Amundsen Seas during the Winter Antarctic Validation Program.

3.3.16 Antarctic Spring Aircraft Experiment (October – November 2004)

The Antarctic Spring campaign is described here for completeness. At present, there are no plans to carry out this campaign due to lack of funding.

3.3.16.1 Rationale and Issues

A second Antarctic aircraft program is planned for the spring of 2004. This second underflight program is required to enable accurate assessment of the accuracy of inferred sea ice parameters during the transition period from the cold and dry surfaces during winter and early spring, to the warm and wet surfaces during the late spring and summer. The transition from dry to wet surface causes large changes in the emissivity of sea ice. This affects ability to accurately estimate the T_I tie point and therefore the accuracy of the retrieval. Good accuracy of the ice parameters during spring and summer is important since the sensitivity in the response of the ice cover to changes in surface temperature is highest during this period (Comiso and Steffen, 2001). Thus, in a global change scenario, accurate quantification of ice parameters during this time period is critical.

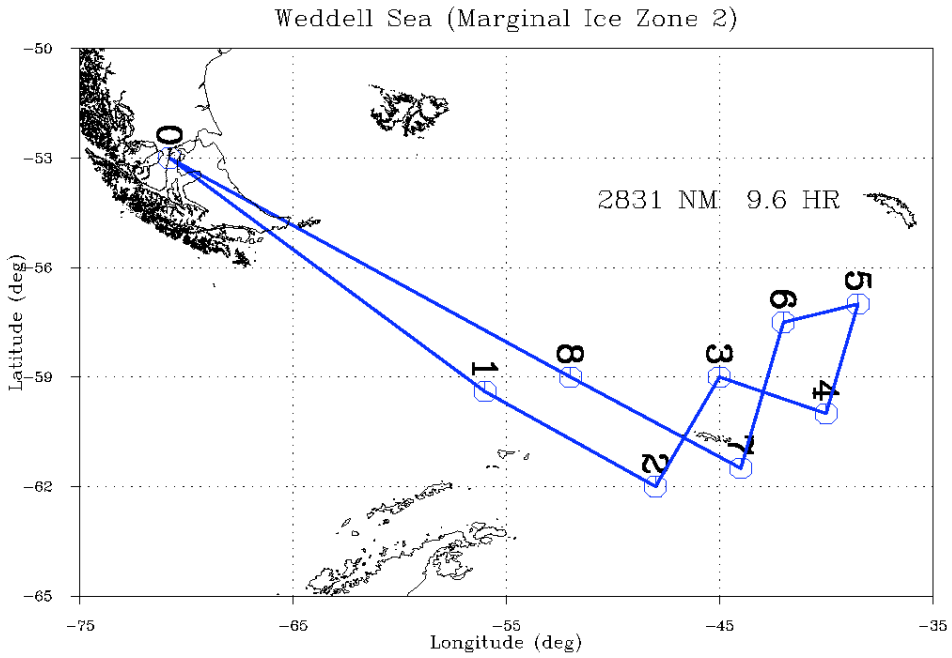

Figure 3.3.15. Sample track for MIZ studies in the Weddell Sea

3.3.16.2 Objectives

As with the winter program, a key objective for the spring program is to provide the means to assess quantitatively the performance of the AMSR-E sea ice algorithm in the Antarctic regionduring this period. The winter and spring projects are needed to ensure that the algorithm is tested as a truly seasonal algorithm. A second objective is to determine quantitatively the magnitude of the change in the emissivity of sea ice from winter to spring and make sure that such change is accounted for by the algorithm. The results will provide the means to better establish the appropriate tie points for sea ice needed to optimize the accuracy of the retrievals. Finally, the overall impact of the spatial variability of the emissivity and temperature of sea ice during spring and summer on the accuracy of the algorithm products will be assessed. With the utilization of intermediate resolution aircraft radiometer data, regional and seasonal changes in emissivities will be quantified. The utility of other AMSR-E channels (i.e., 6 and 10 GHz) not present in currently available satellite data in minimizing retrieval errors and in improving the performance of the algorithm will also be evaluated.

3.3.16.3 Flight Program and Logistics

The strategy is to perform the spring aircraft experiment as soon as feasible after the launch of EOS-Aqua and the completion of the winter aircraft experiment. The plan is to conduct the spring program from mid October to mid-November 2004. If logistical constraint allows it, the preference is to conduct the experiment in the Ross Sea and Western Pacific Ocean regions to complement the data from the Weddell and Bellingshausen Seas and be able to assess how the emissivity varies from one region of the Antarctic to another. Typical flight paths during this compaign are shown in Figure 3.3.16. The flights along the coastal areas are included and is expected to provide quantitatively the extent of open water and thin ice in this region during ice break up. The uncertainties in the assessment of open water in this region includes the percentage of contamination of the sea ice data by data from the continent and the effect unusually cold temperatures in the region. It is very important that retrievals in these regions are validated since these areas are regarded as important oceanographic features and are regimes of intense biological activities. Also, during ice retreat, it is important to know the timing when the

coastal regions are free of sea ice. During each flights, the exact location of the ice edges will also be quantified to assess how accurately the AMSR-E algorithm identify the 15% ice edge. The exact location of the ice edge is key to the calculation of the ice extent, which is an important climate parameter.

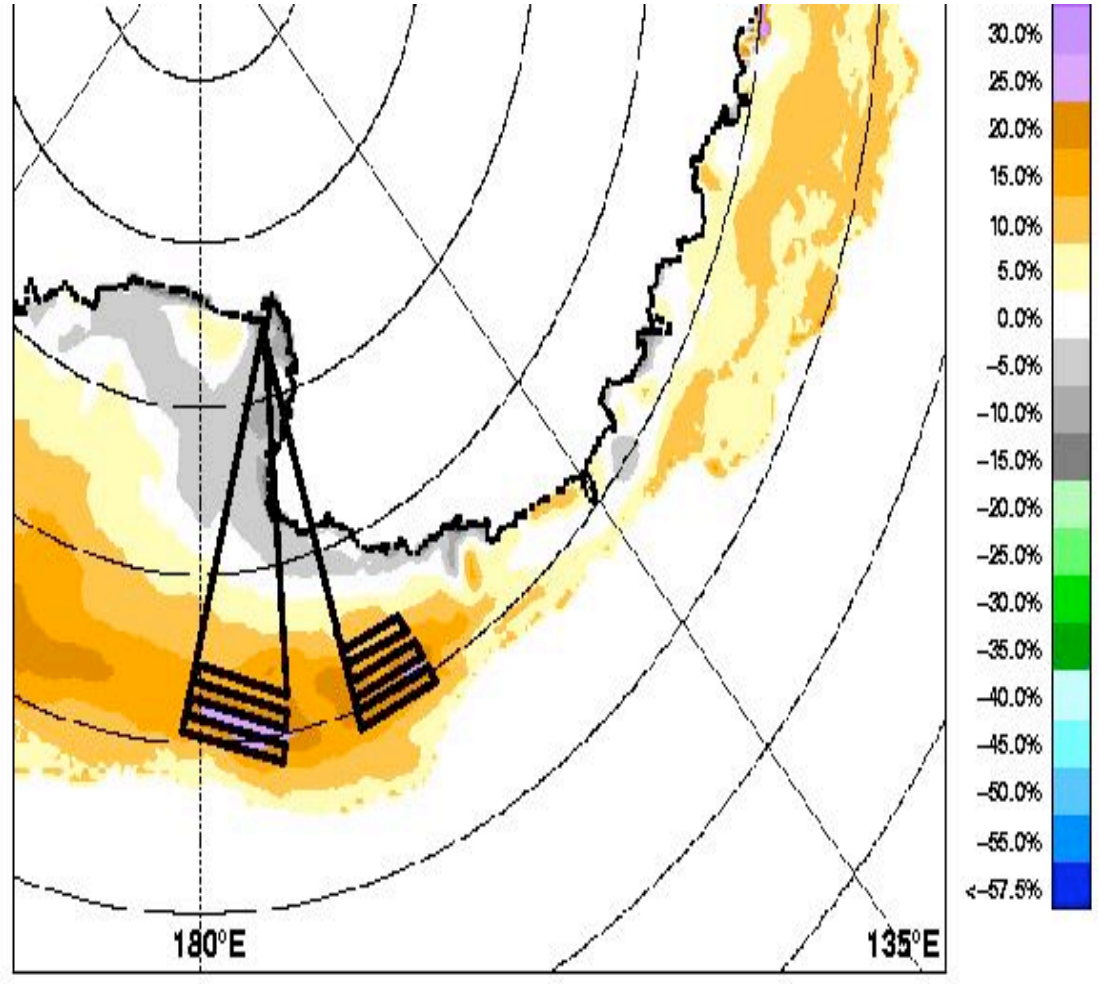

Figure 3.3.16. Sample transects for the P3 Aircraft over the Ross and Western Pacific Ocean during the Spring/Summer Antarctic Validation Program

It is anticipated that the campaign will take about three weeks and will start in mid October to mid November 2004. The specific days of flight will depend, as in the winter case, on weather conditions, which at times are generally unpredictable. Times of flight will also be coordinated such that the chance of coincident AMSR-E overpass is optimized. The patterns are again based on the range of the P-3 as indicated in the section for the winter mission.

It should be mentioned that the P-3 aircraft has not done a scientific mission with McMurdo as the staging base before because of a requirement that an alternate airport for landing is available in case of unexpected change in weather. Such requirement is currently being fulfilled. However, in case of unforeseen problems, the backup location will be Punta Arenas in Chile with flight paths similar to the winter mission but adjusted to account for the rapidly changing ice cover during this time period. Sea ice characteristics and other parameters needed for validation will be collected by sea ice scientists during the period.

Again, the aircraft originates at Wallops, VA but this time, it will refuel at Honolulu, Hawaii (21^{o}N, 158^{o}W) and Christ Church, New Zealand (43^{o}S, 172.5^{o}E). From Christ Church, it will go to

McMurdo, Antarctica (78°S, 167°E) where will be the staging station. The flight sites of interests are:

Ross Sea Site #1: Mosaic pattern centered at 73°S, 180°W
Ross Sea Site #2: Mosaic pattern centered at 75 °S, 170°W
Coastal Regions Site #3: Coastal regions along the edge of the Ross Sea ice shelf.
West Pacific Ocean Site #4: Mosaic pattern centered at 70°S, 90°W
West Pacific Ocean Site #5 Mosaic pattern centered at
Coastal Regions Site #6 Along the Victoria Land coastline up to Cape Adams

The instruments aboard the P-3 during the spring validation period will be basically the same as those that will be used for the Antarctic winter project. New validation instruments that becomes available during the spring period and are relevant and useful to meet the desired objectives will also be installed. If McMurdo is not a feasible staging station for the P3, the experiment will be conducted, as with the winter case, from Punta Arenas, Chile. Such experiment will be coordinated with an international program called ISPOL (ice station Polarstern) which is scheduled for spring 2004 in the Western Weddell Sea.

3.3.16.4 High Resolution Satellite

The relatively large footprint of the AMSR-E sensor makes the sea ice products particularly difficult to validate. The utility of high resolution satellite data for validation studies have been demonstrated in previous studies (Comiso and Zwally, 1982; Steffens and Schweiger, 1991). The validation program for sea ice will therefore rely heavily on the analysis of coincident satellite data not just to complement the aircraft data but also to extrapolate the aircraft results in time and space. The primary AMSR-E satellite validation data set will be those acquired during the AMSR-E validation period. Historical data will also be used to improve statistics and spatial coverage and include data sets previously acquired for validation of sea ice parameters derived from the DMSP SSM/I and Nimbus-7 SMMR (Comiso et al., 1991; Cavalieri, 1992; Grenfell et al., 1994). Coincident data from AMSR-E and SSM/I will also be compared for consistency.

Multi-sensor and multi-platform satellite data, which are approximately coincident in time and space for all seasons and for the southern hemispheres, will be compiled before and during the validation phase. The key sources of satellite validation data for AMSR-E ice products include the following:

(a) Landsat-7, OLS, GLI, AVHRR, MODIS (high-resolution visible);
(b) AVHRR, ATSR, GLI, MODIS (medium-resolution infrared);
(c) SAR (ERS-1, 2, JERS-1, RADARSAT, Envisat ASAR) (high-resolution active microwave);
(d) QuickSCAT, TOPEX Scatt./Altimeter Data (medium-resolution active micr.).

High-resolution SAR, and medium resolution scatterometer and altimeter data are particularly useful in areas of persistent cloudiness and darkness. Geophysical parameters derived from these data are currently research products and will be validated using coincident visible channel data before they are used for AMSR-E validation.

3.3.17 In-Situ Ship and Buoy Data

It is fortuitous that the NSF/RV Gould (a similar ship is shown in figure 3.3.17) is scheduled to go to the Palmer Station for exchange of personnel during the validation period. We are grateful to NSF for agreeing to make this cruise as a platform for collecting in situ data in the Bellingshausen Sea during the period. Dr. Koni Steffen from the University of Colorado and his graduate students will be providing the much needed in situ measurements. Dr. Steffen will be making microwave radiometer measurements as well as physical and environmental measurements in the vicinity of the ship and also on board the ship. The radiometer measurements include the use of radiometers at 11, 21, 35, 48, and 94 GHz to quantify the emissivity of various types of sea ice at these frequencies. The physical characterizations will include temperature, salinity, and structure profiles of the snow and ice cover over several sites

and time periods. Some conductivity measurements will also be made to infer the dielectric property and liquid content of the snow and ice.

Figure 3.3.17. The Antarctic environment as observed from the ground. At the background is RV Polarstern equipped with microwave radiometers mounted at the rail of the ship.

Antarctic Ocean buoy networks will be used for the validation of derived sea ice temperatures and sea ice drift retrievals. Weather station and ice station data will also be used for checking ice temperature and snow depth retrievals. We plan to make use as well of historical ground measurements, like those from Winter Weddell (1986-1992), and Weddell Flux (1994-1995) experiments to better understand how observed brightness temperatures are affected by different ice surface characteristics and conditions. Data from future field experiments, such as those from the Southern Ocean GLOBEC (2001-2002) will be utilized in a similar manner and will be especially valuable because they represent recent ice characteristics and some of the measurements will be made after the launch of AMSR-E and AMSR.

3.3.18 Radiative Transfer Modeling of the Atmosphere and Sea Ice

Atmospheric effects can be estimated using radiative transfer modeling to account for the effects indicated by equation (1). The results from the latter can be used to correct the brightness temperatures observed by the aircraft and satellite and results are used to derive the geophysical parameters that are used in the validation. As indicated earlier, the choice of channel is important and with the set of channels used in the ABA algorithm, the effect appears to be negligible. Further confirmation that this is indeed the case will be done through radiative transfer modeling studies using actual atmospheric profile measurements during the validation period.

Radiative transfer modeling of the microwave radiation emanating from the sea ice cover will also be undertaken because it allows for a better understanding of the emission characteristics of different sea ice surfaces at the different AMSR-E frequencies and

polarizations. Such procedure has been conducted previously (e.g., Tjuatja et al., 1993; Grenfell et al., 1994; Tjuatja et al., 1995) but results were of limited value because of the lack of needed atmospheric and surface data. Some refinements will be implemented and data acquired during the validation program will be used to obtain improved results that will be used to better interpret spatial and temporal changes in the microwave signatures as observed in the aircraft, field, and satellite data sets.

3.3.19 Validation Schedule

The validation of the Basic and AMSR- E Bootstrap algorithm has been a continuing activity that started with the advent of mutichannel passive microwave sytems. The successful launches of the EOS-Aqua/AMSR-E and the NASDA/ADEOS-II/AMSR in 4 May 2002 and 14 December 2002 as well as high performing, high resolution instruments in these satellite, will provide a wealth of data that will enable a greater understanding of the characteristics of the sea ice cover. The aircraft program as discussed will help ensure that the retrieved data from these satellite data will have the accuracy and performance expected. The schedule for key validation programs that includes the aircraft overflight program is shown in Table 3.3.9 below. Initial date is indicated by > while the completion date is indicated by > as well. It is anticipated that some adjustments in the schedule may be necessary since the work needed to calibrate and quality check such kind of data sets is unpredictable. However, the schedule allows for some delays due to unexpected problems and different schedules for different groups.

Table 3.3.9. Antarctic AMSR-E Validation Program Schedule

	2002				2003				2004				2005					
Year/quarter	1	2	3	4	1	2	3	4	1	2	3	4	1	2	3	4	1	2
Pre Launch Val.	_	>																
EOS-Aqua launch		>																
P3 Aircraft Winter							>											
Analysis of Winter data							>	_	_	_	>							
P3 Aircraft Spring												>						
Analysis of Spring data												>	_	_	_	>		
Analysis Satellite Data		>	_	_	_	_	_	_	_	_	_	_	_	_	_	>		
Modeling Studies								>	_	_	_	_	_	_	_	>		
Validation Report											>	_	_	_	_	_	_	>

3.3.20 Data Management, Analysis, and Archival

The basic validation data set will be a compilation of all calibrated data associated with the aircraft program and corresponding co-located satellite AMSR-E observations. This includes data from each of the aircraft sensors during flight days from the time the sensors are turned on after take off up to the time they are turned off before landing. Calibration runs before, during, and after each of the flights will be part of this basic data set. An enhanced validation data set will include in situ measurements from ships or ice camps and high resolution satellite data during each flight day. Also included in this set are ancillary data such as wind, pressure, air temperature, and atmospheric profile data. It is the responsibility of the PI to make sure that the basic data set is archived with proper documentation after the data have been quality checked, calibrated properly, and reduced to a format suitable for archiving. The enhanced version will be put together through collaborative efforts with other PIs. Coordination and management of the enhanced data set will be supervised by the AMSR-E project in collaboration with the PI and coordinated by Elena Lobl.

Scientists and engineers of each sensor will quality check the raw data to make sure that only data that meets certain standards are kept. This will ensure that data collected when instruments are not working properly are not used for validation. The data from various sources will then be calibrated and geolocated according to the specifications of the sensor scientists.

The AMSR-E algorithm will be applied on the calibrated and geolocated aircraft, spacecraft, and field data and the results will be archived as part of the validation data set.

3.3.21 Personnel

The validation program will involve a lot of people and it is not possible to list everybody which will participate at this point. But some of the key people and affiliations are shown below:

PI: Josefino C. Comiso, NASA Goddard Space Flight Center, Code 971
Co Is: D. Cavalieri, NASA Goddard Space Flight Center, Code 971
T. Markus, NASA Goddard Space Flight Center, Code 975
R. Massom, CRC, University of Tasmania, Hobart, Tasmania, Austrialia
S. Jacobs, Lamont-Doherty Earth Observatory, Palisades, NY
AESMIR: Ed Kim, NASA Goddard Space Flight Center, Code 975
PSR: A. Gasiewsky, NOAA Environmental Research Lab
THOR: Robert Cahalan, NASA Goddard Space Flight Center, Code 913
ATM: Bill Krabill and Bob Swift, Wallops Flight Center, Code 972
ESTAR: David Levine, NASA Goddard Space Flight Center, Code 975
D2B: Keith Raney, Applied Physics Laboratory, John Hopskins University
TAMMS: Kennett Lee Thornhill and John Berrick, Langley Flight Center,
RV Gould: Koni Steffen, CIRES, University of Colorado, Boulder, Colorado
Satellite Support: Rob Gersten, Raj Poudyal, SSAI/NASA GSFC, Code 971

3.4 Snow validation (by R. Armstrong, with contributions from R. Kelly)

3.4.1 Validation Criterion and Method Overview

The extent of the seasonal snow cover, which may include as much as 50 percent of the Northern Hemisphere land surface, is an extremely important parameter in global climate and hydrologic systems due to significant effects on energy and moisture budgets. Realistic simulation of snow cover in climate models is essential for correct representation of the surface energy balance, as well as for understanding winter water storage and predicting year-round runoff. When snow covers the ground, some of the microwave energy emitted by the underlying soil is scattered by the snow grains resulting in a sharp decrease in emissivity and associated brightness temperatures. Passive microwave signatures of seasonal snow cover are clearly characterized by this strong dielectric contrast between snow-covered and snow-free ground, by decreasing emissivity (dry snow) with increasing microwave frequency (negative spectral gradient) and by decreasing emissivity with increasing snow mass. Because of this clear capability, a microwave snow cover algorithm is under development by the EOS AMSR-E Science Team

Snow depth and water equivalent can vary greatly with weather conditions and land surface characteristics. Given the large footprint of passive microwave sensors, snow storage within a footprint is seldom uniformly distributed. Therefore, large differences between station or gauge measurements (a point) and satellite estimates (an area integration) are to be expected. Where these differences are small, this apparent success could merely be fortuitous and we cannot always assume that such results represent true validation of a given algorithm. Comparisons of point observations with satellite estimated snow storage at best provide an order of magnitude check on the temporal patterns and spatial distribution. It is necessary to design schemes to compare areal snow storage with satellite derived snow storage. We propose the following types of experiment to validate the snow storage estimates.

(1) Comparisons of AMSR-E derived snow water equivalent (SWE) values with airborne gamma observations.

Airborne gamma data are used by NOAA National Operational Hydrologic Remote Sensing Center (NOHRSC) to derive snow water equivalent over selected basins in the U.S. The accuracy of snow storage estimates over many basins in the north central and western US are well known. We will be able to judge the quality of our derived SWE through comparison with the NOHRSC SWE estimates. Currently we have selected the Red River basin as a primary test site along with the airborne gamma data available from the NASA Cold Land Processes Experiment (CLPX) described below. Coincident airborne gamma and in-situ snow data will be used to validate the snow algorithm at two additional test sites, Black River, Wisconsin and Poplar River, Montana. Each basin is about 10,000 km^2.

(2) Comparisons of AMSR-E derived SWE with snow storage values from a snowmelt runoff models for selected basins.

The procedure to evaluate the accuracy of long term areal SWE estimates will be to compare these results with the water balance output from a hydrological model. The above mentioned three sub-basins will be used in this study which will be undertaken by Dr. J. Foster. A similar study for the Rio Grande basin will be undertaken by Dr. A. Rango. Based on the stream flow output derived from the snowmelt runoff model, it is possible to regress how much snow storage is required to generate the runoff. In addition we will be collaborating with the NASA IDS project (R. Armstrong Co-PI) “A Regional Integrated Monitoring System for the Hydrology of the Pan-Arctic Land Mass “(RIMS) described below.

(3) Comparison of AMSR-E derived SWE with SSM/I algorithm output.

As a baseline check on the accuracy and stability of the AMSR-E Level 1A data going into the snow algorithm we will run the same algorithm in parallel using brightness temperature data from SSM/I. This comparison will be done at the hemispheric scale to evaluate both snow extent and SWE returned by the two data streams over the entire 2002-2003 Northern Hemisphere winter season or over that period for which well calibrated AMSR-E data are available.

3.4.2 Specific Near-term Validation Activities

The quality of the retrieved SWE can be confirmed by thorough comparisons of satellite estimates with independent measurements of areal SWE with known accuracy. This is a challenging effort because areal SWE measurements are very limited. In order to include a wide range of spatial scales, we will evaluate algorithm skill at the local or grid scale, the river basin scale, and the regional to hemispheric scale. Local or grid scale studies will be accomplished through direct participation in the NASA Cold Land Processes Experiment (CLPX) planned for both mid-February and late March of 2002 and 2003 in northwestern Colorado (Cline, 2001). Prior snow validation efforts have primarily relied on what might be termed “data sets of opportunity” - data sets which typically were not entirely appropriate for passive microwave algorithm validation and often introduced as many questions as answers to the process. The optimal sampling scheme comprised of spatially nested sampling areas (Figure 1.) offered by the CLPX represents a major advancement over previous efforts to validate passive microwave snow algorithms. The synergy of multiple investigators and their collective ground-based and airborne meteorological, active and passive microwave and gamma measurement systems will provide the basis for an unprecedented validation campaign for snow cover remote sensing. The overall design and spatial sampling scheme of both the ground-based and airborne measurements constitute an optimal test environment for this validation study. Although this local or grid scale study is limited to three land cover types (grassland, coniferous forest and alpine) these regions are typical of many other locations world-wide where seasonal snow cover is the prevalent land cover during the winter season. Therefore, the algorithms validated in this experiment can be applied and tested over comparable land cover types throughout the world.

Larger river basin scale validation will be facilitated through participation in the ongoing RIMS project, a NASA (IDS) and NSF (OPP) funded program (University of Colorado, University of New Hampshire, Ohio State University and Jet Propulsion Laboratory) that involves an integrated near-real time monitoring and analysis of the major components of the pan-Arctic hydrologic cycle. Output from the AMSR-E snow algorithm will be compared with river discharge data compiled by this project as well as with modeled values of distributed winter precipitation. The Arctic Basin with its relatively non-forested and non-complex terrain and long persisting subfreezing snow cover is an excellent location for the validation of passive microwave snow algorithms. In addition, a number of the rivers draining into the Arctic Ocean are underlain by permafrost, in particular the Lena River, which reduces the amount of runoff going into ground water thus making the relationship between total seasonal SWE on the ground and total snow-melt season river runoff more direct.

For continuous long-term observations of snow extent in diverse environments at the regional to hemispheric scale we will evaluate the snow algorithms by comparison with the EOS MODIS daily global snow extent as well as the NOAA IMS daily Northern Hemisphere snow extent maps. For snow extent and water equivalent we will utilize data from the United States (NWS, NOHRSC and USDA) as well as additional surface station data obtained through our ongoing collaboration with the All-Russia Research Institute of Hydrometeorological Information, Obninsk, Russia, the Satellite Meteorology Institute, Beijing, China, the Cold and Arid Regions Environmental and Engineering Research Institute, Lanzhou, China, The Remote Sensing Group of the Tibetan Meteorological Bureau, Lhasa, Tibet and the Canadian IDS team CRYSYS.

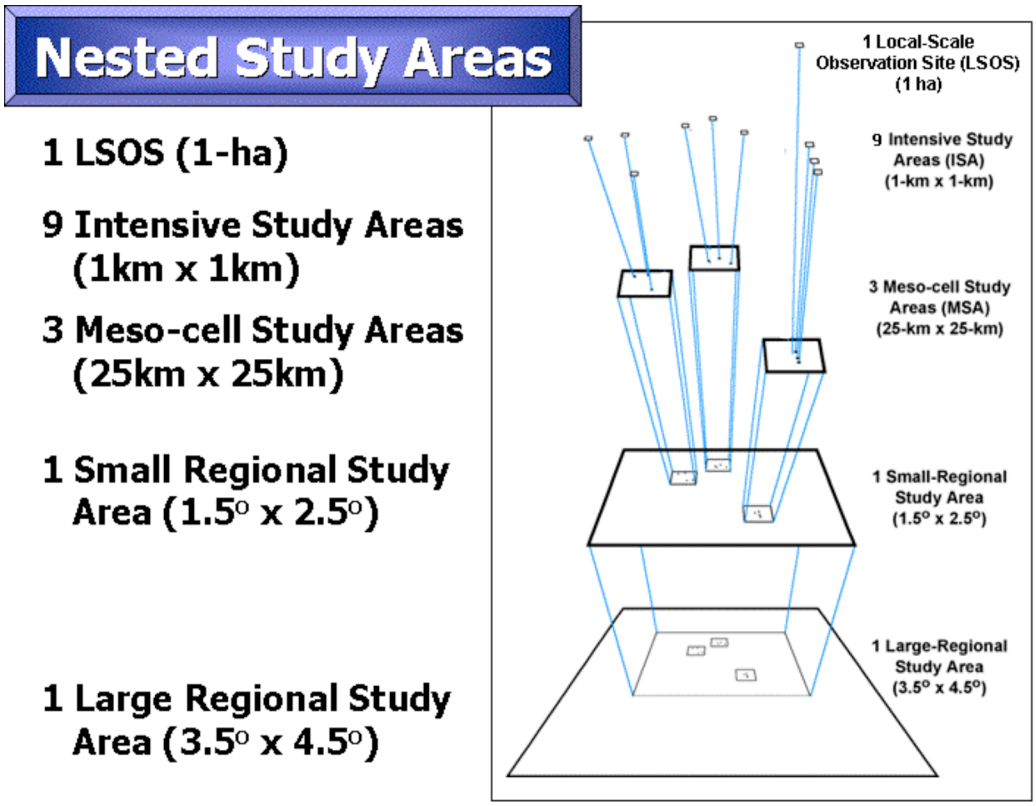

Figure 3.4.1. Cold Land Processes Field Experiment Nested Study Area Concept (Cline, 2001).

3.4.3 Field Experiments

During 2002 (using SSM/I data) and 2003 (using both AMSR-E and SSM/I data) the primary field experiment will be the NASA Cold Land Processes Field Experiment (CLPX) in northwestern Colorado. The CLPX is designed to improve our knowledge of the terrestrial cryosphere by providing a more compete understanding of the fluxes, storage and transformations of water and energy in cold land areas . Details of the CLPX experiment plan can be found in Cline et al. (2001) and on-line at http://www.nohrsc.nws.gov/~cline/clp.html. The CLPX, scheduled for 6 days each during both mid-February and late March of 2002 and 2003 (24 measurement days) will provide this study with unique validation data sets. These will include a wide range of measurements from the ground-based and airborne components of this field experiment. For each six day period, the ground based measurements will provide a spatial density that is unprecedented and will include 4500 snow depth measurements and 144 snow pit profiles (snow water equivalent, snow density, grain size type and size and temperature) to characterize the snow cover over three 25 x 25 km Meso-cell Study Areas (MSAs) providing data at the spatial scale of the AMSR-E footprint.

One component of the CLPX airborne sampling scheme does deserve specific description here. This is the plan for deployment of the NOAA AC690A Turbo Commander aircraft to measure mean areal snow water equivalent and soil moisture along flight lines within the three MSAs of the CLPX. Attenuation of natural terrestrial gamma radiation by water (any phase) in the snow and soil is the basis of the snow water equivalent and soil moistures measurements (Carroll, 1987). Although we will utilize the gamma data from all three MSAs (25-km x 25-km) our analysis will focus on the North Park MSA where the relative flat terrain will allow flight lines to be parallel and uniformly spaced 1-km apart. With a flight line field-of-view of 300-m and a line spacing of 1000-m, this sampling scheme will measure snow water equivalent over approximately 30% of the land area in the MSA. The opportunity to measure snow water

equivalent with this sampling density over an area comparable in size to a passive microwave snow algorithm footprint is unprecedented.

Earlier field experiments were conducted over the Red River valley and Colorado River basin during the 1997-1998 winter season. These field activities were designed to further our understanding of the evolution of snow grain size and spatial inhomogeneity of snow storage over a large area and to validate the pre-launch algorithm. Effects of forest cover on snow parameter estimates were also studied. Several different forest cover fraction indicators were tested. A maximum surface albedo map provided the best results. By applying the forest cover correction, the correlation coefficients of the estimated SWE and the measured SWE improved greatly. SSM/I data were used to test the pre-launch algorithm. Based on these earlier studies, and our ongoing research, forest cover correction coefficients are being applied to the AMSR-E algortim.

In developing the snow algorithm it has been found that the grain size distribution is one of the most critical parameters (Figure 3.4.2.). With a priori grain size profiles built into the algorithm, snow retrieval accuracy has been improved (Kelly et al., in press). Field experiments will be continued to measure snow grain size distribution and its variation with time. This is a part of the on going effort to create a comprehensive database for snow crystal size for different snow conditions. By collecting snowpack profiles for different snow conditions, we will be able to improve our model calculation of the brightness temperatures emerging from the snowpacks. The extensive spatially and temporally distributed ground-based measurements from the CLPX described above will make a fundamental contribution to a better understanding of the relationship between snow grain size and microwave emissivity.

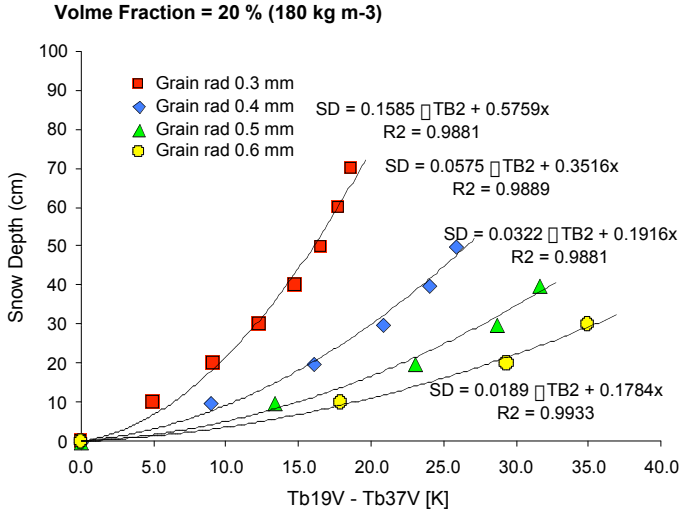

Figure 3.4.2. Model estimates of the relationship between snow depth (cm), microwave brightness temperature spectral gradient (TB) and snow grain radius (mm).

A joint field experiment with Prof. Martii Hallikainen of Helsinki University of Technology (HUT) is being considered for March of 2004 in northern Finland. HUT operates a set of microwave radiometers which match the AMSR frequencies and are mounted on a Skyvan aircraft. The sites selected for Finland include both forested and open areas. Ground teams will make systematic and comprehensive measurements of snow water equivalent, snow wetness and snow structure during the airborne campaign. The experiment plan and details regarding cost sharing are to be determined.

During 2003, in collaboration with Dr. Toshio Koike, we are operating the University of Tokyo, 7 channel, Ground Based Microwave Radiometer (GBMR-7) at the CLPX Local-scale Observation Site (LSOS) near Fraser Colorado. The CLPX LSOS is located within the secure site of the US Forest Service Fraser Experimental Forest Headquarters Facility. The GBMR is an AMSR simulator with the necessary frequencies to conduct fundamental snow and frozen ground

microwave signature studies essential to the improved understanding of the physics behind microwave snow algorithms.

Canadian colleagues are also planning AMSR-E validation activities during 2002-2003 winter as part of the CRYSYS program. This effort entails conducting snow surveys along a 600 km transect in northern Quebec (boreal forest to taiga environment) in support of AMSR-E SWE product validation. Additionally, CRYSYS investigators will be undertaking a lake ice field investigation in northern Canada (around Great Slave Lake) in March 2003.

3.4.4 Operational Surface Networks

Snow water equivalent and depth data are available from a limited number of snow courses world-wide. The number of data collection sites continues to diminish due to budgetary constraints and limited personnel available to make these, typically manual, measurements. One of the more stable programs is represented by the approximately 600 USDA Natural Resources Conservation Service (NRCS) SNOTEL automatic weather stations providing daily snow water equivalent in high snow accumulation regions throughout the western United States. These data are available in real-time for AMSR-E validation studies. Also, through our collaboration with the All-Russia Research Institute of Hydrometeorological Information, Obninsk, Russia (V. Razuvaev) we anticipate that selected snow data sets will become available for near-real-time AMSR-E snow algorithm validation. This collaboration and associated date acquisition is being carried out at the National Snow and Ice Data Center (NSIDC).

Recently the National Climate Data Center (NCDC) has made a web interface available to access data from the WMO/GTS system from more than 8,000 sites worldwide. These data include snow depth at many locations but the exact number, quality and reliability of these data are uncertain at this time (Figure 3.4.3). The degree to which this data set could be of value to this validation study in terms of spatial distribution, consistency in reporting and overall accuracy, is currently being evaluated at NSIDC.

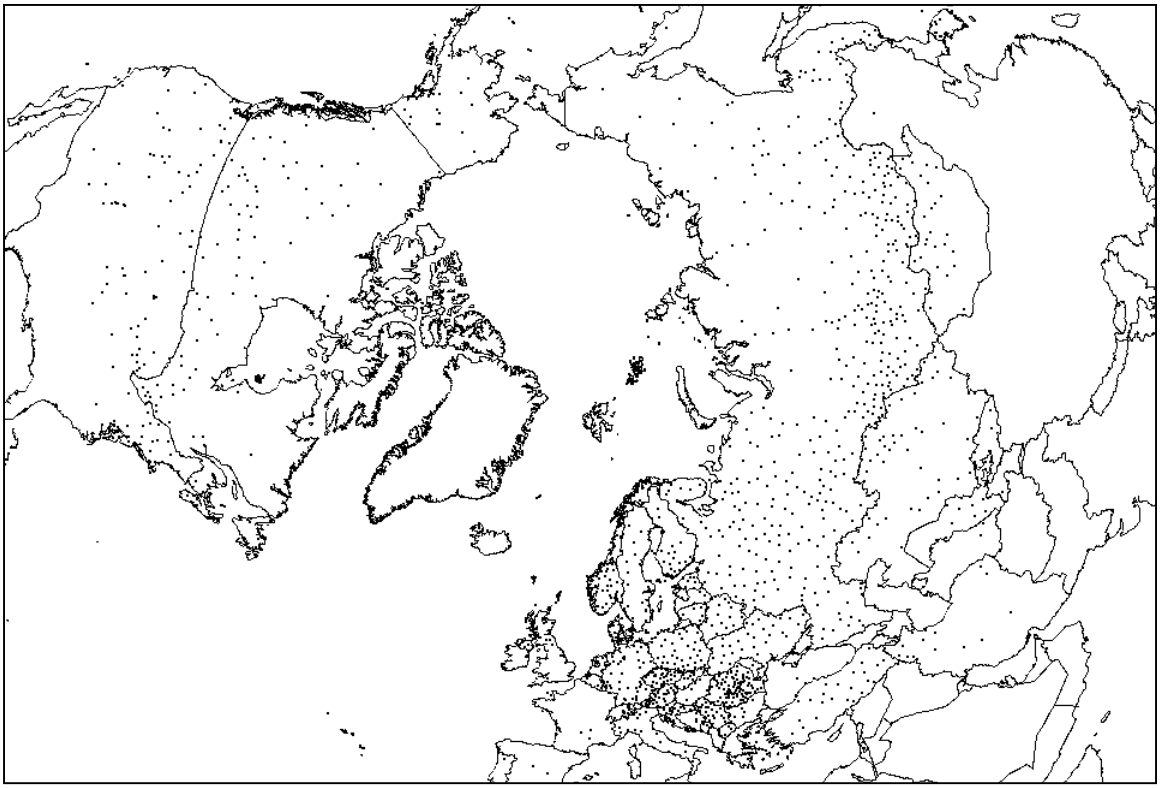

Figure 3.4.3. Location of WMO/GTS stations reporting snow depth greater than 2 cm for 2 February, 2001

3.4.5 Satellite Data

The Special Sensor Microwave Imager (SSM/I) with seven channels (19V, 19H, 22V, 37V, 37H, 85V and 85H) has flown on board the DMSP F-8, F-10, F-11, F-12, F-13 and F-14 satellites. There are over 15 years of SSM/I data available for snow algorithm development and testing. These data have proven to be extremely valuable for AMSR-E algorithm development. Although SSM/I does not provide the lower frequencies of AMSR-E, it is in fact the higher frequency channels that are most important for snow algorithm applications. We are also actively engaged in the NASDA snow algorithm validation comparing SSM/I data with 100 selected surface stations.

Even after the launch of AMSR-E, SSM/I data will continue to be very valuable especially during the period when the snow condition changes rapidly. The overpass time of the EOS Aqua satellite and the DMSP F-13 and F-14 satellites are approximately 6 hours apart allowing enhanced monitoring of diurnal variations in snow amount and properties. More frequent monitoring of snow parameters will help us understand short-term snowpack variability. When the snowpack is not changing rapidly, SWE retrieved from SSM/I data will continue to be used in the direct comparison of AMSR-E snow products.

MODIS, on-board the Terra satellite will provide snow cover maps with 500m spatial resolution. These maps will provide a quantitative snow fraction value over the much coarser AMSR-E footprint. Analysis of coincident MODIS and AMSR-E data will allow us to determine the degree to which the microwave SWE signature is dependent on the percentage of snow cover within the footprint.

3.4.6 Validation Time Line

Pre-launch validation:

Assessment of the quality of the SWE values derived from satellite data has been an ongoing effort (for example, Armstrong and Brodzik, 2001 and 2002; Kelly, 2001, Brubaker et al. 2001). These validation studies using SSM/I data vary in focus and in temporal and spatial scale. The fundamental methodology of such studies has been similar to basic techniques described in the previous sections.

Post-launch validation:

To validate AMSR snow products, focused field campaigns are necessary. Our immediate effort in this area is our collaboration with and participation in the NASA CLPX beginning in February of 2002 and continuing through March of 2003 as described above. Wherever possible we will explore all opportunities to coordinate with other AMSR algorithm teams where interests in land surface characteristics are complementary or where a synergy in the logistics of airborne microwave remote sensing campaigns can be developed.

As noted above, we are discussing a plan with Prof. Hallikainen to include Finland as a validation test site. Finland is an ideal site for snow algorithm validation because of its long snow season. This effort would require some additional support for the Helsinki University of Technology (HUT). Also, our Canadian colleague Dr. Barry Goodison has demonstrated an interest in a joint effort on snow algorithm validation within the Canadian Cyrospheric Systems (CRYSYS) NASA IDS project.

3.5 Land Surface (submitted by E. Njoku, with contributions from T. Jackson, T. Koike)

Soil moisture is the primary parameter retrieved by the AMSR-E land product algorithm. The algorithm also retrieves surface temperature and vegetation water content as diagnostic parameters. These parameters are all output as part of the level 2 (swath) soil moisture product. A level 3 product is generated by compositing the level 2 parameters into daily global maps. The ascending and descending swaths are composited separately so that diurnal effects can be evaluated. Soil moisture is not retrievable where significant fractions of snow cover, frozen ground, dense vegetation, precipitation, open water, or mountainous terrain occur within the sensor footprint (as determined by surface type classification and ancillary information). The products are generated on an Earth-fixed grid with ~25-km nominal grid spacing. The spatial resolution of the products is ~60 km (determined by the 6.9 GHz footprint resolution). (Note: Currently the use of the 6.9 GHz AMSR-E frequency in generating land products is being reconsidered due to the occurrence of radio-frequency interference.) The products are summarized in Table 3.5.1, and are described in the Aqua AMSR-E land surface parameters Algorithm Theoretical Basis Document (ATBD) http://eospso.gsfc.nasa.gov/atbd/amsrtables.html.

Table 3.5.1: AMSR-E Land-Surface Product Parameters

Product Level, Type	Parameter	*Spatial Resolution	+Grid Spacing	Temporal Resolution
2, S	Soil Moisture	56 km	25 km	swath
2, R	Vegetation Water Content	56 km	25 km	swath
2, R	Surface Temperature	56 km	25 km	swath
3, S	Soil Moisture	56 km	25 km	daily
3, R	Vegetation Water Content	56 km	25 km	daily
3, R	Surface Temperature	56 km	25 km	daily
3, S	Gridded Brightness Temps.	12, 56 km	25 km	daily

(S = Standard; R = Research)
* Average 6.9 GHz footprint dimension.
+ Nominal grid spacing (EASE-grid, global cylindrical projection)

The validation program focuses on soil moisture since it is the standard land surface parameter product. The primary validation approach is to conduct instrumented field experiments with comprehensive airborne and in-situ surface sampling of soil moisture, vegetation water content, surface temperature, and other relevant variables. Validation of surface temperature and vegetation water content, which are not standard products, will also be done by intercomparisons with similar parameters retrieved by AIRS and MODIS.

Understanding the spatial and temporal variability of soil moisture is a priority research focus of NASA's Terrestrial Hydrology Program (THP). The AMSR-E instrument was launched on Aqua in May 2002, and a similar AMSR instrument was launched on NASDA's ADEOS-II satellite in December 2002. Soil moisture will be retrieved from the ADEOS-II AMSR initially using four different algorithms including the Aqua AMSR-E algorithm. The AMSR-E soil moisture validation is therefore being coordinated with research investigations of the NASA THP as well as with ADEOS-II AMSR validation activities. This document includes contributions from investigators of both the Aqua and ADEOS-II validation teams.

3.5.1 Validation Criteria and Method

The validation objectives include: (1) assessment and refinement of soil moisture algorithm performance, (2) verification of soil moisture estimation accuracy, (3) investigation of the effects of vegetation, surface temperature, topography, and soil texture in affecting the soil moisture accuracy, and (4) determination of the regions globally where useful soil moisture can be derived. The key objective of the validation is to assess whether and under what conditions the AMSR-derived soil moisture meets the target accuracy goal of 0.06 g-cm^{-3} at 60-km spatial scale. Soil moisture research, and applications using the data are not of themselves primary goals of the validation program.

Since there has been rather limited experience with large-scale soil moisture estimation from space, the expected accuracies of AMSR-derived land surface parameters were estimated by model simulations. With an assumed instrument noise of 0.5 K and allowance for modeling error the retrieval accuracies were estimated as: 0.06 g-cm^{-3}, 0.15 kg-m^{-2}, and 2.5 C for soil moisture, vegetation water content, and surface temperature, respectively, for vegetation water content less than 1.5 kg-m^{-2}. The soil moisture retrieval accuracy decreases significantly as vegetation cover increases due to attenuation of microwave radiation by the vegetation canopy. These accuracies are adequate for some hydrology and climate science applications. However, as hydrologic models improve and experience is gained in understanding large-scale hydrologic processes, increased accuracy and spatial resolution will become desirable, e.g., 0.04 g-cm^{-3} at 10-30 km spatial resolution. This will require a dedicated soil moisture observing mission with lower frequency channels (e.g. L-band) and better spatial resolution than AMSR provides.

Aspects to be considered in retrieving and validating the AMSR soil moisture product include:

- Uncertainties associated with radiative transfer model parameterizations (such as soil roughness, vegetation scattering and opacity, and soil texture) which propagate into soil moisture retrieval algorithm uncertainties.
- AMSR footprints contain mixtures of different surface types. Retrievals represent spatial averages over 60-km 6.9-GHz footprints. Nonlinearities in the radiative transfer processes may give rise to differences between retrieved and area-averaged quantities.
- Retrieved parameters represent averages over the vertical microwave sampling depth. This depth varies with frequency and the amount of moisture in the soil and/or vegetation. Different sampling depths at different AMSR frequencies may give rise to errors in the retrievals and in comparisons between retrievals and in-situ measurements, especially where the moisture and temperature profiles are nonuniform.
- Retrieval errors increase with vegetation cover. A vegetation water content transition threshold for reliability of the retrievals is estimated from simulations as ~1.5 kg-m^{-2}. Experience with AMSR data during the validation phase will help define this threshhold better.

The approaches to be followed in addressing the above issues include the following components:

Algorithm calibration tests will be conducted throughout the AMSR mission to estimate, monitor, and correct bias offsets between AMSR-observed and model-computed brightness temperatures. Offsets may be due to radiometer absolute calibration errors or to errors in parameters of the radiative transfer (RT) model. Algorithm calibration will permit adjustment of the brightness temperatures computed by the RT model (used in the retrieval algorithm) to the AMSR-observed values.

Long-term measurement networks, operated within the U.S. and in other countries, are a source of in-situ soil moisture data for point comparisons with the AMSR observations over continuous seasonal and annual cycles. These networks also provide standard automated

meteorological data that will be useful in correcting and interpreting the AMSR soil moisture information.

Field experiments will provide short-term (~1 month) intensive measurements of soil moisture and other surface and atmospheric characteristics at the AMSR footprint scale, using automated and manual in-situ sampling and airborne radiometers to generate calibrated spatial soil moisture fields.

Hydrologic modeling will be performed to generate soil moisture products at larger (basin-wide and continental) scales using assimilated data independent of AMSR data. The resulting soil moisture fields will be compared with AMSR-derived soil moisture over diurnal and seasonal cycles. The model-derived soil moisture fields will be of lower accuracy than field experiment data, but will extend the comparisons to larger space and time domains.

Satellite data intercomparisons will be performed using data from sensors on the same satellite (AIRS, MODIS) and from microwave sensors on other satellites (SSM/I, TMI, ADEOS II AMSR, Radars). These intercomparisons provide consistency checks for the soil moisture. They will also provide independent information on surface temperature, vegetation cover, brightness temperature, and radar backscatter that can be used to determine the accuracy of the AMSR brightness temperatures, and the effects of temperature, vegetation, topography, and roughness on the AMSR soil moisture retrievals.

Other measurements not specifically described here such as truck-based measurements and augmentations to the operational network stations, will broaden the information available on the temporal variability of microwave brightness temperature, soil moisture, and vegetation biomass over varied ecosystems and seasonal cycles.

3.5.2 Algorithm Calibration

The accuracy of the AMSR retrievals will be affected by calibration offsets between AMSR-observed and radiative transfer model-computed brightness temperatures. Calibration of the models to the satellite data is necessary to eliminate retrieval bias errors. Algorithm calibration includes estimating radiometric calibration errors and tuning the parameterization of the microwave models (i.e. coefficients for surface roughness, vegetation opacity, and vegetation albedo). These parameters have in the past been estimated using ground-based and airborne data, but have not been validated at the satellite footprint scale. Tests of the algorithm calibration procedure have been initiated using existing satellite data (SMMR, SSM/I, TMI) and data from well-instrumented field experiments such as SGP97 and SGP99, as well as data from monitoring sites that have limited in-situ data but are homogeneous and have known surface characteristics.

The calibration monitoring sites are selected for geographic diversity and for homogeneity over the footprint scale, so that they can be characterized by a reduced number of parameters. Operational meteorological data (primarily surface air data and forecast model output) will be acquired over these regions. Desert sites (with minimal soil moisture and vegetation, and little seasonal variability) will be used to calibrate topographic and roughness effects. Dry and humid forests (dense vegetation) will be used to calibrate the opacity and single scattering albedo coefficients. Grasslands and savannas (low vegetation but with seasonal variability) will be used to adjust the vegetation opacity coefficients to provide the correct time-varying vegetation signal.

Sites have been selected in each category that span the continents and northern and southern hemispheres. In this manner, by choosing sites of extreme (but near-constant) vegetation conditions, and intermediate (but time-varying conditions) the brightness temperature

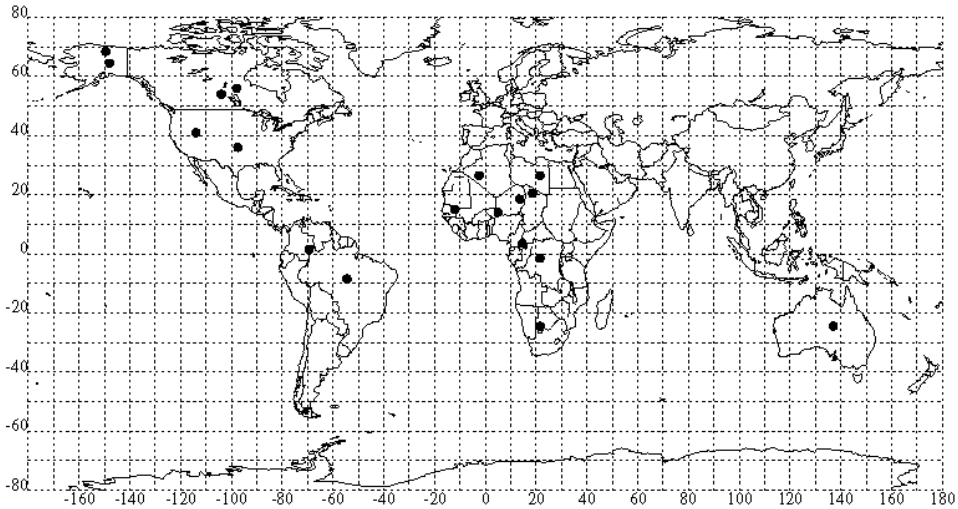

Figure 3.5.1: Locations of AMSR-E land calibration monitoring sites.

calibration offsets and radiative transfer model coefficients can be fine-tuned (the ATBD document provides more details on the algorithm model equations and coefficient estimation). These offsets and coefficients are global constants in the algorithm. Local variability due to specific vegetation types and roughness are corrected in the algorithm using ancillary databases (where available).

The above procedure is analogous to the standard method for estimation of brightness temperature and model calibration offsets over the ocean (in that case using regions of low winds and incorporating ancillary information on sea surface temperature and humidity). Statistics acquired continuously at the calibration sites during the mission will be used to determine and remove long-term algorithm calibration drifts. The locations and summary descriptions of the monitoring sites are given in Figure 3.5.1 and Table 3.5.2. AMSR brightness temperature statistics will be compiled at all the sites, but algorithm coefficient estimation will be done only at those sites where meteorological data are available.

3.5.3 Operational Networks

Operational measurement networks within the U.S. and in other countries are a source of in-situ soil moisture data for long-term point comparisons with the AMSR observations. Some of these data are subject to restrictions (availability and cost) imposed by the sponsoring agencies, and are of varying quality and usefulness. The key measurement networks in the U.S. are the Department of Energy (DOE) Atmospheric Radiation Measurement (ARM) program, the Oklahoma Mesonet, the U.S. Department of Agriculture (USDA) Soil Climate Analysis Network (SCAN), the USDA Agricultural Research Service (ARS) Micronet, and the Illinois State Water Survey. Data from operational measurements in the former Soviet Union, Mongolia, and China have also recently become available. Additional measurement programs in Mongolia and Tibet are being initiated as part of the Global Energy and Water Cycle (GEWEX) Asian Monsoon Experiment (GAME) and the NASDA AMSR validation program.

The operational network measurements are point data, and thus are not representative of footprint-averaged soil moisture. They will not provide accurate point by point validation of the AMSR footprint-averaged soil moisture. However, since they are made routinely and continuously over long time periods they can be used to validate the temporal soil moisture changes observed in the AMSR data. Temporal plots and statistics of the in-situ versus AMSR data will be made over seasonal and annual cycles, and analyzed as a function of local land cover, soil texture, and topographic conditions. Figure 3.5.2 shows operational networks in the SGP region (Oklahoma).

Table 3.5.2: Description of calibration sites

#	Ecosystem	Name	Region	Lat-Lon	Attributes
1	Desert	Simpson Desert	Central Australia	23.5-25.5 S 136-138 E	Low Relief, S. Hemisphere
2	Desert	Kalahari Desert	S.W. Botswana	23-26 S 20-23 E	Low Relief, S. Hemisphere
3	Desert	Western Desert	W. Egypt	25-28 N 25-28 E	Low Relief, N. Hemisphere
4	Desert	Sebkha Mekerrhane	S. Central Algeria	25-28 N 1-4 W	Moderate Relief, N. Hemisphere
5	Desert	Tibesti Mountains	N.W Chad	19-22 N 17-20 E	High Relief, N. Hemisphere
6	Sahel	Bilma	E. Niger	17-20 N 12-15 E	Northern Sahel
7	Sahel	Tahoua	S.W. Niger	13-15 N 4-6 E	Central Sahel
8	Sahel	Kayes	Mali/Senegal	14-16 N 11-13 W	Western Sahel
9	Tropical Forest	Boumba	S.E. Cameroon	2-5 N 13-16 E	Africa, N. Hemisphere
10	Tropical Forest	Salonga	Central Zaire	0-3 S 20-23 E	Africa, S. Hemisphere
11	Tropical Forest	Mitu	Colombia/ Brazil	0-3 N 68-71 W	S. America N. Hemisphere
12	Tropical Forest	Curua	Central Brazil	7-10 S 53-56 W	S. America, S. Hemisphere
13	Boreal Forest	Boreas SSA	Saskatchewan, Canada	53.5-54.5 N 103.5-104.5 W	Southern BOREAS Experiment Site
14	Boreal Forest	Boreas NSA	Manitoba, Canada	55.5-56.5 N 97.5-98.5 W	Northern BOREAS Experiment Site
15	Boreal Forest	Bonanza Creek	Central Alaska, U.S.	64-65 N 147.5-148.5 W	Ecological Forest Experimental Site
16	Tundra	Toolic Lake	N. Central Alaska, U.S.	68-69 N 149-150 W	LTER Site
17	Salt Lake Basin	Great Salt Lake	N.W. Utah, U.S.	38-44 N 111-117 W	Desert Hydrologic Basin
18	Plains Grassland	Southern Great Plains	Oklahoma/ Kansas, U.S.	34-38 N 96-99 W	Sub-humid Hydrologic Basin

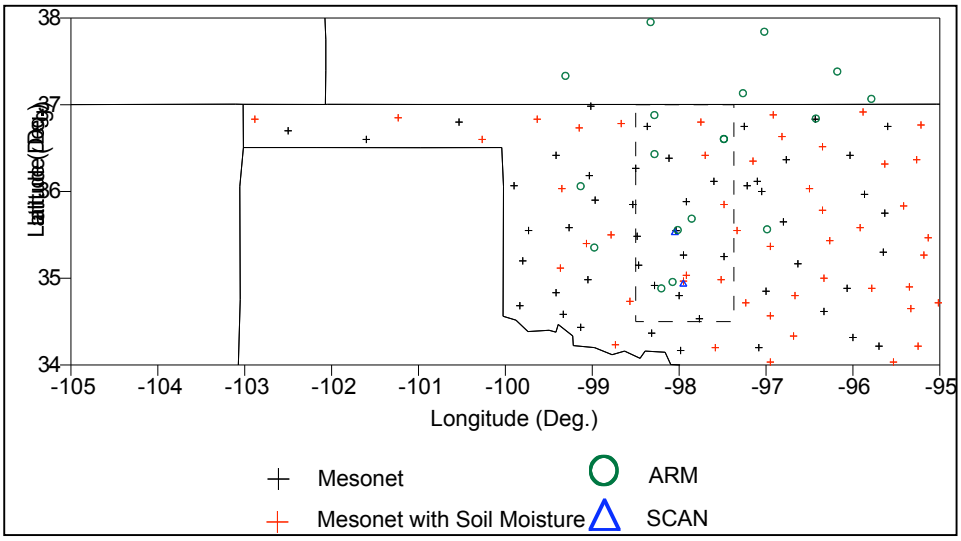

Figure 3.5.2: Operational networks in the SGP (Oklahoma) region

DOE ARM

The DOE ARM program operates a large number, and various types, of instruments within the U.S. Southern Great Plains (SGP) region. The Southern Great Plains is one of the ARM Cloud and Radiation Testbeds (CART). The SGP ARM/CART site layout is based upon a heavily instrumented central facility (CF) surrounded by 22 extended facilities (EF) with fewer instruments, 4 boundary facilities (BF), and 3 intermediate facilities (IF). Soil moisture and meteorological data are collected at the CF and EF sites. Radiosonde observations are made at the CF on weekdays at 530, 1130, 2030, and 2330 (UTC). During intensive observing periods the frequency is increased, weekends are included, and observations are also made at BF sites.

Oklahoma Mesonet

The Oklahoma Mesonet is an automated environmental observing system distributed over the state of Oklahoma. There are 114 stations providing observations every 5 minutes. Data are collected and transmitted to a central point every 15 minutes where they are quality controlled, distributed and archived. Each station consists of a 10 m tower providing measurements of air temperature (1.5 m), relative humidity (1.5 m), wind speed and direction (10 m), barometric pressure, rainfall, solar radiation, and soil temperature (10 cm for both sod and bare soil). About half the stations provide supplemental measurements of air temperature (9 m), wind speed and direction (2 m), leaf wetness, soil moisture (5, 25, 60 and 75 cm under sod), and soil temperature (5 and 30 cm under sod and 5 cm under bare soil). Data files from the Mesonet are copyrighted and must be purchased.

USDA SCAN

The USDA has initiated a nationwide soil moisture and soil temperature analysis network called SCAN. Data are provided to the public on the Internet in real time. Each system provides hourly observations of air temperature, barometric pressure, wind speed, precipitation, relative humidity, solar radiation, soil temperature at 5, 10, 20, 50 and 100 cm, and soil moisture at 5, 10, 20, 50 and 100 cm. There are SCAN sites of interest to AMSR validation operating in the SGP region (Oklahoma), Georgia and, possibly in future, Iowa.

USDA ARS Micronet

The USDA ARS Grazinglands Research Laboratory at El Reno, Oklahoma operates a meteorological network within the Little Washita watershed called the ARS Micronet. There are 42 ARS Micronet stations. The data consist of accumulated rainfall, relative humidity, air temperature at 1.5 m, solar radiation, and soil temperature at 5, 10, 15 and 30 cm below ground surface. Climate data are provided in 5-minute increments and the soil temperature data are provided in 15-minute increments. In addition, ARS also operates an experimental Soil Heat and Water Measurement System. This includes heat dissipation sensors at selected Micronet sites. These sensors provide soil water matric potential data. The data consist of matric potential values at 5, 10, 15, 20, 25, and 60 cm below the ground surface, at 1-hour increments.

Illinois State Water Survey

The Illinois State Water Survey has conducted soil moisture measurements since 1981 at 19 stations distributed over the state. The measurements are made using the neutron-probe technique at depths of 0-10, 10-30, and 20-200 cm. Measurement frequency is about every two weeks during the growing season and once per month during the rest of the year.

FSU, Mongolia, China

Data from operational measurements in the former Soviet Union, Mongolia, and China have recently become available through the Global Soil Moisture Data Bank, a web-based archive compiled by investigators at Rutgers University and their colleagues. The data are in-situ gravimetric measurements from mostly grassland and agricultural sites measured in the top 10-cm of soil. Due to the considerable effort required to compile and quality-control these data most of the data are not current, and are useful primarily for retrospective analyses. Data from Mongolian sites in closer to real time will be available through the ADEOS-II AMSR validation program.

3.5.4 Field Experiments

The AMSR soil moisture field experiments are designed to take advantage of short-term (~1 month) intensive sampling of soil moisture and other surface and atmospheric characteristics using automated and manual in-situ measurements and airborne radiometers. The data can be analyzed to provide validation products at the AMSR footprint scale. Test sites are selected for feasibility of characterizing the spatial variability of surface moisture, temperature, and vegetation over a region encompassing a few (3 to 6) AMSR footprints, and for geographic diversity of vegetation, topography, and climate. (Experiments of this type were carried out in 1997 and 1999 in the SGP region of the U.S. (SGP97 and SGP99).

The first AMSR-E soil moisture validation experiment (SMEX02) was carried out in June/July 2002 over the Walnut Creek watershed and regional area near Ames, Iowa. A description of this experiment and the experiment plan can be found at the web site: http://hydrolab.arsusda.gov/smex02. A workshop reviewing data from the experiment was held on January 14/15, 2003 in Columbia, MD. Data from the experiment will be available as of February, 2003 from the National Snow and Ice Data Center Distributed Active Archive Center (NSIDC DAAC) http://nsidc.org/data/amsr_validation/soil_moisture/. Figure 3.5.3 shows an overview of the SMEX02 experiment.

Additional experiments at U.S. sites are planned in the summers of 2003 and 2005. The 2003 sites include Oklahoma, Georgia, and Alabama in June and July, while the 2005 sites will likely include Arizona and possibly Idaho. Site selections for 2005 are intended to provide sites with some topographic variability and contrast between semi-arid and vegetated conditions. Also in September 2003, sites in Brazil are being considered for aircraft overflights and ground sampling to support AMSR validation. Descriptions of the 2003 experiments in the U. S. and

Brazil, designated SMEX03, can be found at the SMEX03 experiment planning web site: http://hydrolab.arsusda.gov/smex03.

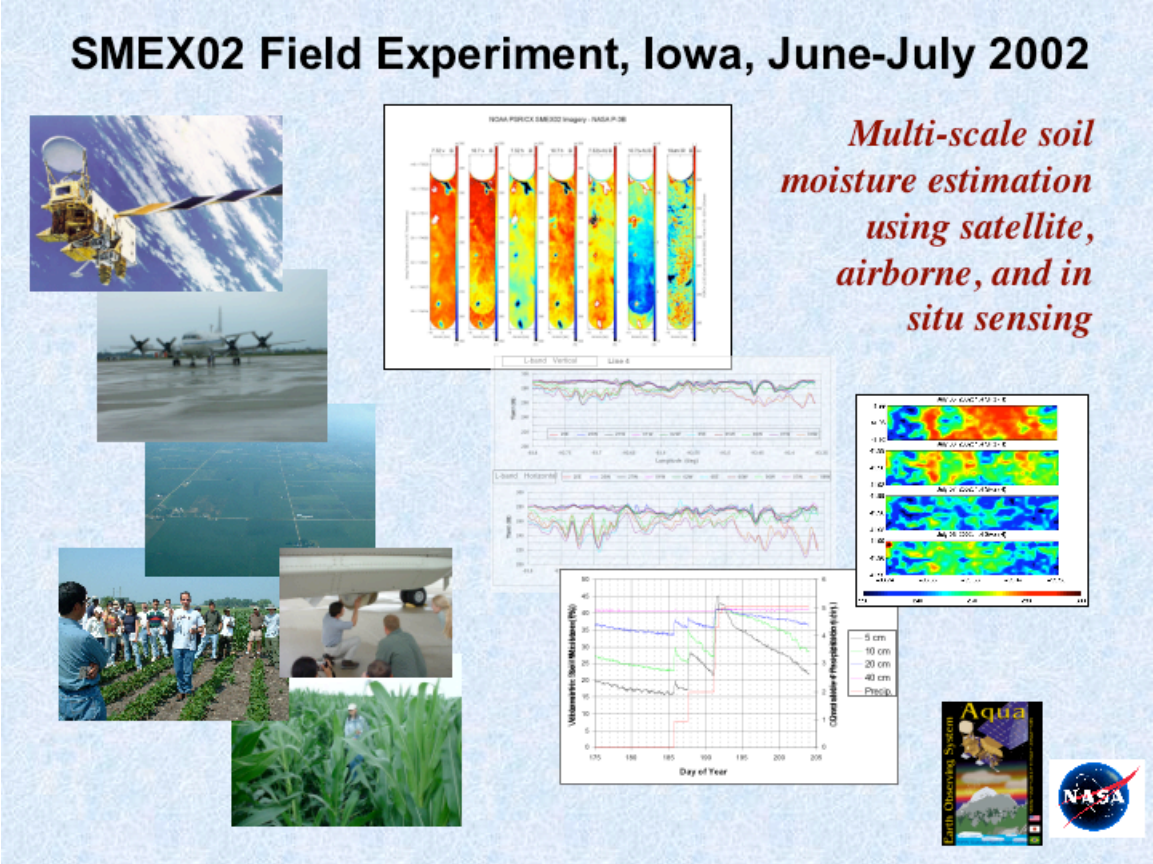

Figure 3.5.3. Overview of SMEX02 Experiment

ADEOS-II AMSR soil moisture validation experiments are planned at sites in Asia as Japanese NASDA-funded validation activities. Sites have been identified and instrumented in Thailand, Tibet, and Mongolia for experiments in 2001, 2002, and beyond (ADEOS-II AMSR Validation Plan).

U. S. Sites

The approach for the U. S. field experiments is to use airborne radiometers and in-situ sampling to generate daily soil moisture maps over regions spanning a few AMSR footprints. These can be compared with the AMSR soil moisture retrievals over a range of soil moisture conditions during the one-month experiment duration. The airborne soil moisture mapping is done using a variety of microwave airborne sensors. Sensors flown to date, e.g. in SGP99 and SMEX02, include the NOAA Environmental Technology Laboratory (ETL) Polarimetric Scanning Radiometer (PSR) which has the same frequencies, polarizations, and viewing angle as the AMSR, and the Jet Propulsion Laboratory (JPL) Passive/Active L/S-band sensor (PALS) which has L- and S-band radiometer and radar channels. The PSR is flown on the NASA P3 aircraft at high-altitude (~7 km) to map a 100 x 300 km region at ~2-km spatial resolution. The PALS is flown on the NCAR C-130 aircraft to underfly the P-3 at ~1-km altitude over a limited region (10 x 50 km), to provide field-resolution (~0.4 km) soil moisture maps. In SMEX02, within the regions mapped by the PSR and PALS several fields with vegetation covers representative of the larger region were intensively sampled to obtain soil moisture and temperature profiles, soil textures and bulk densities, and surface roughness and vegetation characteristics. Other microwave

radiometers were also flown to take advantage of available accommodations on the P-3 and C-130 aircraft. These include the ESTAR and GPS-reflection instruments.

The in-situ measurements are averaged for each field and applied with established L-band brightness temperature versus soil moisture relationships to generate L-band aircraft sensor-derived regional soil moisture maps. Results from SGP99 show that this can be done to about 3% volumetric soil moisture accuracy. The in-situ and L-band data are used to calibrate the wide coverage C-band sensor-generated soil moisture maps which in turn provide comparisons with the AMSR data at the AMSR footprint scale. The airborne C-band sensor maps also provide insights into the effects of heterogeneity within the AMSR footprint. The accuracy of the soil moisture data maps at the different scales can be estimated using statistical techniques, and is estimated from previous experiments as ~3-4% volumetric.

Factors to be considered in implementing this procedure include: variability of soil texture, vegetation, and topography at different scales; logistical difficulties of coordinating in-situ and airborne radiometer measurements with the AMSR-E overpass times; reliability of equipment; availability of human resources for field sampling; and uncertainty of meteorological conditions (precipitation and drying) such that a good soil moisture dynamic range can be observed. Sufficient measurements are required to assess the effects of vegetation, temperature, texture, and topography on the soil moisture accuracy. Available soils, vegetation, and topographic maps, as well as Landsat and MODIS images, are used for these purposes.

While the core Aqua/ADEOS-II soil moisture validation team members have overall responsibility for the validation planning, a much larger group of investigators is typically involved in collecting, processing, and analyzing the data. Following procedures implemented successfully for SGP97 and SGP99, Aqua project validation funds are used to support government agency, university faculty, and student personnel in the data acquisition, processing and analysis. All experiment data are placed in the public archive (NSIDC DAAC) for availability to other researchers funded by NASA's EOS and Terrestrial Hydrology programs.

Mongolia, Tibet, Thailand

Experiments at Asian field sites in Mongolia, Tibet, and Thailand are planned as part of the ADEOS-II AMSR validation activities. Details of these experiments can be found in the ADEOS-II Validation Plan. Data from these experiments are expected to be made available by NASDA for joint AMSR team validation. Exchanges between U.S and Japanese team members of data acquired in the SGP99 and Tibetan Plateau experiments has already occurred, and such exchanges are expected to continue. The approach for the Asian field sites is to use long-term measurements from automated stations and gravimetric sampling during periodic intensive field campaigns to acquire soil hydrology and surface meteorological data. The Mongolian Plateau experiment will cover a region 160 x 160 km in southern Ulaanbaatar where the terrain is generally flat with grass and bare surface conditions. Automated measurements include soil moisture, temperature air temperature, and precipitation. Intensive sampling to be carried out includes the above, plus plant water content and LAI, surface roughness, and soil bulk density and texture.

3.5.5 Modeling and Data Assimilation

Airborne radiometers provide one means for deriving satellite-footprint-scale soil moisture over a limited region and time period. Another method for producing soil moisture fields, over larger areas and longer time periods, is hydrologic modeling with data assimilation. The data assimilated include atmospheric forcing and surface in-situ data. The models used are land-surface hydrologic models or more sophisticated surface-atmosphere coupled models. The models operate at various time and space scales, and with varying schemes for data assimilation. Key parameters at the model grid scale, such as precipitation and surface net radiation, depend on the input data quality and parameterizations of the models, and their errors can be difficult to

assess. Thus, model output fields will be used mainly for consistency checking of the spatial and temporal patterns of AMSR-derived soil moisture rather than for quantitative validation of the soil moisture accuracy.

The generation of specific model output fields for AMSR validation is part of the broad-based AMSR-E validation plan. These include model products currently being developed by the GSFC Data Assimilation Office (DAO) and the operational forecast centers (NCEP and ECMWF) and through the Aqua Validation NASA Research Announcement (NRA) research investigations

3.5.6 Satellite Data Intercomparison

Satellite data intercomparisons will be performed: (1) to assess brightness temperature (TB) calibration levels over land, (2) to intercompare geophysical products between AMSR, AIRS, and MODIS, and (3) to evaluate effects of heterogeneity within the AMSR footprint.

Brightness temperatures from ADEOS-II AMSR (at 6.9, 10.7, 18.7, and 36.5 GHz), TRMM Microwave Imager (TMI) (at 10.7, 19.35, and 37 GHz), and DMSP Special Sensor Microwave Imager (SSM/I) (at 19.35 and 37 GHz) will be registered to the Aqua AMSR grid and compared with the Aqua AMSR 6.9, 10.7, 18.7, and 36.5 GHz brightness temperatures. Statistics will be compiled of the means and standard deviations of the TB differences as functions of time during the mission. Although the launch dates, sampling times, spatial resolutions, frequencies, and incidence angles are somewhat different between the sensors the statistics compiled over time will indicate relative sensor calibration offsets and drifts, as well as the relative instrument sensitivities.

Geophysical validation will be carried out at the AMSR footprint scale by intercomparisons between products from the Aqua AMSR, AIRS, and MODIS instruments. Specifically, using infrared (IR) land surface temperature (LST) from AIRS and MODIS, and leaf area index (LAI) from MODIS. The IR LST products will be averaged and co-registered to the AMSR footprint resolution and locations and compared with the AMSR LST. Differences will be interpreted in terms of terrain, soil moisture, and landcover characteristics. The LAI product will be averaged to the AMSR footprints and compared against the AMSR-derived vegetation water content. Relationships will be developed between LAI and vegetation water content for different vegetation types, and these relationships will be evaluated against published relationships derived at local scales for similar vegetation classes. Over limited regions, principally at the AMSR validation experiment sites (Figure 3.5.3) MODIS high-resolution landcover data will be accumulated for each AMSR footprint and used to interpret the effects of vegetation heterogeneity on AMSR soil moisture retrievals.

Data from synthetic aperture radars (SARs) such as Radarsat and ERS (if operating during the AMSR mission) can be analyzed jointly with AMSR data as case studies. Such studies may provide additional insights into effects of surface heterogeneity and microwave surface signatures at different scales. The use of SAR data is not emphasized in this plan, however, since the quantitative interpretation of vegetation, roughness, and soil moisture effects in SAR data itself requires research and careful study.

4 IMPLEMENTATION OF VALIDATION RESULTS IN DATA PRODUCTION

4.1 Approach

AMSR-E's primary heritage is SSM/I. SSM/I is an externally calibrated instrument and over the thirteen years that it has been flying it proved to be a very stable instrument. After the initial on-orbit calibration, where the ground calibration (instrument characterization) is verified, all data should be ready to be processed routinely. A second instrument, the TRMM Microwave Imager, is currently expected to last until the end of 2001. Should TMI still be operating at the time of the AMSR-E launch, it will offer an opportunity for direct calibration when the two sensors intersect their orbits. Since TMI will be routinely compared to SSM/I, this opportunity will insure that the AMSR-E instrument calibration is commensurate with the SSM/I sensors and would give additional confidence to the radiance measurements.

Once the radiance measurements are verified, geophysical algorithm verification must begin. Experience tells us that 2-4 months are typically needed to insure that a variety of artifacts typically found in new data sets are understood and properly handled by the algorithms. These situations vary from the mundane quality control issues to the subtle conditions such as satellite maneuvers when the data appears valid but in fact require geometric corrections or are altogether unusable. Where AMSR-E algorithms utilize channels not available on SSM/I, an initial period is also required to build up the required statistics from ground based networks. Geophysical parameters that have been scrubbed of any physically implausible solutions should realistically be expected approximately six months after launch.

After the initial checkout of the instrument, the AMSR-E team will concentrate on comparing results to the routine observations gathered as part of the validation program. This process will insure that the products contain no systematic biases and will help define some of the uncertainties within the geophysical products. Systematic deviations between satellite derived and ground based products should be corrected within the first year. From an overall implementation strategy, it therefore makes sense to consider doing routine product generation 6 months after launch, with an initial reprocessing one year after launch.

The routine collection of validation data, as well as the data collected during focused experiments is intended to refine assumption within the geophysical algorithms. It should therefore be expected that the AMSR-E products would continue to improve throughout the lifetime of the AMSR-E. To make these improvements available to the research community, the AMSR-E products therefore need to be regenerated periodically to incorporate the new understanding offered by the routine and special validation campaigns. We recommend that the AMSR-E team convene annually for the purpose of examining if the scientific advances in the previous year warrant that the data be reprocessed or not.

4.2 Role of EOSDIS

EOSDIS has contracted the AMSR-E Science Investigator-led Processing System (SIPS) to process the higher level (2 and up) standard products. The AMSR-E SIPS is composed of Remote Sensing Systems (RSS) and the Global Hydrology Resource Center (GHRC) group managed by M. Goodman, co-located with the AMSR-E Team leader, at MSFC. Once the standard products are processed they will be sent to NSIDC. NSIDC DAAC will archive and distribute the AMSR-E standard products. They will also archive the Level 1A data. These data will be processed and delivered to the US by NASDA, in Japan.

4.3 Archival of Validation Data

The validation data will be archived by different DAACs. The following is a proposal that has not yet been approved by EOSDIS.

a) The sea ice and snow validation data to be archived at NSIDC. NSIDC is a well known facility, with vast experience in sea ice and snow data sets.

b) The GSFC DAAC to archive the rainfall and soil moisture validation data sets

In the next year, as specific AMSR-E validation data will be collected this proposal will be discussed and decided upon.

REFERENCES

Aagaard, K., L. K. Coachman, and E. C. Carmack, On the halocline of the Arctic Ocean, Deep Sea Res., 29, 529-545, 1981..

Armstrong, R.L. and Brodzik, M.J. 1999. A twenty year record of global snow cover fluctuations derived from passive microwave remote sensing data, 5th Conference on Polar Meteorology and Oceanography, American Meteorological Society, Dallas, TX: 113-117.

Armstrong, R.L. and Brodzik, M.J. 1995. An earth-gridded SSM/I data set for cryospheric studies and global change monitoring. Advances in Space Research, 16(10): 155-163.

Armstrong, R.L. and Brodzik, M.J. 1998. A comparison of Northern Hemisphere snow extent derived from passive microwave and visible remote sensing data. IGARSS-98, Proceedings: 1255-1257.

Armstrong, R.L. and M.J. Brodzik, 2002. Hemispheric-scale comparison and evaluation of passive microwave snow algorithms, Annals of Glaciology Volume 34:38-44.

Armstrong, R.L. and M.J. Brodzik, 2001. Recent Northern Hemisphere snow extent: a comparison of data derived from visible and microwave sensors, Geophysical Research Letters, Vol. 28, No.19.

Armstrong, R.L. and M.J. Brodzik, 2001. Validation of Passive Microwave Snow Algorithms, Remote Sensing and Hydrology 2000, IAHS Pub. No. 267, Eds. M. Owe, K. Brubaker, J. Ritchie and A. Rango, p.p. 87-92.

Armstrong, R.L., A. Chang, A. Rango and E. Josberger, 1993. Snow depths and grain size relationships with relevance for passive microwave studies, Annals of Glaciology, no.17:171-176.

Austin, R. T. and G. L. Stephens, 2001: Retrieval of stratus cloud microphysical parameters using millimetric radar and visible optical depth in preparation for CloudSat, Part I: Algorithm formulation. J. Geophys. Res., 106, 28233-28242.

Barber, D. G. and J. Yackel, The physical, radiative, and microwave scattering characteristics of melt ponds on sea ice, Int. J. Remote Sensing, 20, 2069-2090, 2000.

Bauer, P. and N. Grody, 1995: The potential of combining SSM/I and SSMT/2 measurements to improve the identification of snowcover and precipitation. IEEE Trans. Geosci Rem. Sens., 33, 252-261.

Bell, T. L. and P. K. Kundu, 2000: Dependence of satellite sampling error on monthly averages rain rates: Comparison of simple models and recent studies. J. Climate, 13, 449-462.

Bell, T. L., P. K. Kundu, and C. D. Kummerow, 2001:Sampling errors of SSM/I and TRMM rainfall averages: Comparison with error estimates from surface data and simple model. J. Appl. Meteor., 40, 938-954.

Bennartz, R. and D. B. Michelson, 2001: Correlation of precipitation estimates from spaceborne passive microwave sensors and weather radar imagery for BALTEX PIDCAP. In press Int. J. Remote Sensing.

Bennartz, R. and Petty G. W., 2001: The sensitivity of microwave remote sensing observations of precipitation to ice particle size distributions. J. Appl. Meteor., 40, 345-364.

Bjørgo, E., O.M. Johannessen, and M.W. Miles, Analysis of merged SSMR-SSMI of Arctic and Antarctic sea ice parameters 1978-1995. Geophys. Res. Lett., 24(4), 413-416, 1997.

Björk, G., A one-dimensional time-dcpendent model for the vertical stratification of the upper Arctic Ocean, J. Phys. Oceanogr., 19, 52-67, 1989.

Brown, E., C. Friehe and D. Lenschow, The use of pressure fluctuations on the nose of an aircraft for measuring air motion. J. Clim. Appl. Meteor., 22, 171-180, 1983.

Brubaker, K. L., M. Jasinski, A.T.C. Chang, E. Josberger, 2001. Interpolating sparse surface measurements for calibration and validation of satellite-derived snow water equivalent in Russian Siberia. Remote Sensing and Hydrology 2000, IAHS Pub. No. 267, Eds. M. Owe, K. Brubaker, J. Ritchie and A. Rango, p.p. 93-98.

Carroll, T. Operational airborne measurements of snow water equivalent and soil moisture using terrestrial gamma radiation in the United States, in Large Scale Effects of Seasonal Snow Cover, Proceedings of the Vancouver Symposium, IAHS Publ. No. 166:213-233.

Carroll, S.S., G.N. Day, N. Cressie and T.R. Carroll, 1995: Spatial modeling of snow water equivalent using airborne and ground based snow data. Enviornmetrics, 6, 127-139.

Cavalieri, D. J., NASA Sea Ice Validation Program for the Defense Meteorological Satellite Program Special Sensor Microwave Imager, *J. Geophys. Res.*, 96, 21, 969-21,970, 1991.

Cavalieri, D. J., The validation of geophysical parameters using multisensor data, Chapter 11 in Microwave Remote Sensing of Sea Ice, edited by F. D. Carsey, American Geophysical Union Monograph 68, 233-242, 1992.

Cavalieri, D. J., A microwave technique for mapping thin sea ice, J. Geophys. Res., 99, 12,561-12,572, 1994.

Cavalieri, D. J., EOS Aqua Sea Ice Validation Program: Meltpond2000, NASA Technical Memorandum 2000-209972, National Aeronautics and Space Administration, Goddard Space Flight Center, Greenbelt, MD 20771, pp. 31, December 2000

Cavalieri, D. J., J. Crawford, M. R. Drinkwater, D. Eppler, L. D. Farmer, R. R. Jentz and C. C. Wackerman, Aircraft active and passive microwave validation of sea ice concentration from the DMSP SSM/I, J. Geophys. Res., 96, 21,989-22,008, 1991.

Cavalieri, D. and S. Martin, The Contribution of Alaskan, Siberian, and Canadian coastal polynyas to the cold halocline layer of the Arctic Ocean, J. Geophys. Res., 99, 18343-18362, 1994.

Cavalieri, D. J., P. Gloersen, and T. T. Wilheit, Aircraft and satellite passive-microwave observations of the Bering Sea ice cover during MIZEX West, IEEE Trans. Geoscience and Remote Sensing, GE-24, 368-377, 1986.

Cavalieri, D.J., C.L. Parkinson, P. Gloersen, J.C. Comiso, and H.J. Zwally, Deriving long-term time series of sea ice cover from satellite passive microwave data sets, J. Geophys. Res., 104(C7), 15803-15814, 1999.

Chang, A. T. C., L. S. Chiu, and T. T. Wilheit, 1993: Random errors of oceanic monthly rainfall derived from SSM/I using probability distribution functions. Mon. Wea. Rev., 121, 2351-2354.

Chang, A.T.C., J.L. Foster and D.K. Hall, 1996: Effects of forest on the snow parameters derived from microwave measurements during the BOREAS winter field experiment. Hydrological

Processes, 10, 1565-1574.

Chang, A.T.C., J.L. Foster, D.K. Hall, B.E. Goodison, A.E. Walker and J.R. Metcalfe, 1997: Snow parameters derived from microwave measurements during the BOREAS winter field experiment. JGR, 102, 29663-29671.

Cho, K., N. Sasaki, H. Shimoda, T. Sakata, and F. Nishio, Evaluation and improvement of SSM/I sea ice concentration algorithms for the Sea of Okhotsk, J. Remote Sensing Soc. of Japan, 16(2), 47-58, 1996.

Cline, D. 2001. NASA Cold Land Processes Field Experiment Plan 2002-2004. Cold Land Processes Working Group, NASA Earth Science Enterprise, Land Surface Hydrology Program, http://www.nohrsc.nws.gov/~cline/clpx.html .

Comiso, J.C., and A.L. Gordon, Interannual variabilities of summer ice minimum, coastal polynyas, and bottom water formation in the Weddell Sea, in Antarctic sea ice physical properties and processes, AGU Antarctic Research Series Volume, edited by M. Jeffries, 293-315, 1998.

Comiso, J. C. and K. Steffen, Studies of Antarctic sea ice concentrations from satellite data and their applications, J. Geophys. Res. (in press, 2001).

Comiso, J. C., and H. J. Zwally, Antarctic Sea Ice Concentrations Inferred from Nimbus-5 ESMR and LANDSAT imagery, J. Geophys. Res., 87(C8), 5836-5844, 1982.

Comiso, J.C., and H.J. Zwally, Temperature Corrected Bootstrap Algorithm, IEEE IGARSS'97 Digest, Volume 3, 857-861, 1997.

Comiso, J. C. and C. W. Sullivan, Satellite microwave and in-situ observations of the Weddell Sea Ice Cover and its Marginal Ice Zone, J. Geophys. Res., 91(C8), 9663-9681, 1986.

Comiso, J. C., D. J. Cavalieri, C. P. Parkinson, and P. Gloersen, Passive Microwave Algorithms for Sea Ice Concentration - A Comparison of Two Techniques, Remote Sensing of the Environment, 60 (3), 354-384, 1997.

Comiso, J.C., D. J. Cavalieri, and T. Markus, Sea ice concentration, ice temperature, and snow depth using AMSR-E data, IEEE Trans. Geoscience and Remote Sensing, in press, 2003.

Comiso, J. C., P. Wadhams, W. Krabill, R. Swift, J. Crawford, and W. Tucker, Top/Bottom multisensor remote sensing of Arctic sea ice, *J. Geophys. Res.*, 96(C2), 2693-2711, 1991.

Comiso, J. C., T. C. Grenfell, D. L. Bell, M. A. Lange, and S. F. Ackley, Passive Microwave In Situ Observations of Winter Weddell Sea Ice, J. Geophy. Res., 94, 10891-10905, 1989.

Comiso, J.C, T.C. Grenfell, M. Lange, A. Lohanick, R. Moore, and P. Wadhams, "Microwave remote sensing of the Southern Ocean Ice Cover," Chapter 12,Microwave Remote Sensing of Sea Ice, (ed. by Frank Carsey), American Geophysical Union, Washington, D.C., 243-259, 1992.

Comiso, J.C., Sea ice geophysical parameters in the Arctic and the Sea of Okhotsk using multichannel passive microwave data, Journal of Japanese Remote Sensing, 16(2), 32-46, 1996.

Durden, S. L., E. Im, F. K. Li, W. Ricketts, A. Tanner, and W. Wilson, 1994: ARMAR: an airborne rain mapping radar. J. Atmos. & Oceanic Technol., 11, 727-737.

Ferraro, R.R, F. Weng, N.C. Grody and L. Zhao, 2000: Precipitation characteristics over land from the NOAA-15 AMSU Sensor. Geophys. Res. Letters, 27, No. 17, 2669-2672.

Fuhrhop, R., C. Simmer, M. Schrader, G. Heygster, K-P. Johnsen, P. Schussel, Study of Passive Remote Sensing of the Atmosphere and the Surface Ice: Executive Summary and Final Report, ESA ESTEC Contract No.11198/94/NL/CN, Berichte IfM Kiel, Nr. 29, 1997.

Gawarkiewicz, G., and D. C. Chapman, A numerical study of dense water formation and transport on a shallow, sloping continental shelf, J. Geophy. Res., 100, 4489-4507, 1995.

Gloersen P., W. Campbell, D. Cavalieri, J. Comiso, C. Parkinson, H.J. Zwally, Arctic and Antarctic Sea Ice, 1978-1987: Satellite Passive Microwave Observations and Analysis, NASA Spec. Publ. 511, 1992.

Gordon, A. L., and J. C. Comiso, Polynyas in the Southern Ocean, Scientific American, 256, 90-97, 1988.

Grenfell, T. C., J. C. Comiso, M. A. Lang, H. Eicken, and M. R. Wensnahan, Passive microwave observations of the Weddell Sea during austral winter and early spring, J. Geophys. Res., 99, 9,995-10,010, 1994

Haggerty, C.D. and Armstrong, R.L. 1996: Snow Trends within the former Soviet Union. EOS, Transactions American Geophysical Union, Vol. 77, No. 46:F191

Holland, G. J., T. McGeer and H. Youngren, Autonomous Aerosondes for economical atmospheric soundings anywhere on the globe. Bull. Amer. Met. Soc., 73, 1987-1998, 1992.

Holland, G. J., P. J. Webster, J. A. Curry, G. Tyrell, D. Gauntlett, G. Brett, J. Becker, R. Hoag, and W. Vaglienti, The Aerosonde robitic aircraft: A new paradigm for environmental observations. Bull. Amer. Met. Soc., 82 (5), 889-901, 2001.

Holmgren, J., M. Sturm, N. E. Yankielun, and G. Koh, Extensive measurements of snow depth using FM-CW radar. Cold Regions Sci. & Tech. 27, 17-30, 1998.

Jacobs, S.S., and J.C. Comiso, A climate anomaly in the Amundsen and Bellingshausen Seas, J. Climate, 10(4), 697-709, 1997.

Jezek, K. C., D. K. Perovich, K. M. Golden, C. Luther, D. G. Barber, P. Gogineni, T. C. Grenfell, A. K. Jordan, C. D. Mobley, S. V. Nghiem, and R. G. Onstott, A broad spectral, interdisciplinary investigation of the electromagnetic properties of sea ice, IEEE Trans. Geosci. and Remote Sensing, Vol.36, No.5, 1633-1641, 1998.

Kelly, R. 2001. Remote sensing of UK snow covers using multi-sensor satellite imagery. . Validation of Passive Microwave Snow Algorithms, Remote Sensing and Hydrology 2000, IAHS Pub. No. 267, Eds. M. Owe, K. Brubaker, J. Ritchie and A. Rango, pp.72-76.

Kelly, R.E.J., Chang, A.T.C, Tsang, L. and Foster, J.L. (in press) Development of a prototype AMSR-E global snow area and snow volume algorithm, IEEE Transactions on Geoscience and Remote Sensing.

Kidd, C., 1998: On rainfall retrieval using polarisation correct temperatures. Int. J. Remote Sensing, 19, No. 5, 981-996.

Kozu, T., T. Kawanishi, H. Kuroiwa, M. Kojima, K. Oikawa, H. Kumagai, K. Okamoto, M. Okumura, H. Nakatsuka, and K. Nishikawa, 2001: Development of precipitation radar onboard the Tropical Rainfall Measuring Mission (TRMM) satellite. IEEE Trans. Geosci. Rem. Sensing, GE-39, 102-143.

Krajewski, W. F., G. J. Ciach, J. R. McCollum, and C. Bacotin, 2000: Initial validation of the global precipitation climatology project monthly rainfall over the United States. J. Appl. Meteor., 39, 1071-1087.

L'Ecuyer, T. S. and G. L. Stephens, 2002: An estimation-based precipitation retrieval algorithm for attenuating radars. J. Appl. Meteor., accepted

Liu, A. K. and D. J. Cavalieri, Sea ice drift from wavelet analysis of DMSP SSM/I Data, *Int. J. Remote Sensing*, 19, 1415-1423, 1998.

Liu, G., and J. A. Curry, 1997: Precipitation characteristics in the Greenland-Iceland-Norwegian Seas determined using satellite microwave data. J. Geophys. Res., 102, 13,987-13,997.

Liu, A. K., Y. Zhao, and S. Y. Wu, Arctic sea ice drift from wavelet analysis of NSCAT and special sensor microwave imager data, J. Geophys, Res., 104, 11,529-11,538, 1999.

Markus, T. and D. J. Cavalieri, An enhanced NASA Team sea ice algorithm, IEEE Trans. Geosci. and Remote Sensing, 38, 1387-1398, 2000.

Markus, T. and D. J. Cavalieri, Snow depth distribution over sea ice in the Southern Ocean from satellite passive microwave data, In, Antarctic Sea Ice: Physical Processes, Interactions and Variability, Antarctic Research Series, Volume 74, pp 19-39, American Geophysical Union, Washington, DC, 1998

Markus, T. and D. J. Cavalieri, A revision of the NASA Team sea ice algorithm, IEEE Transactions on Geoscience and Remote Sensing, 38(3), 1387-1298, 2000.

Markus, T., D.J. Cavalieri, and A. Ivanoff, The potential of using Landsat 7 ETM+ for the classification of sea ice surface conditions during summer, Ann. Glaciol., in press, 2001.

Martin, S., B. Holt, D. J. Cavalieri, and V. Squire, Shuttle Imaging Radar B (SIR-B) Weddell Sea ice observations: A comparison of SIR-B and Scanning Multichannel Microwave Radiometer ice concentrations, J. Geophys. Res. 92, 7173-7179, 1987.

Martin, S., K. Steffen, J.C. Comiso, D.J. Cavalieri, M. Drinkwater, B.M. Holt, "Microwave Remote Sensing of Polynyas," Chapter 15, Microwave Remote Sensing of Sea Ice, (ed. by Frank Carsey), American Geophysical Union, Washington, D.C., 303-311, 1992.

Martinec, J., A. Rango and E. Major, 1983: The Snowmelt-Runoff Model (SRM) User's Manual. NASA Ref. Publ. 1100, 11 8pp.

Massom, R.A., J.C. Comiso, A.P. Worby, V. Lytle, and L. Stock, Satellite and in situ observations of regional classes of sea ice cover in the East Antarctic pack in winter, Remote Sensing of the Env., 68(1), 61-76, 1999.

Mätzler, C., R.O. Ramseier, and E. Svendsen, Polarization effects in sea ice signatures, IEEE J. Oceanic Eng. OE-9, 33-338, 1984.

Maykut, G. A., Energy exchange over young sea ice in the central Arctic, J. Geophys. Res., 83, 3646-3658, 1978.

McConnell, A. and G. R. North, 1987: Sampling errors in satellite estimates of tropical rain. J. Geophys. Res., 92D, 9567-9570.

Menasi, J., C. Swift, K. St. Germain, J. Comiso, and A. Lohanick, Passive microwave measurement of sea ice thickness, J. Geophys. Res., 98(C12), 22569-22578, 1993.

Mognard, N. M. & Josberger, E.G. 2000: Application of a Passive Microwave Snow Depth Algorithm that includes snow metamorphism, proceedings IAHS Remote Sensing and Hydrology 2000 Symposium, Sante Fe, NM, 2-7 April, 2000 (in press).

Morrissey, M. L., J. A. Maliekal, J. S. Greene, and J. Wang, 1995: The uncertainty in simple spatial averages using raingage networks. Water. Resour. Res., 31 (8), 2011-2017

NASA 1982: Plan of Research for Snowpack Properties Remote Sensing (PRSPRS), The Snowpack Properties Working Group, Goddard Space Flight Center, Greenbelt, Maryland.

National Snow and Ice Data Center(NSIDC), NSIDC, DMSP SSM/I Brightness Temperatures and Sea Ice Concentration Grids for the Polar Regions on CD-ROM User's Guide, National Snow and Ice Data Center, Special Report - 1, Cooperative Institute for Research in Environmental Sciences, University of Colorado, Boulder, CO, January 1992.

National Snow and Ice Data Center(NSIDC), NSIDC, DMSP SSM/I Brightness Temperatures and Sea Ice Concentration Grids for the Polar Regions on CD-ROM User's Guide, National Snow and Ice Data Center, Special Report - 1, Cooperative Institute for Research in Environmental Sciences, University of Colorado, Boulder, CO, January 1996.

Oelke, C., Atmospheric signatures in sea-ice concentration estimates from passive microwaves: modelled and observed, Int. J. Remote Sensing, 18, 1113-1136, 1997

Peixoto, J.P. and A.H. Oort, *Physics of Climate.* American Institute of Physics, New York, 1992.

Rango, A., J. Martinec, A. Chang, J. Foster and V. Van Katwijk, 1989: Average areal water equivalent of snow on a mountainous basin using microwave and visible data. IEEE Trans. on Geoscience and Remote Sensing, 27, 740-745.

Seed, A. and G. L. Austin, 1990: Variability of summer Florida rainfall and its significance for the estimation of rainfall by gauges, radar and satellite. J. Geophys. Res., 95D, 2207-2215

Steffen, K. and J. A. Maslanik, Comparison of Nimbus 7 Scanning Multichannel Microwave Radiometer radiance and derived sea ice concentrations with Landsat imagery for the North Water area of Baffin Bay, J. Geophys, Res., 93, 10,769-10,781, 1988.

Steffen K. and A. Schweiger, NASA Team algorithm for sea ice concentration retrieval from the Defense Meteorological Satellite Program (DMSP) Special Sensor Microwave/Imager (SSM/I): comparison with Landsat imagery, *J. Geophys. Res*., 96, 21, 971-21,987, 1991.

Steffen, K., D. J. Cavalieri, J. C. Comiso, K. St. Germain, P. Gloersen, J. Key, I. Rubinstein, D. Thomas, Passive microwave algorithms, Chapter 10 in Microwave Remote Sensing of Sea Ice, American Geophysical Union Monograph 68, edited by F. D. Carsey, 201-231, 1992.

Steiner, M., R. A. Houze, and S. Yuter, 1995: Climatological characteristics of three-dimensional storm structure from operational radar and rain gauge data. J. Appl. Meteor., 34, 1978-2007.

Stephens, G. L., D. G. Vane, and S. J. Walter, 2002: The ClouSat mission: A new dimension to space-based observations of cloud in the coming millennium. Bull. Amer. Met. Soc., submitted.

Stroeve, J., J. Maslanik, and X. Li, An Intercomparison of DMSP F11- and F13-derived Sea Ice Products, Remote Sensing of the Environment, Vol. 64, 132-152, 1998.

Sturm, M., K. Morris, and R. Massom, The winter snow cover of the west Antarctic pack ice: its spatial and temporal variability. In Antarctic Sea Ice: Physical Processes, Interactions and Variability, M. Jeffries, ed., Ant. Res. Series, 74, 1-18, 1998.

Sturm, M., J. Holmgren, and D. Perovich, In review, The winter snow cover on the sea ice of the Arctic Ocean at SHEBA: Temporal evolution and spatial variability. Journal of Geophysical Research-Oceans

Tao, W.-K. and J. Simpson, 1999: Tropical Oceanic Precipitation Processes over the Warm Pool: 2D and 3D Cloud-Resolving Model Simulations. WMO/WCRP, F. Bradley and R. Lukas (Eds.), 407-408

Tjuata, S., A.K. Fung, and J.C. Comiso, Effects of Snow Cover on Sea Ice Emission, IEEE IGARSS'95 Digest, Vol. 1, 697-699, 1995.

Tjuata, S., A.K. Fung, and M. Dawson, An analysis of scattering and emission from sea ice, Remote Sensing Review, 7, 83-106, 1993.

Todd, M. C. and J. O. Bailey, 1995: Estimates of rainfall over the United Kingdom and surrounding seas from SSM/I using polarization-corrected temperature. J. Appl. Meteor., 34, 1254-1265

Walter, B., A Study of the Planetary Boundary Layer over the Polynya Downwind of St. Lawrence Island in the Bering Sea using Aircraft Data, Bound-Layer Meteor., 48, 255-282, 1989.

Weingartner, T. J., D. J. Cavalieri, K. Aagard, and Y. Sasaki, Circulation, dense water formation, and outflow on the northeast Chukchi shelf, J. Geophy. Res., 103, 7647-7661, 1998.

Wentz F.J., C.L. Gentemann, D.K. Smith, D.B. Chelton, Satellite Measurements of Sea-Surface Temperature Through Clouds, *Science*, 288(5467), p. 847, 2000.

Wentz, F.J., A well-calibrated ocean algorithm for SSM/I, *J. Geophys. Res.,* 102(C4), p. 8703, 1997.

Wentz, F.J., L. A. Mattox, and S. Peteherych, New algorithms for microwave measurements of ocean winds: Applications to SeaSat and the Special Sensor Microwave Imager, *J. Geophys. Res., 91,* 2289-2307, 1986.

Wentz, F.J., Measurement of Oceanic Wind Vector Using Satellite Microwave Radiometers, *IEEE Transactions on Geoscience and Remote Sensing*, 30 (5), 960-972, 1992.

Wiesmann, A. and C. Metzler, Microwave Emission Model of Layered Snowpacks, Remote Sens. Environ., 70, 307-316, 1999.

Winsor, P., and G. Björk, Polynya activity in the Arctic Ocean from 1958 to 1997, J. Geophy. Res., 105, 8789-8803, 2000.

Worby, A.P., and J. Comiso, A study of the Antarctic Sea Ice Edge using SSM/I-Derived and in situ Observations, IGARSS Digest 2001, Sydney, Australia, July 2001.

Yuter, Sandra E., and Robert A. Houze Jr., 1995: Three-dimensional kinematic and microphysical evolution of Florida cumulonimbus. part II: Frequency distributions of vertical velocity, reflectivity, and differential reflectivity. Mon. Wea. Rev., 123, 1941–1963.

Zwally, H. J., J. C. Comiso, C. L. Parkinson, W. J. Campbell, F. D. Carsey, and P. Gloersen, Antarctic Sea Ice 1973-1976 from Satellite Passive Microwave

Acronyms

4DDA	four-dimensional data assimilation
ACR	Airborne Cloud Radar
ADEOS-II	ADvanced Earth Observation Satellite
AIRS	Atmospheric InfraRed Sounder
AIJEX	
AMeDAS	Automatic Meteorological Data Acquisition System
AMMR	Airborne Multichanel Microwave radiometer
AMPR	Airborne Microwave Precipitation Radiometer
AMSR-E	Advanced Microwave Scanning Radiometer for EOS
AMSU	Advanced Microwave Sounding Unit
APR-2	2nd generation Airborne Precipitation Radar
ARM	Atmospheric Radiation Measurement
ARM-CART	ARM-Clouds And Radiation Testbed
ARMAR	Airborne Rainfall Mapping Radar
ARS	
asc	ascending
ATBD	Algorithm Theoretical Basis Document
ATM	Airborne Topographic Mapper
ATSR	Along Track Scanning Radiometer
AVHRR	Advanced Very High Resolution Radiometer
Baltex	BALTic EXperiment
BOREAS	BOReal. Ecosystem-Atmosphere Study
BRDC	Baltex Radar Data Center
BSRN	Baseline Surface Radiation Network
CAMEX	Convection And Moisture Experiment
CFAD	Contoured Frequency by Altitude Diagrams
C	degree Celsius
Cm	centimeter
COADS	
CRM	Cloud Resolving Model
CZCS	Coastal Zone Color Scanner
dB	deciBell
DCG	Digital chirp generator
DMSP	Defense Meteorological Satellite Program
DOE	Department of Energy
dsc	descending
EASE-grid	Equal-Area projections grid
ECMWF	European Center for Medium-Range Weather Forecasts
EIA	Extended Interaction Amplifier
EOC	Earth Observation Center
EOS	Earth Observing System
EOSDIS	EOS Data and Information System
ERS	European Research Satellite
ESDIS	EOS Science Data Information system
ESMR	Electrically Scanning Microwave Radiometer
ETL	Environmental Technology Laboratory
FIRE	First ISCCP Regional Experiment
FL	freezing level
FOV	field of View
ftp	file transfer protocol
g	gram
GAC	Global Area Coverage
GAME	GEWEX ASIAN Monsoon Experiment
GCIP	GEWEX Continental-scale International Project
GCM	Global Circulation Model

GEWEX	Global Energy and Water cycle EXperiment
GHz	Giga Hertz
GLOBEC	GLOBal ocean ECosystem dynamics
GLI	GLobal Imager
GOES	Geostationary
GPCP	Global Precipitation Climatology Project
GSFC	Goddard Space Flight Center
GT	Ground Truth
GTS	Global Telecommunications System
H	horizontal (polarization)
Hr	hour
HR	Hydroscience and Engineering
HSB	Humidity Sounder from Brazil
IANZONE	International ANtarctic ZONal Experiment
IFOV	Instantaneous Field of View
IGBP	International Geosphere- Biosphere Programme
IMS	Interactive Multisensor Snow and Ice Mapping System
IR	infra red
ISCCP	International Satellite Cloud Climatology Program
ITA	integrated team algorithm
JCET	Joint Center for Earth Science Technology.
JERS	Japanese Earth Resources Satellite
JPL	Jet Propulsion Laboratory
K	degrees Kelvin
Km	kilometer
KWAJEX	KWAJalein EXperiment
L	columnar liquid water
LAI	Leaf-Area-Index
Landsat	LAND SATtelite
LBA	Large-scale Biosphere-atmosphere experiment in Amazonia
LNA	Low-noise amplifier
LTER	Long Term Ecological Research
LWC	liquid water content
M	meter
m_e	soil moisture
MAS	MODIS Airborne Simulator
MCSST	Multi-Channel SST
MEDS	marine Environmental Data Services
MHz	Mega Hertz
MIR	Millimeter Imaging Radiometer
MIZ	Marginal Ice Zone
MIZEX	Marginal Ice Zone EXperiment
MODIS	MODerate-resolution Imaging Spectraradiometer
mm	millimeter
Ms	milisecond
m/s	meter per second
MSS	Multi-Spectral System
MTPE	Mission to Planet Earth
NASA	National Aeronautics and Space Administration
NASDA	National Space Development Agency of Japan
NCAR	National Center for Atmospheric Research
NCDC	National Climatic Data Center
NCEP	National Center for Environmental Prediction (NOAA)
NDBC	National Data Buoy Center
NDVI	Normalized Difference Vegetation Index
NESDIS	National Environmental Satellite, Data, and Information Service
NEXRAD	NEXt generation RADar

NMC	National Meteorological Center
NOAA	National Oceanic and Atmospheric Administration
NOHRSC	National Operational Hydrologic Remote Sensing Center
NSCAT	NASA SCATterometer
NSF	National Science Foundation
NSIDC	National Snow and Ice Data Center
NWP	numerical weather prediction
NWS	National Weather Service
OLS	Optical Line Scanner
OMT	ortho mode transducer
OPPS	Operational Product Processing System
pdf	probability density function
PIRATA	Pilot Research Moored Array in the Tropical Atlantic
PMEL	Pacific Marine Environmental Laboratory
PO.DAAC	Physical Oceanigraphy Distributed Active Archive Center
PR	precipitation radar
prf	pulse repetition frequency
PSR	Polarimetric Scanning Radiometer
PV	Physical Validation
PWC	precipitable water content
QC	Quality Control
RADARSAT	Canadian Synthetic Aperture Radar Satellite
RAOB	RAdiosonde OBservations
RCE	Regional Continental-scale Experiment
rms	root mean square
rpm	rotations per minute
RTM	Radiative Transfer Model
S	second
SAR	Synthetic Aperture Radar
SCF	Scientific Computing Facility
SGP	Southern Great Plains
SISEX	Shuttle Imaging Spectrometer EXperiment
SHEBA	Surface HEat Budget of the Arctic Ocean
SLFMR	Scanning Low-Frequency Microwave Radiometer
SMMR	Scanning Multichannel Microwave Radiometer
SMOS	Soil Moisture and Ocean Salinity
SSM/I	Special Sensor Microwave/Imager
SSM/T-2	Special Sensor Microwave/temperature-2 (humidity)
SST	Sea surface temperature
SWE	Snow Water Equivalent
TAO	Tropical Atmosphere-Ocean
T_e	surface temperature
T_s	Sea Surface Temperature
Tb	brightness temperature
TL	Team Leader
TLSCF	Team Leader Science Computing Facility
TMI	TRMM Microwave Imager
TOGA	Tropical Ocean Global Atmosphere
TR	(brightness) temperature – rain rate
TRMM	Tropical Rainfall Microwave Mission
USGS	United States Geological Survey
V	columnar water vapor, vertical (polarization)
VIS/IR	Visible/InfraRed
W	wind speed
w_e	vegetation water content
WCRP	World Climate Research Program
WMO	World Meteorological Organization